
Radio Frequency Identification (RFID) Tags and Reader Antennas Based on Conjugate Matching and Metamaterial Concepts

Ph.D. Thesis written by
Gerard Zamora González

Under the supervision of

Jordi Bonache Albacete

and

Ferran Martín Antolín



Bellaterra (Cerdanyola del Vallès), July 2013



The undersigned, Dr. **Jordi Bonache Albacete** and Prof. **Ferran Martín Antolín**,

Professors of the Electronic Engineering Department (Engineering School) of the *Universitat Autònoma de Barcelona*,

CERTIFY:

That the thesis entitled “*Radio Frequency Identification (RFID) Tags and Reader Antennas Based on Conjugate Matching and Metamaterial Concepts*” has been written by **Gerard Zamora González** under their supervision.

And hereby to acknowledge the above, sign the present.

Signature: Jordi Bonache Albacete

Signature: Ferran Martín Antolín

Bellaterra, July 29th 2013

Contents

Acknowledgements.....	ix
Summary.....	xi
1 Motivation and Objectives.....	1
2 Introduction.....	5
2.1 Introduction to RFID Technology	5
2.1.1 Automatic Identification Systems	6
2.1.2 Operating Frequency Ranges and Applications	8
2.1.3 Brief History	12
2.1.4 Standardization.....	13
2.1.5 Market Trend	16
2.2 UHF-RFID Systems: Overview and State of the Art	17

2.2.1	UHF-RFID Frequency Bands and Operating Principle.....	17
2.2.2	Read Range: Definition and Measurement.....	19
2.2.3	Lumped element Equivalent-Circuit Model of UHF-RFID Chips.....	21
2.2.4	Physical Bandwidth Limitations: The Bode Criterion	22
2.2.5	State of the Art.....	24
2.3	Introduction to Leaky-Wave Antennas Based on Metamaterial Transmission Lines	32
2.3.1	Metamaterial Transmission Lines Based on SRRs.....	32
2.3.2	Leaky-Wave Antennas	35
2.4	References.....	37
3	Single Resonant Passive Circuit Network for Conjugate Matching and Bandwidth Optimization	49
3.1	Circuit Network Analysis	50
3.2	Limitation of the -3 dB Bandwidth	52
3.3	Design of a Broadband UHF-RFID Tag.....	54
3.3.1	Equivalent-Circuit Model for Tag Bandwidth Optimization	55
3.3.2	Tag Antenna Design	56
3.4	Fabrication and Experimental Results	59

3.5	Conclusions.....	60
3.6	References.....	61
4	Design and Synthesis Methodology for UHF-RFID Tags Based on the T-match Network	65
4.1	Previous Equivalent-Circuit Models of T-match Based Tags	65
4.2	Proposed Circuit Approach and Requirements.....	66
4.3	Design and Synthesis of T-match Based Tags.....	69
4.3.1	Design of a T-match Based Tag using a Resonant Antenna	71
4.3.2	Tag Bandwidth Related to the Antenna Impedance	73
4.3.3	Frequency Range of Validity of the Proposed Approach.....	74
4.3.4	Synthesis of a T-match Based Tag using a Resonant Antenna	74
4.4	Design of a Broadband UHF-RFID Tag using the Proposed Method	75
4.5	Fabrication and Experimental Results	79
4.6	Synthesis Technique of the Proposed Method.....	80
4.7	Conclusions.....	82
4.8	References.....	83
5	Microwave and UHF-RFID Devices Based on Metamaterial Concepts for Reader Applications	85
5.1	Fundamental Mode LWA using Slot Line and SRR-Based Metamaterials for	

Microwave RFID Reader Applications	86
5.1.1 Design of a Balanced CPW CRLH Transmission Line.....	86
5.1.2 Proposed Structure.....	87
5.1.3 Simulation and Experimental Results	90
5.1.4 Automatic Vehicle Identification (AVI) Applications	92
5.2 Design Strategy of Near Field Communication Devices for UHF-RFID Reader Applications	94
5.3 Conclusions.....	98
5.4 References.....	98
6 Conclusions and Future Work	101
APPENDIX A	107
APPENDIX B	109
APPENDIX C	111
Author list of publications	113
Patents	117

Acknowledgements

The present work would have never been possible without the help and support of many people who helped me during the PhD, and hence this thesis is partially their merit.

I have to give special thanks to my supervisors, Jordi Bonache and Ferran Martín, for their constant guidance, support and encouragement. Thank you Ferran for giving me the opportunity to start my professional trajectory as a researcher, and for your invaluable efforts, making things in my research much more understandable and simpler. Jordi, you have been the great master who has hugely contributed in my training as a researcher in the art of engineering and science. I do not find words for you, so I will simply say deep thanks. Also, I would like to thank all the members from GEMMA/CIMITEC and the Electronic Engineering Department for their support and help. Gonzalo, Jose, Paris, Núria, Albin, Miqui, Simone, G. Sisó, Naqui, Albert and J. Hellín. I have to give special mention to F. Paredes who has worked with me side by side during this period, and J. Selga for his help and patience.

Thanks to my family for their kindness and affection, and to all my friends have provided me with so many laughs and good times during these last years.

Of course, this is also a tribute to a very important person in my life, who knows the pains of this thesis better than I, and without whom the bad moments would have been infinitely worse: thank you Cristina.

Summary

Radio frequency identification (RFID) is a fast developing technology that provides wireless identification and tracking capability by using simple devices used for tagging objects or people on one end, called tags, and more complex devices on the other end of the link, called readers. RFID is an emerging technology and one of the most rapidly growing segments of today's automatic identification and data capture (AIDC) industry. RFID is used for hundreds, if not thousands, of applications at present. RFID is revolutionizing supply chain management, replacing bar codes as the main object tracking system, and it is rapidly becoming a cost-effective technology. However, the design of tags able to cover the whole UHF-RFID regulated bands, providing appropriate read performance, becomes an important challenge. Also, there is a lack of systematization in the design methodology of UHF-RFID tags. Another problem which prevents a faster expansion of the UHF-RFID technology is found in the retail item management, in the difficulty of simultaneously offer the possibility of controlling items payment in stores and inventory of elements present in the store. Cost reduction is a special concern in the implementation of microwave RFID systems since they typically use active tags whose power consumption should be minimized.

The main objective of this thesis is to provide solutions to the aforementioned problems, contributing to the progress and improvement of the RFID technology. This is achieved by proposing new strategies and a simple methodology for the design of UHF-RFID tags based on conjugate matching, and RFID reader antennas based on metamaterial concepts.

CHAPTER 1

Motivation and Objectives

Radio frequency identification (RFID) technology is a wireless communication technology that is used to uniquely identify tagged objects or people. RFID is an emerging technology and one of the most rapidly growing segments of today's automatic identification and data capture (AIDC) industry. Whether we realize it or not, RFID is an integral part of our life. RFID is used for hundreds, if not thousands, of applications such as preventing theft of automobiles and merchandise, inventory management, collecting tolls without stopping, managing traffic, gaining entrance to buildings, automating parking, controlling access of vehicles to gated communities, corporate campuses and airports, dispensing goods, providing ski lift access, tracking library books, and the growing opportunity to track a huge amount of assets in supply chain management. RFID is revolutionizing supply chain management, replacing bar codes as the main object tracking system. RFID technology is also being used in U.S. Homeland Security with applications such as securing border crossings and freight container shipments. RFID is rapidly becoming a cost-effective technology. This is in large part due to the efforts of Wal-Mart (the world's largest retailer) and the U. S. Department of Defense (the world's largest supply chain operator) to incorporate RFID technology into their supply chains.

In recent years, the applications of RFID passive systems operating in the UHF band have experienced a progressive growth. UHF-RFID tags are usually designed to operate at a single frequency band. However, due to the different worldwide regulations, the UHF-RFID frequency bands have different locations in the spectrum and vary in the different world regions. Therefore, the design of UHF-RFID tags able to cover the whole regulated bands (i.e., global band tags), providing appropriate read performance, becomes an important challenge. Another major problem which prevents a faster expansion of the UHF-RFID technology at present is found in a potential application from which high expectations arises: the retail item management. The problem is found in the difficulty of simultaneously offer the possibility of controlling items payment in stores and inventory of elements present in the store. Cost reduction is of special concern in the implementation of microwave RFID systems since they typically use active tags, which are powered by means of a battery, and power consumption should be minimized.

The main objective of this thesis is to provide solutions to the aforementioned problems, thus contributing to the progress and improvement of the RFID technology. This will be achieved by providing new strategies for the design of UHF-RFID tags based on conjugate matching, and microwave and UHF-RFID reader antennas based on metamaterial concepts. Accordingly, the outline of this work is as follows:

- The second chapter presents an overview of RFID technology, paying special attention to UHF-RFID systems. The concept of metamaterials is defined and metamaterial transmission lines based on a coplanar waveguide (CPW) transmission line and SRRs are introduced. Leaky-wave antennas (LWAs) based on metamaterial transmission lines are also described.
- In chapter three, the passive circuit network required for tag bandwidth broadening, by introducing a single resonance with conjugate matching at the intermediate frequency of the UHF-RFID band is obtained. According to this analysis, a global band UHF-RFID tag prototype is designed and fabricated.
- In chapter four, a new method for the design of global band UHF-RFID tags based on the T-match network is proposed. Such method is based on the equivalent-circuit network for bandwidth broadening obtained in Chapter 3. As a proof of concept, a global band tag is designed using this method and fabricated.
- Chapter five is focused on the design of RFID devices based on metamaterial concepts for reader applications. A leaky-wave antenna (LWA) is proposed to be used as microwave RFID reader antenna in the field of automatic vehicle identification (AVI). Moreover, a new methodology for designing near field (NF)

communication devices able to confine the electric and magnetic field in a controlled coverage region is presented for applications in the retail item management.

- Lastly, in chapter six, the conclusions and future research that result from this thesis are outlined.

The work conducted during the realization of this thesis was carried out within the Group GEMMA/CIMITEC, which is part of the Electronics Engineering Department of the *Universitat Autònoma de Barcelona*. GEMMA/CIMITEC has been part of the European Network of Excellence NoE 500252-2 METAMORPHOSE (Metamaterials organized for radio, millimeter wave and photonic super lattice engineering), the main objective of which was to research, study and promote artificial electromagnetic materials and metamaterials within the European Union. It has recently given rise to the Virtual Institute for Artificial Electromagnetic Materials and Metamaterials (METAMORPHOSE VI AISBL). Furthermore, CIMITEC is one of the centers of the Technological Innovation Network of TECNIO (ACCIÓ) of the Catalan Government, created with the objective of promoting the transference of technology to industry in the field of Information and Communication Technology and has been recognized as a Consolidated Group by the Catalan Government (AGAUR). This work was, thus, supported by the European, Spanish and Catalan Governments by means of several projects and contracts. Among the projects and contracts with the different institutions and companies that have given support to the developed research activities, we would like to highlight:

- International Project Eureka METATEC granted to a consortium composed of two companies and three research institutions from Serbia and Spain and funded in Spain by a PROFIT and an AVANZA I+D project. Title: *METAmaterial-based TEchnology for broadband wireless Communications and RF identification*. This project is linked to the following two projects. Period: 2006-2008.
- Project FIT-330225-2007-15 funded by the Spanish Government (Ministerio de Industria, Turismo y Comercio) by a PROFIT project. Title: *Metamaterial-based technology for broadband wireless communications and RF identification*. Period: 2007.
- Project TSI-020400-2008-119 funded by the Spanish Government (Ministerio de Industria, Turismo y Comercio) by a AVANZA I+D project. Title: *Metamaterial-based technology for broadband wireless communications and RF identification*. Period: 2008.
- Project TEC2007-68013-C02-02 META-INNOVA from the Spanish Government (*Dirección General de Investigación*). Project coordinated by the *Universitat*

Autònoma de Barcelona and the Universidad de Sevilla. Title: Tecnologías basadas en metamateriales y su aplicación a la innovación en componentes y subsistemas de RF microondas y milimétricas: circuitos de radiocomunicación. Period: 2007-2010.

- Project CSD2008-00066 CONSOLIDER INGENIO 2010 granted to a consortium composed of eight research groups from different Spanish Universities and funded by the Spanish Government. Title: *Ingeniería de Metamateriales (EMET)*. Period: 2008-2013.
- Project TSI-020100-2009-778 funded by the Spanish Government (Ministerio de Industria, Turismo y Comercio) by a AVANZA I+D project. Title: *Implementación de etiquetas de identificación por radio frecuencia de reducidas dimensiones y altas prestaciones*. Period: 2009.
- Project TEC2010-17512 METATRANSFER granted to the Universitat Autònoma de Barcelona by the Spanish Government. Title: *Nuevas estrategias de diseño y síntesis de componentes de microondas basados en conceptos de METAmateriales con orientación a la TRANSFERencia tecnológica*. Period: 2010-2013.

CHAPTER 2

Introduction

In this chapter, the main characteristics of RFID technology are introduced, as well as a brief history and a market prediction for the near future. RFID systems operating within the UHF regulated frequency bands are explained with more detail, including the most relevant features and the state of the art of such technology. Next, the concept of metamaterials is defined and metamaterial transmission lines (MTM TLs) based on a coplanar waveguide (CPW) and split ring resonators (SRRs) are described. Finally, leaky-wave antennas (LWAs) are briefly described, focusing the attention on planar implementations using MTM TLs, since a LWA based on metamaterial concepts is proposed in Chapter 5 for RFID reader applications.

2.1 Introduction to RFID Technology

Radio frequency identification (RFID) is a fast developing technology that provides wireless identification and tracking capability. Nowadays, many applications such as preventing theft of automobiles and merchandise, collecting tolls without stopping, gaining entrance to buildings, controlling access of vehicles to gated communities, corporate campuses and airports, providing ski lift access, tracking library goods, asset

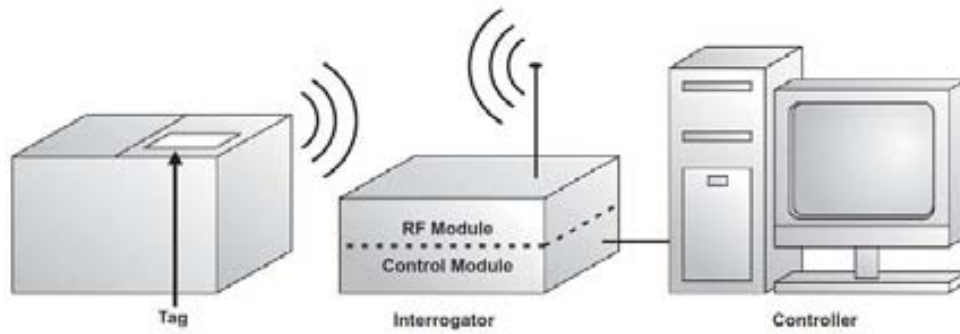


Fig. 2.1 The basic building blocks of an RFID system, including a host controller. Fig. extracted from [2].

identification, retailing and supply chain management, animal tracking, among others, take advantage of RFID systems [1],[2]. This section gives an overview of RFID technology and includes a short explanation about the main operating frequency ranges, as well as a brief history of RFID and the market trend.

RFID is generally characterized by the use of simple devices on one end, called tags or transponders, and more complex devices on the other end of the link, called readers or interrogators. The tags are made up of an antenna and an application specific integrated circuit (ASIC) chip, which contains memory where data is stored. Occasionally, they can include a matching network, located in between the antenna and the chip, to achieve proper impedance matching. The readers are composed of an antenna, an RF electronic module, which is responsible for communicating with the tag, and a control electronic module, which is responsible for communicating with a host computer (or controller), usually connected to the reader in order to centrally process information coming from readers. Fig. 2.1 shows the schematic of a typical RFID system. RFID systems can be read only (data is transferred in one direction, from the tag to the reader) or read-write (two way communication). Tags can be powered by a battery (active tags) or by rectification of the radio signal sent by the reader (passive tags). This thesis delves into passive RFID systems.

2.1.1 Automatic Identification Systems

Auto-ID (Automatic Identification) technology, also called automatic identification and data capture (AIDC), is a big set of identification procedures which include the very well-known barcode, as well as Optical Character Recognition (OCR), infrared identification and RFID. Among the various forms of Auto-ID, optical barcodes clearly



Fig. 2.2 (a) Traditional one-dimensional barcode (UPC code) and (b) two-dimensional barcode (QR code).

dominate the Auto-ID market being used in almost everything and everywhere today in the world. The main reason is their ultra-low cost, which is almost negligible. However, they are limited in memory storage capability and ‘line-of-sight’ operation is required. The latter makes the presence of an operator necessary to read a barcode. Since RFID systems do not have these limitations and, therefore, remove the human intervention in the reading process, RFID technology is coming into the Auto-ID market with a huge potential. In addition, unlike barcodes, RFID technology provides security by means of data encryption, and read/write capability. Nevertheless, RFID tags require a chip to store the data, which makes the tags expensive to be implemented in certain Auto-ID market applications. Barcodes typically cost under 0.01 €, whereas RFID tags cost over 0.10 €, as indicated in Table 2.1 where a comparison between optical barcodes and RFID systems is shown [2],[3]. Thus, there is a big demand of low-cost RFID technology around the world, and it is believed that someday RFID tags will be as pervasive as barcodes.

Table 2.1 Comparison of barcode vs. RFID system characteristics

	Barcode	RFID
Data Transmission	Optical	Electromagnetic
Memory/Data Size	Up to 3 KB	Up to 64 KB (passive tags) Up to 128 KB (active tags)
Tag Writable	No	Possible
Position of Scan/Reader	Line-of-sight	Non-line-of-sight possible
Read range	Typically up to several cm	Up to 15 m (passive tags) Up to > 100 m (active tags)
Access Security	Low	High
Environmental Susceptibility	Dirt	Low
Multiple reading	Not possible	Possible
Price	< 0.01 €	From 0.1 € to 1 € (passive tags) From 10 € to 100 € (active tags)

2.1.2 Operating Frequency Ranges and Applications

RFID systems operate at widely different frequency bands, as shown in Fig. 2.3, including frequencies from 125 KHz to 5.8 GHz in the microwave range. There are four main frequency bands used in RFID technology [2],[3]:

Low frequency (LF). These systems operate between 125 KHz and 134.2 KHz being available for use in the United States, Europe and Japan. Due to the electromagnetic properties at these frequencies, LF tags can be read even when they are attached to objects containing water, animal tissues, metal, wood, and liquids. However, they are only suitable for proximity applications, because they can be interrogated from a very short range of only a few centimeters (generally LF tags are passive). LF tag antennas are usually made of a copper coil with hundreds of turns rolled around a ferrite core. Because of these properties of LF tags, they are used for specific applications such as animal identification, access control, asset tracking, vehicle immobilizer, healthcare, and various point-of-sale applications. In particular, LF tags have been intensively used for animal tracking since the early 1980s.

High frequency (HF). Working around a central frequency of 13.56 MHz, this frequency band is also available for use in the United States, Europe and Japan at very similar power levels. HF tags are passive and their operating principles are similar to LF tags. However, HF tags have a better read range than LF tags and can be read up to half a meter away. The tag includes an *LC* resonant antenna usually made of several turns (~ 5-20 turns) of conductive materials such as copper, aluminum, or silver as a flat

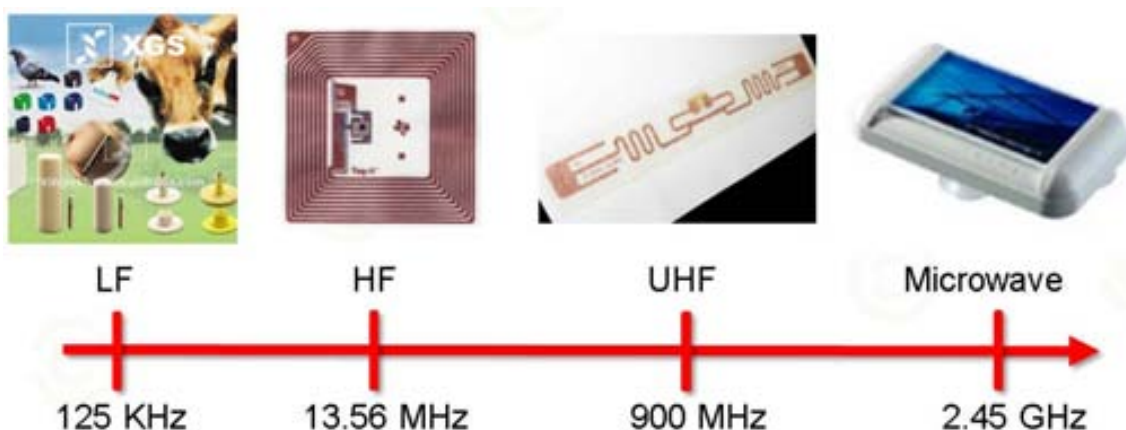


Fig. 2.3 Main RFID frequency bands and photographs of typical tags.



Fig. 2.4 Examples of LF-RFID tags for animal tracking (left) and vehicle immobilizer (right).

spiral, connected to a capacitor. Therefore, HF tags are usually very thin (as thick as paper). As it occurs with LF tags, HF tags can be easily read while attached to objects containing water, tissues, metal, wood, and liquids. Their performance, however, is affected by metal objects in the close vicinity. Tagging metal objects is not possible since metals cancel significantly the magnetic field perpendicular to the object, which is required to excite HF tags attached on metal surfaces. Their Applications include near-field communications (NFC), credit cards, smart cards, library book tags, airline baggage tags, and asset tracking.

Ultra high frequency (UHF). These systems operate in the vicinity of 433 MHz (active tags) and from 840 MHz to 960 MHz (passive and semi-passive tags). There are significant differences between regulations in different countries around the world, such as the United States, Europe, China and Japan. UHF tags have a read range of up to 15 m approximately. Unlike LF and HF tags, all the protocols in the UHF range have some type of anti-collision capability, allowing multiple tags to be read simultaneously. The UHF tag antennas are mostly based on dipole antennas and made of copper,



Fig. 2.5 Some applications of the NFC technology using a mobile phone.



Fig. 2.6 Examples of UHF-RFID applications in (a) supply chain management and (b) retail item management.

aluminum, or silver deposited on the substrate. The length of a resonant half-wave dipole antenna at 900 MHz is approximately 17 cm. However, the overall antenna size can be reduced through proper design techniques. The UHF antennas are easy to manufacture and, as HF tags, can be made thin using planar design. UHF tags offer more memory size and better read range, in comparison with LF and HF tags. As it is well-known, UHF tag performance changes when it is placed on different objects. This can generally be solved by taking into account the content on which the tag will be placed in the design stage. However, objects containing metals and water may degrade even more the read range of the tag through energy absorption and detuning. This problem can be overcome by designing tags specifically for tagging metal contents or for liquid contents. However, tags mountable on metallic objects that exhibit good performance are usually too expensive, big and occasionally heavy for certain applications. The reason of the efficiency degradation of common tags (not specially designed for metals) due to metal objects is that most UHF tags need to be excited by an electric field, tangentially oriented to the object metal surface, which extremely cancels such field. Regarding water (or liquid) contents, UHF's short wavelengths tend to get highly absorbed by liquids. Applications of UHF-RFID systems include supply chain management, retail item management and parking access control. (UHF-RFID technology will be explained with more detail in Section 2.2).

Microwave. The systems operating around the central frequencies of 2.45 GHz and 5.8 GHz industrial, scientific and medical (ISM) bands fall into this category. Passive, semi-passive and active tags are available in this frequency range and in most regions. The read range for passive tags are similar to UHF tags (up to around 15 m), whereas active ones can be read within a maximum range of up to more than 100 m. Their performance can be degraded when tags are close to water or metals, just like UHF tags.

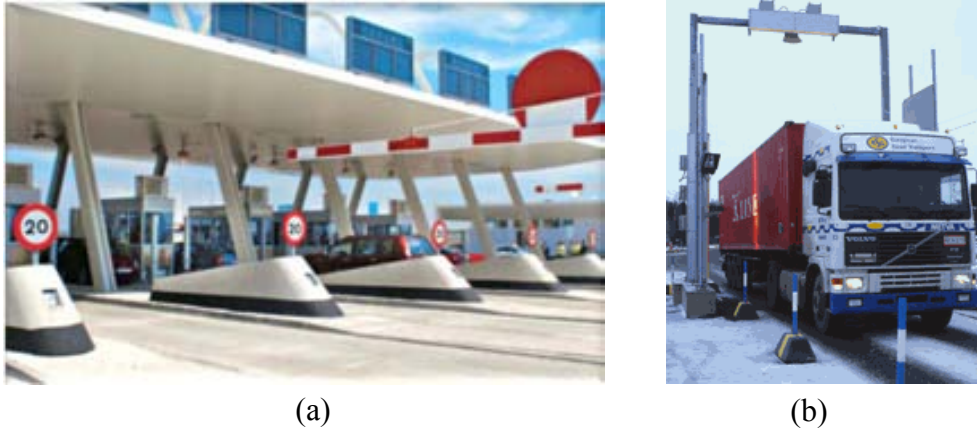


Fig. 2.7 Examples of Microwave-RFID applications in (a) highway toll collection and (b) automatic vehicle identification.

Multiple tags can also be read at the same time since anti-collision protocols exist. Nonetheless, other microwave devices sharing the same ISM band such as WLAN, cordless phones and microwave ovens, provide RF noise. Among their applications, highway toll collection, fleet identification, controlling access of vehicles to gated communities, hospitals, corporate campuses and airports and real-time location systems (RTLS) must be pointed out.

The most common physical coupling method used in LF and HF is based on inductive coupling, although there are also a few systems with capacitive coupling. The main reason is that magnetic field is affected only by objects with high magnetic permeability and metals, and such objects are not common in everyday life. On the other hand, capacitive coupling systems are affected by objects with high dielectric permittivity and loss. By contrast, UHF and microwave systems are coupled using electromagnetic fields and, occasionally, surface acoustic waves (see Fig. 2.8).

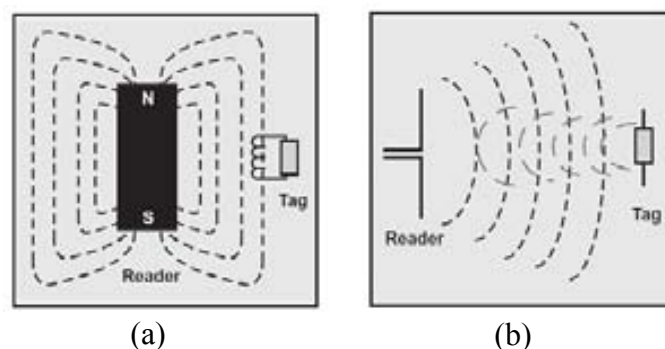


Fig. 2.8 Physical coupling method based on (a) near-field magnetic induction, used in LF and HF systems, and (b) far-field electromagnetic coupling, used in UHF and microwave systems.

2.1.3 Brief History

The first landmark work on the basic principles of passive RFID technology was published by Harry Stockman in 1948, and it was titled “Communication by Means of Reflected Power” [4]. In [4] Stockman stated: “Evidently, considerable research and development work has to be done before the remaining basic problems in reflected-power communication are solved and before the field of useful applications is explored.” Indeed, it took thirty years of investigation before the first RFID transponder was developed. Following, some of the most relevant events in the context of the history of RFID are chronologically listed [5].

During the 1950s, many of the technologies related to RFID were explored by researchers, taking advantage of developments in radio frequency communications and radar theory carried out in the 1930s and 1940s. In the 1950s, the U.S. military began to implement an early form of a long range identification system called identification, friend or foe (IFF), designed to distinguish between allied and enemy aircrafts. RFID technology commercial activities were beginning in the 1960s, thanks largely to the works on electromagnetic theory by R.F. Harrington, including “Fields Measurements Using Active Scatterers” [6] and “Theory of Loaded Scatterers” [7] published in 1963 and 1964, respectively. In this decade, electronic article surveillance (EAS) equipment for anti-theft and security applications was developed. These systems were 1-bit systems which allowed only detect the presence of objects, rather than identify them.

The RFID explosion took place in the 1970s, when companies, academic institutions, and government laboratories were increasingly working on RFID. During this decade RFID developments were applied to animal tracking, vehicle tracking and factory automation. An important development was published in a paper titled “Short-Range Radio-Telemetry for Electronic Identification using Modulated Backscatter” [8], written by Alfred Koelle, Steven Depp and Robert Freyman, in 1975. By 1978, a passive microwave transponder had already been accomplished. In the 1980s, commercial RFID systems began to extend in various parts of the world. Examples include livestock management, keyless entry, personnel access systems, and transportation applications, which appeared late within this decade. The world’s first toll application emerged in Europe in 1987, followed by the United States in 1989. In this same period, the development of the personal computer (PC) gave rise to a rapid expansion of RFID applications, since it made possible a more convenient and economical collection and management of data from RFID systems. Tags using custom CMOS integrated circuits and discrete components started to be built. This allowed further reductions in the size

of tags and increase in functionality. Consequently, the antenna size started to be crucial in determining the size of the tags.

Also, the 1990s were an important decade for RFID since it began to enter the mainstream of business and technology. RFID systems began to be used for toll collection, access control and a wide variety of other applications in commerce. In mid-1990s, RFID toll systems were operating at highway speeds enabling vehicles to pass toll collection points, unimpeded by plazas or barriers. The success of electronic toll collection led to important advancements, such as the first use of tags across different business segments. This allowed a single tag to be used for different applications such as electronic toll collection, parking lot access and gated community access. New RFID applications were also created for dispensing fuel, ski pass systems and vehicle access systems. For the first time, microwave RFID tags containing only a single integrated circuit (capability previously limited to inductively coupled RFID transponders) were constructed. This together with the rapid expansion of PC's and internet left the RFID industry with the unique problem of expensive tags to overcome, in order to develop commercially viable systems. In 1999 the Auto-ID centre was established at the Massachusetts Institute of Technology to gather RFID manufacturers, researchers and users, in order to develop standards and guidelines, together with other standard organizations including the European Conference of Postal and Telecommunications Administrations (CEPT) and the International Standards Organization (ISO).

By the early 2000s microwave tags were built as adhesive labels consisting of only two components: a simple integrated circuit and an antenna. Since then, the size of tags is clearly limited by the size of the antenna. In 2003, the Auto-ID was merged into EPC (Electronic Product Code) Global and assumed the task of standards for supply chain applications. The ISO also had very active standards activities for a variety of application areas in the beginning of the 2000s. Currently, all of these organizations are working on standards for RFID technology.

2.1.4 Standardization

The huge amount of applications where RFID is used and the necessity of interoperability between different systems demands a standardization of the RFID technology. The purpose of RFID standards is to create uniformity in the RFID industry and, therefore, to improve the efficiency of RFID systems and increase the industry

growth. Among the many standards bodies existing around the world, the following should be mentioned [2]:

- International Organizations for Standardization (ISO).
- International Electro-technical Commission (IEC).
- International Telecommunications Union (ITU).
- Electronic Product Code Global (EPC Global).

This section will delve into ISO and EPC Global standards, since they have influenced RFID industry to a greater extent.

2.1.4.1 International Organizations for Standardization (ISO)

Among the more relevant ISO standards, we can find (i) the two standards for animal tracking systems, which use LF, known as ISO 11784 and ISO 11785, (ii) standards for RFID identification cards, working at HF, such as ISO 10536, ISO 14443 and ISO 15693, and finally (iii) standards for RFID AIDC and item management technologies, some of which were published recently, in 2004, and became very important to the promotion of RFID technology.

Standards for RFID AIDC include ISO 15961, ISO 15962, ISO 15963, ISO 18001 for RFID item management and ISO 18000 to provide common communications protocols for international use of RFID. The ISO 18000 addresses the full range of RFID frequencies (LF, HF, UHF and microwave) to minimize the problems of migration between different frequency range operating systems. Specifications from this standard are divided into seven parts, as shown in Table 2.2.

Table 2.2 ISO 18000 Parts

Part 1	Generic Parameters for Air Interference Communication for Globally Accepted Frequencies
Part 2	Parameters for Air Interference Communication below 125 KHz
Part 3	Parameters for Air Interference Communication at 13.56 MHz
Part 4	Parameters for Air Interference Communication at 2.45 GHz
Part 5	Parameters for Air Interference Communication at 5.8 GHz
Part 6	Parameters for Air Interference Communication at 860-930 MHz
Part 7	Parameters for Air Interference Communication at 433 MHz

2.1.4.2 Electronic Product Code Global (EPC Global)

The EPC Global standards seem to be the standards choice for retailing and supply chain management applications. In fact, it is expected that EPC Global standards will have a significant influence over the direction the technology finally takes. The EPC can be understood as the electronic version of the UPC (the barcode standard). Indeed, EPC Global is trying to establish a large group called Global Trade Identification Numbers (GTIN), in order to enclose both EPC and UPC standards. An EPC number is made up of four parts, as shown in Fig. 2.9. The first part corresponds to the header, which identifies the EPC version (in this case version 1). The other three sections contain data akin to the product the tag is attached to in the following way. The second part, just after the header, identifies the product manufacturer. The third part stands for the object class or the exact type of product. Finally, the fourth part contains the serial number of the product. As it can be seen in Fig. 2.9, this tag is 96 bits long. This type of tag (with 28 bits for the manager number, 24 bits for the object class, and 36 bits for the serial number), is capable to uniquely identify 268 million companies, each of which could have up to 16 million different products and 68 billion unique serial numbers for each product. This is more than enough to identify all the world's manufactured goods for many years.

There are five classes of EPC tags summarized in Table 2.3. In addition to these classes, there exists the class 5, not shown in this table. This class defines the reader, which can communicate and power up the tags belonging to the classes 1 to 4, defined in Table 2.3.

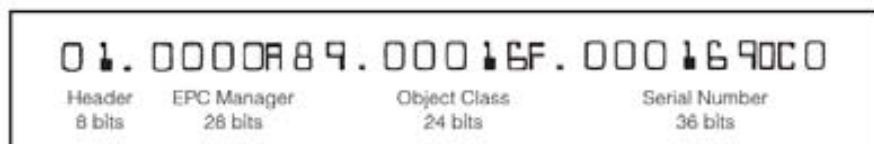


Fig. 2.9 An example of a EPC tag numbering system. Fig. extracted from [2].

Table 2.3 Classes of EPC tags

EPC Class	Definition	Programming
Class 0	Read-Only passive tag	Programmed during the semiconductor manufacturing process
Class 1	Write-Once-Read-Many passive tags	Programmed once by the end user
Class 2	Re-Writable passive tags	Can be Reprogrammed Many Times
Class 3	Semi-passive tags	Can be Reprogrammed Many Times
Class 4	Active tags	Can be Reprogrammed Many Times

Currently, there is a second generation of EPC labels known as EPC Gen 2, which was implemented in 2006. While keeping the same class structure, the Gen 2 tags functionality has been increased as compared with first generation. The Gen 2 standards has been adopted by the ISO standards organization and they concern, to a greater extend, for UHF-RFID systems. Their main aim is to provide uniformity between different RFID systems when operating at different locations around the world. Furthermore, Gen 2 protocols are much more secure than the previous ones, which allowed illegal data capturing. For example, the Gen 2 protocols include an option to kill a tag. In other words, once a tag is killed, it will not respond to a reader anymore, thus providing more privacy.

2.1.5 Market Trend

Currently, the most mature technology among all the RFID systems is the HF-RFID technology. However, there is a big acceleration in the development of UHF-RFID systems due mainly to its global standardization. Costs associated with UHF-RFID systems are not only limited to the tag price, but also to the software and hardware that is required to implement any RFID system. However, one of the biggest obstacles to extend the use of this technology is the high price of tags. Today, passive tags price ranges between 0.10 € and 1 €, as indicated in Table 2.1. These prices can be easily absorbed in high-cost products, while for low cost products would be prohibitive. Certainly, UHF-RFID tags are, at present, not able to compete with barcodes in terms of price, not even producing tags in billions. Nevertheless, according to a reliable prediction of RFID market given by [3] and [9], the price of passive tags is expected to decrease significantly in the coming years, as Fig. 2.10 shows, due to the development in semiconductor technology and mass productions.

An alternative technology based on chipless RFID tags was recently proposed. The functionality of such tags is largely reduced, but it is enough for many of today business processes, where the identification of the items is sufficient. For this reason this technology has become an object of study for many researchers and several chipless tags have been reported in the literature [10]-[12]. Fig. 2.10 shows the projection of the RFID chipped tag price versus the chipless tag price from 2004 to 2018. It can be seen that both curves tend to converge in the near future.

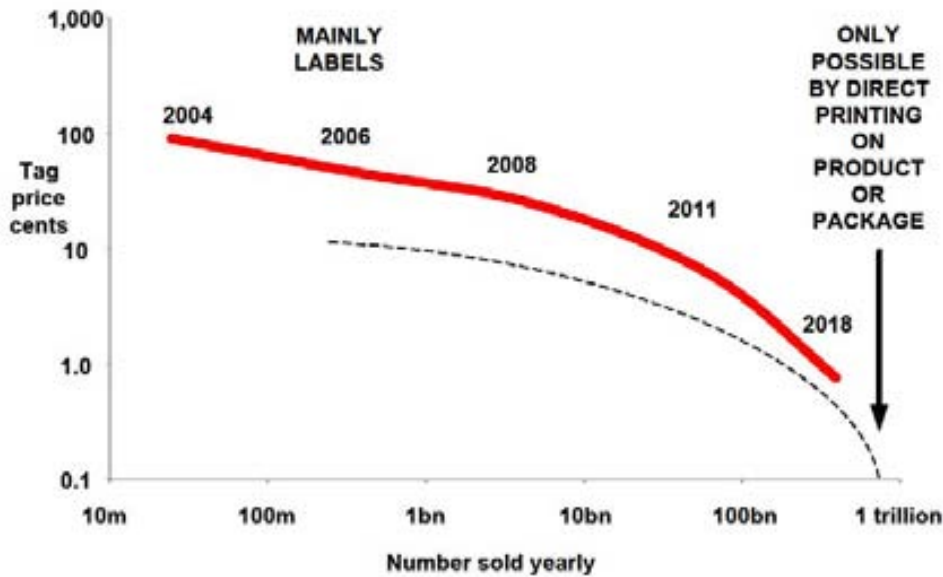


Fig. 2.10 Prediction of chip (solid line) and chipless (dashed line) tag prices (expressed in dollars) versus the number of tags sold yearly, from 2004 to 2018. Fig. extracted from [9].

2.2 UHF-RFID Systems: Overview and State of the Art

Particularly, ultra-high frequency (UHF) RFID systems are very attractive in comparison with RFID regulated systems using low frequency (LF) and high frequency (HF) bands, since they can provide superior read range, larger memory, faster signal processing and more secure data transmission [1]. Although microwave RFID systems provide similar performance than UHF systems, regulations and standards are available minimally at this frequency band. This is because they work at the ISM band and, therefore, it is especially susceptible to interferences introduced by other microwave devices sharing this frequency range, as mentioned in Section 2.1.2. This is the reason why attention is focused largely on UHF-RFID today and most emerging applications take advantage of the benefits of this technology. Thus, this section is devoted to UHF-RFID technology and it includes some basic characteristics, physical bandwidth limitations and the state of the art. Special attention is paid to passive systems.

2.2.1 UHF-RFID Frequency Bands and Operating Principle

The UHF-RFID regulated bands vary in the different world regions and they include frequencies between 840 MHz and 960 MHz, as it is shown in Fig. 2.11. UHF-RFID is



Fig. 2.11 Worldwide UHF-RFID operating frequency bands.

operated at 840-845 MHz in China, 866-869 MHz in Europe, 902-928 MHz in USA, and 950-956 MHz in Japan. Hence, the design of UHF tags able to cover the whole regulated bands (i.e., global band tags) becomes an important challenge.

The vast majority of UHF-RFID passive systems use the principle of modulated backscatter. In this type of RFID systems the reader transmits a modulated signal with periods of un-modulated carrier, which is received by the tag antenna. The chip converts the un-modulated signal to DC and sends back its information by varying its complex RF input impedance, Z_{chip} . This impedance typically toggles between two different states, corresponding to conjugate matching and to some other impedance, effectively modulating the back-scattered signal [13]. Fig. 2.12 shows the operation of a typical UHF-RFID system.

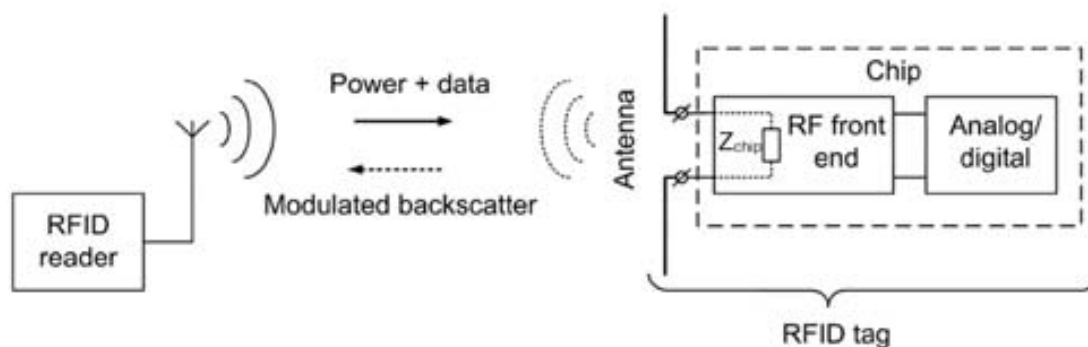


Fig. 2.12 Operating principle of a typical UHF-RFID system. The backscatter signal is modulated by changing the chip impedance Z_{chip} . Fig. adapted from [13].

2.2.2 Read Range: Definition and Measurement

The most important tag parameter indicative of the performance of an RFID system is the read range. That is, the maximum distance at which a reader can read information from the tag. Because the reader sensitivity is typically high in comparison to that of the tag, the read range is defined by the tag response threshold. The read range is also sensitive to the tag orientation, the material where the tag is attached, and the environment [13]. The read range r can be calculated using the Friis free-space formula (valid only in the far-field region) as [13]

$$r = \frac{\lambda}{4\pi} \sqrt{\frac{EIRP G_r \tau}{P_{chip}}} \quad (2.1)$$

where λ is the wavelength and $EIRP$ is the equivalent isotropically radiated power, determined by local country regulations ($EIRP = 3.3W$ in Europe, and $EIRP = 4W$ in USA). P_{chip} is the minimum threshold power necessary to activate the RFID chip, G_r is the gain of the receiving tag antenna, and τ is the power transmission coefficient between the chip and the antenna, which is related to the power reflection coefficient $|s|^2$ by $\tau = (1 - |s|^2)$. It is important to emphasize that (2.1) gives the maximum distance in free space at which the reader can detect the backscattered signal from a given tag, that is, both reader antenna and tag antenna are oriented towards each other in the direction of maximum gain and their polarizations are matched.

There exist various techniques for measuring the read range of RFID tags. It can be done by using a commercial RFID reader, resulting in the most economic method. It simply consists of moving the tag away from the reader until the tag stops responding. The read range curve as a function of the frequency is obtained by repeating the same procedure varying the frequency within a certain RFID frequency band. The main problem of this technique is that commercial readers are designed to operate only at a specific frequency band (e.g. Europe). This reduces the read range measurements to a limited frequency range, unless one has multiple readers, able to operate each one in a different UHF-RFID frequency band. Even in this case, it is not possible to obtain a continuous range curve as a function of frequency, due to the existing frequency band gaps between regulated bands. To overcome this problem, an arbitrary function generator, able to generate RFID frames and connected to a characterized antenna, can be used instead of an interrogator.

On the other hand, tag read range measurement can be carried out in a controlled environment by using an anechoic chamber or a transverse electromagnetic (TEM) cell. In both methods, tag can be located inside the anechoic chamber or TEM cell at a fixed position and transmitted output power can be varied. Thereby, large chambers or cells can be avoided. Even so, the read range measurement using a TEM cell is much more economic than using an anechoic chamber. Recently, a new method for tag characterization by means of a reverberation chamber was introduced in [14], achieving good accuracy in comparison with most common methods based on an anechoic chamber or a TEM cell.

The RFID setup available in our laboratory is shown in Fig. 2.13. The configuration of this measurement system has been entirely developed within this thesis. It includes an *Agilent N5182A* vector signal generator, which creates RFID frames and plays the role of a reader with variable frequency and variable output power. Such a generator is connected to a TEM cell by means of a circulator. The tag under test is located inside the TEM cell and it is excited by the frame created by the generator. Then the tag sends a backscatter signal to an *Agilent N9020A* signal analyzer through the circulator. At each frequency, the minimum power at the input of the TEM cell required to communicate with the tag is recorded. Finally, the tag under test is replaced by an electric probe inside the TEM cell, in order to determine the root mean square of the incident electric field, E_{rms} , corresponding to the minimum power at each frequency. This electric field is related to the power delivered to the chip according to

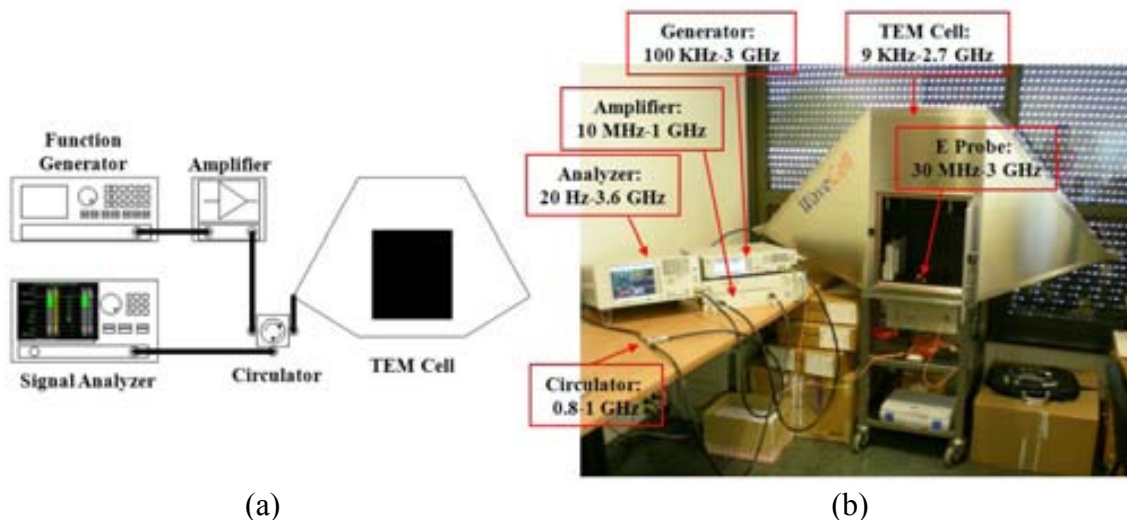


Fig. 2.13 (a) Schematic and (b) photograph of the RFID measurement setup available in our laboratory.

$$P_{chip} = SA_{ef}\tau = \frac{|E_{rms}|^2}{\eta} \frac{\lambda^2 G_r}{4\pi} \tau \quad (2.2)$$

where S is the incident power density, A_{ef} is the effective area of the tag antenna, and η is the wave impedance of free space. The measured read range can be inferred by introducing (2.2) into (2.1), resulting in the following expression

$$r = \frac{\sqrt{30EIRP}}{E_{rms}} \quad (2.3)$$

2.2.3 Lumped element Equivalent-Circuit Model of UHF-RFID Chips

The use of low-cost CMOS process to implement RFID chips has been imposed due to the need for cheap tags in many applications. In these applications, passive tags using back-scatter modulation are considered. In order to activate the chip, an RF-to-dc converter, also named voltage multiplier, is used as a first stage. Traditionally voltage multipliers consisted of capacitors and Schottky diodes. However, the use of MOS transistors to synthesize diodes became an interesting alternative allowing a significant reduction of the chip fabrication cost [15]. For this reason, low-cost RF-to-dc converter based on MOS transistors is extensively used in RFID chip implementations at present. In Fig. 2.14 a CMOS based voltage multiplier can be appreciated as part of an UHF-RFID chip.

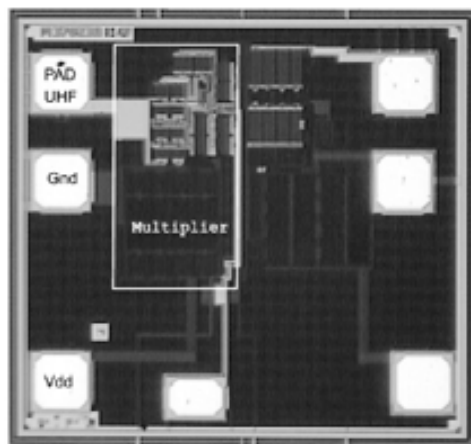


Fig. 2.14 Photograph of an UHF-RFID chip using a CMOS based voltage multiplier. Fig. extracted from [15].

The input impedance of an UHF-RFID chip is mainly determined by the voltage multiplier stage of the integrated circuit transponder. Thus, the chip impedance can be modeled by a parallel combination of a resistance R_c (that accounts for the losses of the multiplier) and a capacitance C_c (that includes all the capacitive effects). Typically, UHF-RFID chips exhibit high-impedance phase-angle and small resistance within the UHF-RFID frequency range [15],[16]. The ASIC has, therefore, a complex impedance which varies not only with frequency, but also with the input power applied to the chip [13]. The impedance reported by manufacturers is commonly referred to the minimum threshold power necessary to activate the chip, in order to ensure tag response at the maximum possible reading distance.

2.2.4 Physical Bandwidth Limitations: The Bode Criterion

Appropriate impedance matching between the antenna and the chip is of substantial importance in RFID. It directly influences the read range of the tag. Since the impedance of RFID chips is complex and depends on the manufacturer, specific RFID tag antennas must be designed for the considered chips available in the market. RFID tags are typically designed to achieve conjugate matching between the chip and the antenna (this maximizes the read range). As explained in the previous section, the chip impedance is always capacitive, hence requiring the antenna impedance to be inductive in order to obtain a proper impedance matching.

The qualitative behaviour of antenna impedance, chip impedance, and read range as a function of frequency for a typical UHF-RFID tag is illustrated in Fig. 2.15. It can be seen that the chip impedance is always capacitive and has a small resistance, as mentioned in the previous section. It can be observed that the peak read range of a typical RFID tag occurs at the frequency where conjugate matching between the chip and the antenna is achieved. This is because, among the parameters of (2.1), the power transmission coefficient τ is typically dominant in frequency dependence. Since the chip impedance has a complex value, which is frequency dependent, it is difficult to obtain broadband matching between the chip and the antenna, even in the case of using an external matching network for this purpose.

Regardless of whether a matching network is placed between the chip and the antenna or not, a theoretical limit on the minimum reflection coefficient magnitude that can be obtained within a certain frequency band, by means of an arbitrary ideal network cascaded to the chip, can be deduced from the Bode criterion. This fundamental limitation will be applied in Chapter 3 to obtain the optimum equivalent-circuit network

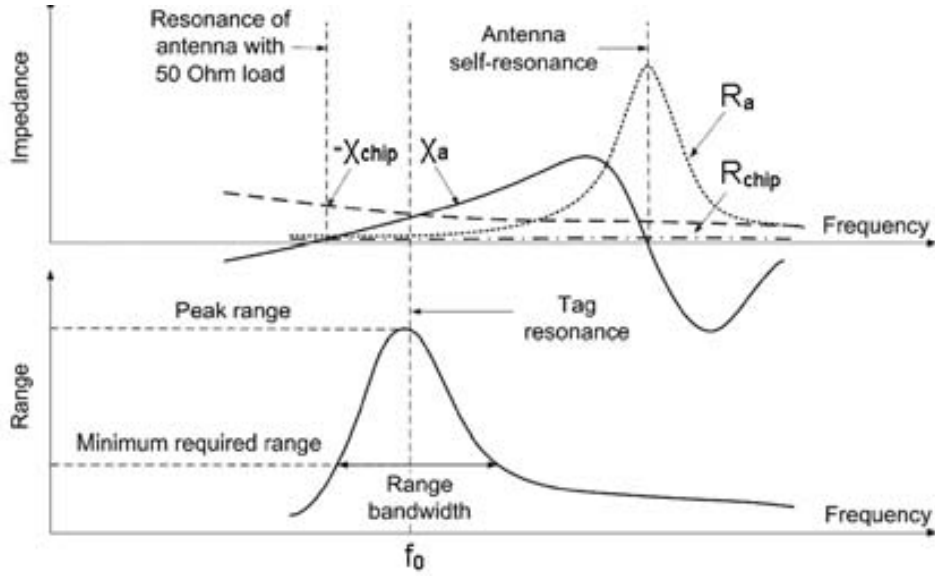


Fig. 2.15 Antenna impedance, chip impedance, and read range as functions of frequency for a typical RFID tag. R_{chip} and χ_{chip} are the resistance and reactance of the chip, respectively, and R_a and χ_a are the resistance and reactance of the tag antenna, respectively. Fig. adapted from [13].

necessary for bandwidth broadening in single resonant UHF tags with conjugate matching.

Let us assume the scenario depicted in Fig. 2.16. According to Bode's limit [17]-[18], the reflection coefficient achievable by any passive and lossless network cascaded to a parallel RC load impedance is limited by

$$\int_0^{\infty} \ln \left(\frac{1}{|s|} \right) d\omega \leq \frac{\pi}{R_c C_c} \quad (2.4)$$

where s denotes the reflection coefficient, ω the angular frequency and R_c and C_c are the equivalent resistance and capacitance, respectively, of the chip. Since $\ln(1/|s|)$ can be expressed in terms of the return loss (in dB) at the input of the matching network, expression (2.4) can be written as

$$-\int_0^{\infty} |s|_{\text{dB}} df \leq \frac{10 \log e}{R_c C_c} \quad (2.5)$$

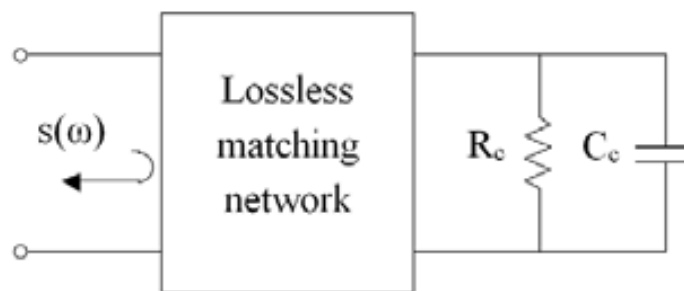


Fig. 2.16 Lossless matching network cascaded to a parallel RC load to determine the Bode's limit for the reflection coefficient $s(\omega)$.

Expression (2.5) forces the area given by the return loss curve to be less than, or equal, to a constant¹. Bandwidth optimization implies assuming $|s|^2$ to be a constant over the band of interest, and $|s|^2 = 1$ ($RL = 0\text{dB}$) elsewhere. This is the response with maximum bandwidth, but it cannot be realized in practice because it would require an infinite number of elements in the matching network [19]. The necessity of multiple stages to approximate the optimum response makes this objective prohibitive due to the increment of cost and tag dimensions. In fact, UHF-RFID tags are typically designed with a single resonant frequency in their frequency response. For this reason, in Chapter 3, a single resonant UHF tag is considered to obtain the equivalent-circuit network required for bandwidth optimization.

2.2.5 State of the Art

Currently, further development of RFID technology is taking place in the UHF band. This is due to the high expectations arising from item level tagging in many applications, especially in retailing and supply chain management. Such expectations are possible thanks to (i) the existence of the UHF Gen 2 as a single standard which opens up new applications, and (ii) the rapid cost reduction of passive UHF-RFID tags (see Fig. 2.10), mainly due to a decrease in the chip price and mass production, as indicated in Section 2.1.5.

¹ The maximum area achievable between the return loss curve and the $|s|^2 = 1$ axis for a given chip is referred as Bode area throughout this thesis.

At present, there are many manufacturers of passive tags to which one can outsource for the fabrication of tags. By contrast, in the case of active tags, there are less market initiatives. This is because passive UHF tags have been imposed over active tags, not only because they are much cheaper, but also because the read ranges achieved by new passive tags are continuously increasing. This allows the use of passive tags for long-range applications in which active tags were required in the past. The increase in the read range of passive tags is primarily due to the development of better chips with higher power sensitivities. Fig. 2.17(a) shows the dependence of the read range with the chip minimum threshold power over the recent past years. It can be appreciated a significant improvement of both, the read range and the chip power sensitivity, with time.

The current trend consists in implementing small-sized UHF-RFID chips with large user memory and minimum threshold power, according to specifications of the EPC Class 1 Gen 2 standard (see Fig. 2.17b). Until 2006, this market was mainly controlled by the manufacturer Impinj. Nowadays, the market of UHF-RFID chips is shared by Impinj and other companies such as NXP Semiconductors, Alien Technologies and Texas Instruments. Table 2.4 shows some examples of the mostly used UHF-RFID chips available in the market today. This table includes the minimum threshold power, P_{chip} , the value of the equivalent-circuit model parameters, R_c and C_c , and the Bode area for each chip.

Current developments are directed primarily towards creating global band UHF tags containing the new chips developed by industry and size optimized antennas exhibiting

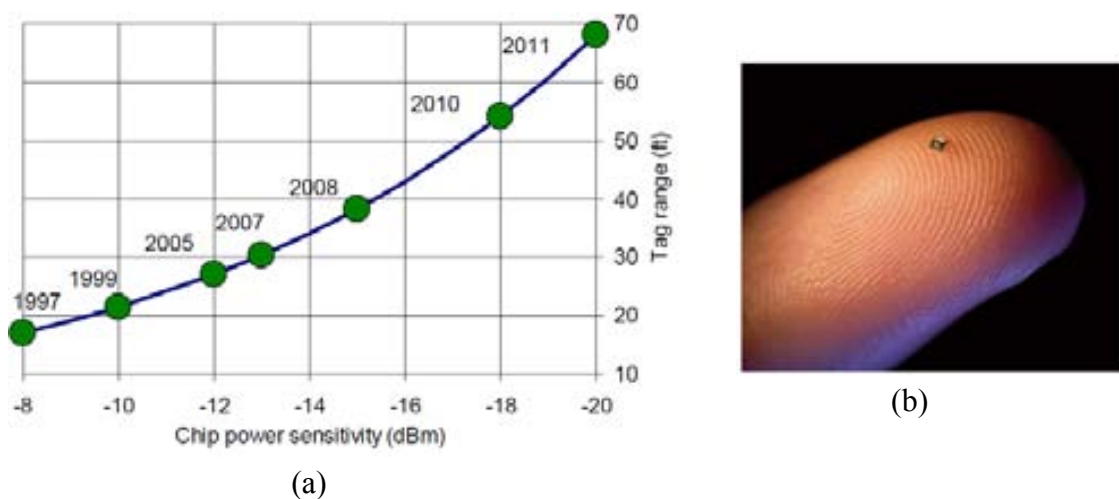


Fig. 2.17 (a) Tag read range (expressed in feet) versus chip power sensitivity over the recent past years and (b) photograph of an UHF-RFID commercial chip. Fig. 2.17(a) has been extracted from [20].

Table 2.4 Examples of UHF-RFID chips available in the market today

Chip	P_{chip} (dBm)	R_c (Ω)	C_c (pF)	Boode Area (MHz·dB)
Impinj Monza 4	-17.4	1650	1.21	2175
Impinj Monza 5	-17.8	1800	0.825	2924
Impinj Monza X-2K Dura	-17	1600	1	2714
Alien Higgs 3	-18	1500	0.85	3406
Alien Higgs 4	-18.5	1500	0.85	3406
NXP UCODE G2XM/ G2XL	-15	1385	1.16	2700

preferably dipole-like radiation pattern and linear polarization. One of the essential requirements in RFID applications is tag cost reduction. Hence, the use of external matching networks implemented with lumped elements is usually prohibitive. To overcome this situation, the antenna can be directly matched to the chip or by means of a matching network based on quasi-lumped or distributed components. Several techniques for achieving conjugate matching can be found in the literature [13],[21]-[25]. In [25], matching at two of the UHF-RFID regulated bands (Europe and USA) was considered, and it was demonstrated that optimum matching can be achieved by using dual-band tags, rather than broadband ones. This is of special interest when tags mountable on metallic objects are considered, since they are more robust against detuning. By contrast, broadband tags are usually preferred for general purposes, since they can continue working well in spite of suffering detuning effects when attached to objects with different contents. Other commonly used matching techniques are based on an inductive coupling, where the chip is matched to the antenna by means of an inductive coupled loop [26]-[29], and the strategy based on a nested slot, useful to match large planar dipoles or suspended patches, typically used to design tags for metal containers [30]-[33]. However, most commercial UHF-RFID tags are based on dipole antennas using some variant of the T-match network [24],[34],[35]. Such a matching network is extensively used in UHF-RFID tags since it allows achieving conjugate matching between the chip and the tag antenna at a certain frequency by means of a simple and small structure, without involving a significant increase of the tag cost and size. Examples of the aforementioned matching techniques are depicted in Fig. 2.18.

The T-match connection was first proposed by Uda [36], and more recently explained in [37] as an effective shunt-matching technique. Although the Uda transmission line model was initially analyzed as a general form of a cylindrical folded dipole, it has been applied to design planar structures [38]-[40] and even RFID tags [22],[24],[34]. However, it results difficult to match the antenna impedance to real RFID chips [22].

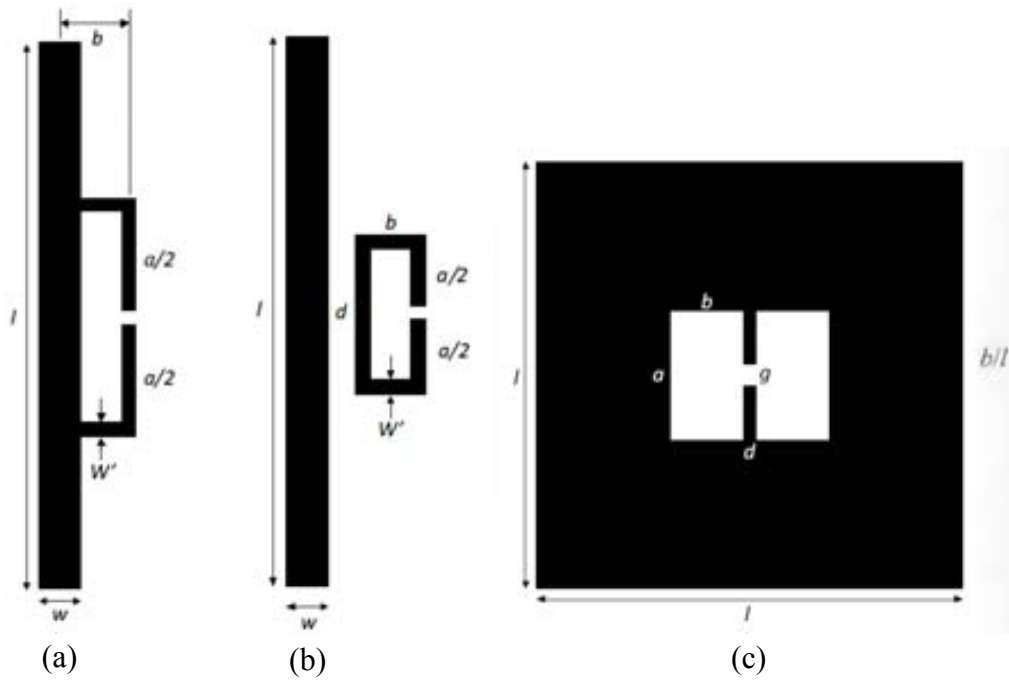




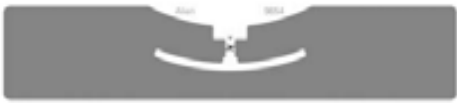
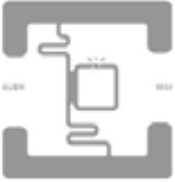















Fig. 2.18 An example of the (a) embedded T-match configuration and (b) inductively coupled feed for planar dipoles, and (c) geometry of the nested slot suspended patch.

Moreover, by this means, only a special case of the T-match structure can be used to design RFID tags, the embedded T-match, which is constructed by embedding the T-match structure into the antenna [35], as shown in Fig. 2.18(a). This is the main drawback since most commercially available T-match based tags have more complex geometries which cannot be analyzed by means of this planar model, in which the T-match is analyzed as a coplanar strip line embedded to the antenna. Table 2.5 shows some examples of passive UHF tags from leading manufacturers. It can be observed that the T-match network is almost always present with a loop shape in commercial tags. In order to overcome this problem, some efforts to deviate from Uda classic analysis and focus on a circuit-based approach have been made [24],[41],[42]. In these works, equivalent-circuit models of a dipole antenna (only valid over a relatively small frequency range near resonance) matched to the chip by means of a T-match have been developed. Nevertheless, the synthesis process of the tags from the obtained circuits is not fully explained. For this reason, a new systematic methodology for the design of broadband T-match based UHF-RFID tags is proposed in Chapter 4.

Often, UHF-RFID applications require small tags since they have to be attached to objects with reduced sizes. Then, the tag antenna must be miniaturized without unacceptable degradation of the radiation gain. Since antenna size and frequency of

Table 2.5 Examples of passive UHF-RFID tags in the market. Tags are not drawn to scale.

 <h2 style="margin: 0;">Alien Technology</h2>		
 <p>ALN 9640. IC: Higgs 3</p>	 <p>ALN 9728. IC: Higgs 4</p>	 <p>ALN 9762. IC: Higgs 4</p>
 <p>ALN 9654. IC: Higgs 3</p>	 <p>ALN 9634. IC: Higgs 3</p>	 <p>ALN 9710. IC: Higgs 4</p>
 <h2 style="margin: 0;">UPM Raflatac</h2>		
 <p>UPM Frog 3D. IC: Monza 4</p>	 <p>UPM Belt. IC: Monza 5</p>	 <p>UPM DogBone. IC: Monza 4</p>
 <p>UPM Web. IC: UCODE G2XM</p>	 <p>UPM Web. IC: UCODE G2XL</p>	
 <h2 style="margin: 0;">Avery Dennison</h2>		
 <p>AD-224. IC: UCODE G2XM</p>	 <p>AD-814. IC: Monza 3</p>	 <p>AD-110. IC: Monza 5</p>
 <p>AD-231D. IC: Monza 4</p>	 <p>AD-233. IC: Monza 5</p>	

operation impose limitations on maximum achievable gain and bandwidth [43]-[45], there exists a tradeoff between size miniaturization of antennas and maximum achievable gain and bandwidth. It means that reducing the electrical size of the tag antenna involves unavoidable gain and bandwidth degradation, which directly influences the tag performance. One of the most common used strategies for tag miniaturization is meandering, which consists in a single or even multiple folding of the antenna [46]. This can be observed in Table 2.5, wherein the majority of tags have been miniaturized using this technique. By this means, new extra degrees of freedom are introduced to achieve better matching between the chip and the antenna. However meandering involves far field cancellation due to the existence of currents in the antenna flowing in opposite directions. It is clear from (2.1) that a reduction on the gain of the receiving tag antenna involves a degradation of the read range of the tag. Therefore, for certain RFID applications where miniaturization is not mandatory, size reduction techniques may be avoided in order to achieve better tag performance.

2.2.5.1 Near field UHF-RFID

Currently, near field (NF) UHF-RFID receives a lot of attention as a possible solution for item level tagging in pharmaceutical and retailing industry, where LF/HF RFID has traditionally been used [47]-[52]. This technology uses standard UHF Gen 2 chips but instead of using far field (electric field) for communication between tag antennas and readers, they are designed to communicate by using NF, in a similar way that an HF antenna communicates (magnetic field). The main purpose of NF UHF is to make UHF-RFID systems work at short distances and on different objects, including liquid containers, as reliably as LF/HF-RFID [51]. In [52] the authors investigated and compared the use of HF (magnetic coupling) and UHF-RFID (electric coupling) systems for the item level identification of pharmaceutical products throughout their supply chain, and they conclude that UHF-RFID systems provide significantly superior readability in comparison with passive HF systems. A description of the main approaches to implement NF UHF-RFID systems are given below [53]:

1. The most obvious approach is to use a standard UHF-RFID system with conventional (far field) reader antennas and tags. It is expected that tags, which are able to work at the far field region, should receive more than enough power to be activated close to the reader antenna within the near field region. However, for applications where a short range reading zone is required, this system may detect undesired tags present in the far field region.

2. Another approach consists of using the same standard (far field) UHF-RFID system but with low reader output power. This becomes a straightforward solution for the problem presented above. However, due to the slow decay of the far field with distance r (decay as $1/r$, in contrast with the typical $1/r^2$ decay of the near field), undesired tags could be read within the far field region even reducing the reader output power. Moreover, because of the low reader output power, only high performance tags (long range and material insensitive) could be used to provide appropriate read performance on *RF non-friendly* objects.

3. Another method is to use a standard (far field) UHF-RFID reader and short range tags which only respond to strong fields in the vicinity of the reader antenna. These tags can either use magnetic or electric small antennas or even conventional tags intentionally mismatched by tuning. By this means, unintentional tag reads from the far field region are possible.

4. Finally, the most common solution reported in the literature consists of using special near field readers and tags. Such systems provide the best performance but also the highest cost. Although there are a few systems using electric (capacitive) coupling [54],[55], most solutions are based on magnetic (inductive) coupling between tags and reader antennas. Different versions of near field UHF RFID tags are supplied by companies nowadays. On one hand, there exist special tags sensitive only to the magnetic field [56],[62]. These types of tags are not compatible with far field RFID readers, since the magnetic field level generated at certain distance from the reader (subjected to power regulation) is not enough to activate them, being suitable for near field applications. On the other hand, the most common structures use dipole-like antennas (providing better sensitivity to the tags in the far field region), with the T-match loop acting as a matching network and allowing at the same time for magnetic excitation². As a result, these UHF tags have the capability to operate not only using electric far-fields but also by the use of magnetic near-fields. A fundamental advantage of UHF tags (840-960 MHz) using the T-match network over HF (13.56 MHz) tags relies on the Faraday's law

² Magnetic excitation of UHF tags is only possible in the near field region determined by the reader antenna, since magnetic field level generated at a certain distance, within the far field region, is not enough to activate UHF tags, due to power regulation.

$$\oint_{\partial S} \vec{E} d\vec{l} = -\frac{d}{dt} \int_S \vec{B} d\vec{s} \quad (2.6)$$

which states that the voltage induced (line integral of the induced electric field \vec{E}) on a single coil (with contour ∂S) by a magnetic field \vec{B} is proportional to the intensity and frequency of the field. Therefore, the magnetic coupling strength, in the case of considering UHF tags, is between 62 (at the low UHF-RFID frequency limit) and 70 (at the high UHF-RFID frequency limit) times greater than that of HF tags. This allows using a very small single turn loop in UHF tags (e.g. T-match connection) instead of HF complex multi-turn coils and even achieving longer communication distance than HF tags. Thus, UHF tags with far-field and near-field performance can be designed with similar size than typical HF tags, as it can be seen in Fig. 2.19.

Regarding the NF UHF interrogators, most solutions use magnetic reader antennas based on the so-called segmented loop technique [63]-[68]. By this means, strong and uniform magnetic fields can be achieved around the reader antenna. However, with these types of devices it is difficult to achieve a good compromise between low radiation gain and a large near field coverage. This is due to the fact that the radiation gain of a current loop increases strongly with its radius and also the distance where the near field is present is always of the same order of the size of the loop [69],[71]. Thus, to achieve a proper coverage zone (within the near field region) the size of the antenna is always of the order of the wavelength of the UHF-RFID signal in free space, giving rise to excessive values of radiation gain. This makes prohibitive the use of those tags capable to operate with electric far-field and magnetic near field (T-match based tags) in order to avoid unintentional tag reads. For this reason, most existing NF UHF applications are based on segmented loops and tags sensitive only to the magnetic field³.

One of the problems at present with the introduction of RFID technology in the retail item management is found in the difficulty of simultaneously offer the possibility of controlling items payment in stores and inventory of elements present in the store. The reason for this difficulty is found in the inability of the UHF-RFID readers to confine

³ As well as in the magnetic case, solutions based on electric coupling between the RFID tag and readers provide a very small coverage area for small radiation gains, since these devices are based on small antennas or resonators whose radiation gain increases dramatically with dimensions.

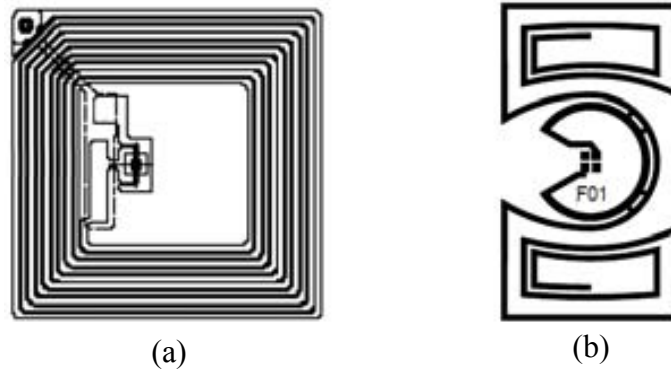


Fig. 2.19 (a) Typical HF tag and (b) Impinj's UHF tag. The UHF tag is smaller and exhibits both near-field and far-field performance characteristics.

the RF Electromagnetic power in a controlled space. A near field reader is needed in the payment point while a far field reader is needed for inventory purposes. Far field readers based on antennas are very suitable for carrying inventory without having to approach to the product, so that a complete inventory of every store can be made within seconds. Because the existing NF readers present high levels of radiation gain, the decay of the field towards the distance is difficult to control. Thus, these devices are not appropriate for payment applications, since the definition of a clear coverage zone is not possible and it is impossible to ensure that only the products of a single customer are accounted. For this reason, a strategy for the design of UHF-RFID NF communication devices to overcome the aforementioned problem is proposed in Section 5.2.

2.3 Introduction to Leaky-Wave Antennas Based on Metamaterial Transmission Lines

In this section, the concept of metamaterials is introduced. Special emphasis is given to planar metamaterials consisting of a CPW transmission line loaded with SRRs and wires. Leaky-wave antennas are presented as well, with focus on planar implementations using MTM TLs.

2.3.1 Metamaterial Transmisison Lines Based on SRRs

Metamaterials are commonly defined as artificial effectively homogeneous structures with advantageous and unusual electromagnetic properties. An effectively homogeneous structure is a periodic (or quasi-periodic) structure whose period is much

less than the wavelength at the frequencies of interest (refractive phenomena of the incident waves dominate over diffraction phenomena), thereby achieving effective medium properties (or continuous), which can be controlled at will (to some extent) by an appropriate design of the constitutive elements. Metamaterials have been under broad investigation over the past decade [72]-[75]. Specifically, one-dimensional composite right/left-handed transmission line (CRLH TL) metamaterials, also called MTM TLs, have been extensively applied to design planar guided-wave and radiated-wave structures. The MTM TL is a TL composed of a periodic repetition of a unit cell which provides left-handedness (anti-parallel phase and group velocities), usually at lower frequencies, and right-handedness (parallel phase and group velocities) at higher frequencies. The controllable electromagnetic properties of such structures and the possibility of device miniaturization, due to the small electrical size of the constituent cells, allows for the design of devices with improved performance and novel functionalities, in comparison with conventional structures.

There are two main approaches to implement MTM TLs: (i) the one based on the dual transmission line concept, initially proposed by Iyer *et al.* [76], Oliner [77], and Caloz *et al.* [78], and (ii) the resonant-type approach, initially proposed by Martín *et al.* [79]. This section will focus on the resonant-type approach and, more specifically, on the structure proposed in [79], which is characterized by using the split ring resonator (SRR) proposed by Pendry in [80].

The SRR is formed by two concentric open metallic rings printed on a microwave dielectric circuit board, as depicted in Fig. 2.20. The presence of a time-varying external magnetic field along the rings axial direction forces the electric current to flow from one

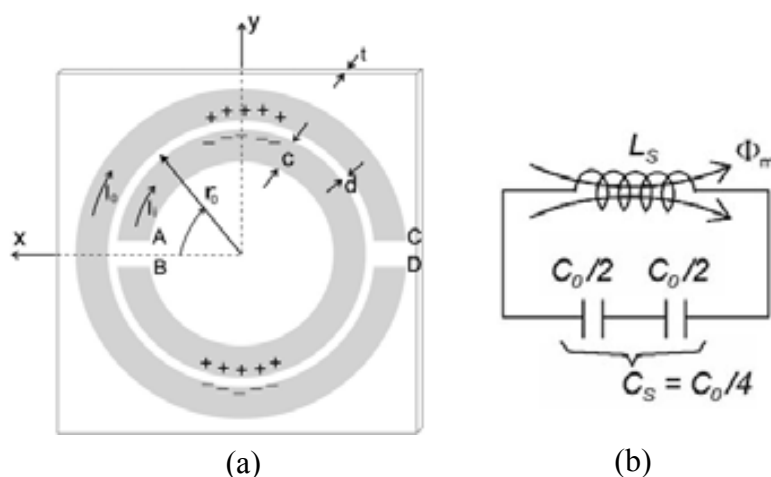


Fig. 2.20 (a) Topology and relevant dimensions of the SRR and (b) its equivalent-circuit model. Fig. extracted from [81].

ring to another (in the form of displacement current) across the slots between them, because the cuts in each ring are placed on opposite sides of the SRR. Hence, the current loop is closed through the distributed capacitance existing between the rings. A quasistatic circuit model for the SRR is shown in Fig. 2.20 [75],[82]. In this circuit L_s is the SRR self-inductance, C_0 is the total capacitance between rings, that is $C_0 = 2\pi\epsilon_0 C_{\text{pul}}$, where C_{pul} is the per unit length capacitance along the slot between the rings and C_s is the total capacitance of such a circuit. C_s is obtained from the series connection of the capacitances of both SRR halves, giving $C_s = C_0/4$. The SRR has a small electrical size at the first resonance frequency, given by

$$\omega_0 = \frac{1}{\sqrt{L_s C_s}} \quad (2.7)$$

The sub-wavelength characteristic of the SRR makes this resonator perfectly suitable to constitute the elemental unit cells in the synthesis of MTM TLs. The structure proposed in [79] consists of a set of SRRs periodically etched on the back substrate side of a CPW and a set of wires connecting the central strip and the ground plane, just above the SRRs, as Fig. 2.21(a) shows. This allows the SRRs to be magnetically coupled to the CPW.

The lumped element equivalent-circuit for the elemental cell (Fig. 2.21a) is shown in Fig. 2.21(b), which is valid in the long-wavelength regime ($\beta l \ll 1$, where β is the phase constant for guided waves) [79],[83]. The lumped elements of this equivalent circuit were found to be

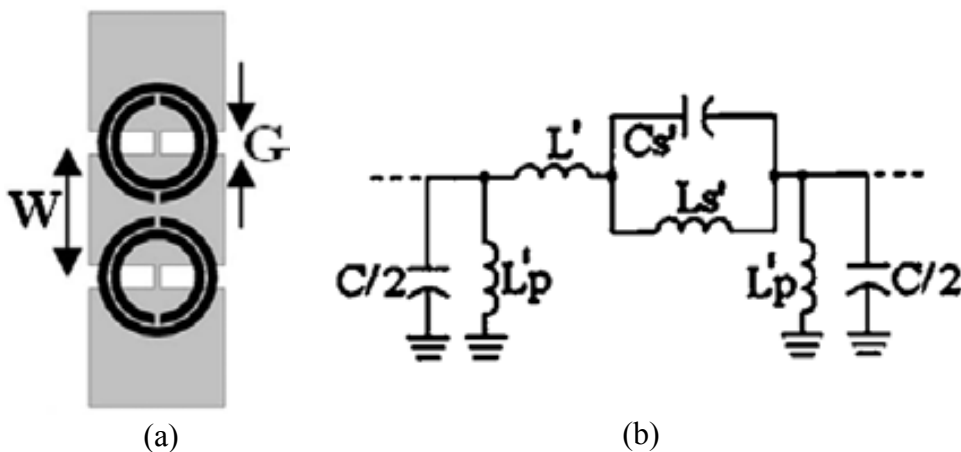


Fig. 2.21 (a) Layout of the unit cell of the considered CPW structures with SRRs and shunt strips and (b) simplified equivalent circuit model. Fig. extracted from [83].

$$C'_s = \frac{L_s}{2\omega_0^2 M^2} \left(\frac{1 + \frac{M^2}{2L_p L_s}}{1 + \frac{L}{4L_p}} \right)^2 \quad (2.8)$$

$$L'_s = 2\omega_0^2 M^2 C_s \frac{\left(1 + \frac{L}{4L_p}\right)^2}{1 + \frac{M^2}{2L_p L_s}} \quad (2.9)$$

$$L' = \left(2 + \frac{L}{2L_p}\right) \frac{L}{2} - L'_s \quad (2.10)$$

$$L'_p = 2L_p + \frac{L}{2} \quad (2.11)$$

where L and C are the per-section inductance and capacitance of the host CPW, L_p is the equivalent inductance of connecting wires and the SRRs, with resonance frequency given by (2.7), are inductively coupled to the line through a mutual inductance, M . The resulting dispersion diagram exhibits backward (or left-handed) wave propagation at low frequencies and forward (or right-handed) wave propagation at high frequencies. Typically, a frequency gap is present between the left-handed and the right-handed bands of the transmission line, unless it is designed to be balanced. In this case, the gap collapses and there is a continuous transition between the left-handed and the right-handed band at the so-called transition frequency, where the phase velocity is ideally infinity and the group velocity takes a finite value [84].

2.3.2 Leaky-Wave Antennas

LWAs are known since the 1940s, when W.W. Hansen introduced the first LWA consisting of a slotted rectangular waveguide [85]. The basic working principle of LWAs is based on a wave propagating along a guiding structure and gradually leaking

out a small amount of energy in the form of coherent radiation. Its advantages are the ability to offer sharp directional beams with a frequency scanning over a large bandwidth [86]. There are two different basic types of LWAs: uniform (or quasi-uniform) and periodic. In uniform LWAs the guiding structure is uniform along its length. In this case, the structure supports a wave that is fast with respect to free space. A quasi-uniform LWA operates in a similar way as does a uniform one, except that a periodic structure is used to guide the wave. However, the period is much smaller than the wavelength, and periodicity does not play an active role in the radiation phenomenon. In periodic LWAs, the guiding structure supports slow waves with respect to free space. However, the periodic modulation of the guiding structure produces infinite space harmonics, some of which may be fast, hence providing leaky-wave radiation [87],[88].

Specifically, planar LWAs have recently attracted much attention due to their structural simplicity, easy fabrication, and integration with other planar components [86],[87]. The interest in printed LWAs has increased significantly, mainly due to the advent of MTM TLs. Over the past years, MTM TLs have been proposed as backward, forward or backward-forward frequency scanning LWAs [89]-[97]. A very interesting property of these leaky-wave antennas is their capability to operate in the fundamental mode. This avoids the need for a complicated and costly feeding network, as typically used in a phased array. Moreover, most of these antennas can radiate at broadside direction [90],[94]-[97]. Despite the fact that these fundamental modes are fast in a certain region of the dispersion diagram, there is a cancelation of the leaky-wave radiation when open planar waveguides such as microstrip, coplanar waveguide and coplanar strip (CPS) lines are used to design LWAs, due to the presence of antiparallel currents. Such antennas are usually treated as antenna arrays in which radiation is mainly achieved by virtue of periodically loaded radiating elements, which are excited by the fundamental propagating mode [89],[91],[98].

Planar MTM TLs based on SRRs and wires can be tailored to produce backward and forward leaky-wave radiation, as it was shown in [92]. Although the original structure proposed in [79] supports fast-waves in a certain frequency range, it results inefficient to produce leaky-wave radiation from the fundamental mode (CPW mode), as it has been mentioned before. Due to the symmetry of the line and excitation, a magnetic wall in the symmetry plane appears. The radiation properties can be obtained by considering the equivalent magnetic currents, which are antisymmetric by virtue of the presence of the magnetic wall. Therefore, a significant cancellation of the far field will take place, as it occurs in a dipole antenna parallel to a tiny close electric conductor. In [92], in

order to achieve efficient leaky-wave radiation, a strong asymmetry was forced in the SRR-loaded CPW. Such asymmetry was obtained by removing the set of SRRs present at one of the sides of the symmetry plane of the CPW. This reduces the far field cancelation from the magnetic current balance between both slots and provides an excitation of the slot line mode, which results in an important contribution to increase the leaky-wave radiation. In Section 5.1, the problem of far field cancelation due to the existence of parallel currents is overcome by designing a new slot line LWA, inspired by the structure presented in [79], with forward, backward and broadside leaky-wave radiation from the fundamental mode, for reader applications in the microwave RFID band.

2.4 References

- [1] K. Finkenzeller, *RFID handbook: Radio-Frequency Identification fundamentals and applications*, 2nd ed: John Wiley and Sons, 2003.
- [2] V. S. Hunt, A. Puglia, and M. Puglia, *RFID: A Guide to Radio-Frequency Identification*, John Wiley and Sons, NY, 2007.
- [3] N. C. Karmakar, *Handbook of Smart Antennas for RFID Systems*, John Wiley and Sons, NJ, 2010.
- [4] H. Stockman, “Communication by means of reflected power”, *Proc. IRE*, pp. 1196–1204, Oct. 1948.
- [5] J. Landt, “The history of RFID”, *IEEE Potentials*, vol. 24, no. 4, pp. 8–11, Oct.–Nov. 2005.
- [6] R. F. Harrington, “Fields measurements using active scatterers”, *IEEE Transactions on Microwave Theory and Techniques*, vol. 11, no. 5, pp. 454–455, Sep. 1963.
- [7] R. F. Harrington, “Theory of loaded scatterers”, *Proceedings of the Institution of Electrical Engineers*, vol. 111, no. 4, pp. 617–623, April 1964.
- [8] A. R. Koelle, S. W. Depp and R. W. Freyman, “Short-range radio-telemetry for electronic identification using modulated backscatter”, *Proceedings of the*

IEEE, vol. 63, no. 8, pp. 1260–1261, Aug. 1975.

- [9] R. Das and P. Harrop, *Printed and Chipless RFID Forecasts, Players and Opportunities 2009–2019*, IdTechEx report, 2009.
- [10] S. Preradovic and N. C. Karmakar, “Chipless RFID: bar code of the future”, *IEEE Microwave Magazine*, vol. 11, no. 7, pp. 87–97, Dec. 2010.
- [11] F. J. Herraiz-Martínez, F. Paredes, G. Zamora, F. Martín and J. Bonache, “Printed magnetoinductive-wave (MIW) delay lines for chipless RFID applications”, *IEEE Transactions on antennas and propagation*, vol. 60, no. 11, pp. 5075–5082, Nov. 2012.
- [12] F. J. Herraiz-Martínez, F. Paredes, G. Zamora, F. Martín and J. Bonache, D. Segovia- Vargas “Chipless RFID and Wireless Sensors Based on Planar Magnetoinductive-Wave (MIW) Delay Lines”, *Unión Científica Internacional de Radio (URSI)*, Elche, España, Sep. 2012.
- [13] K. V. Seshagiri Rao, P.V. Nikitin and S.F. Lam, “Antenna design for UHF-RFID tags: a review and a practical application”, *IEEE Trans. Antennas and Propagation*, vol. 53, no. 12, pp. 3870–3876, Dec. 2005.
- [14] J. H. Rudander, P. S. Kildal and C. Orlenius, “Measurements of RFID tag sensitivity in reverberation chamber”, *IEEE Antennas and Wireless Propagation Letters*, vol. 10, pp. 1345–1348, Nov. 2011.
- [15] E. Bergeret, J. Gaubert, P. Pannier and J.M. Gaultier, “Modeling an design of CMOS UHF voltage multiplier for RFID in a EEPROM compatible process”, *IEEE Trans. Circuits and Systems*, vol. 54, no. 10, pp.833-837, Oct. 2007.
- [16] G. De Vita and G. Iannaccone, “Design criteria for the RF section of UHF and microwave passive RFID transponders”, *IEEE Trans. Microwave Theory Tech.*, vol. 53, no. 9, pp. 2978–2990, Sep. 2005.
- [17] H. W. Bode, “Network analysis and feedback amplifier design”, pp. 360–371, D. Van Nostrand co., N.Y., 1945.
- [18] R. M. Fano, “Theoretical limitations on the broadband matching of arbitrary impedances”, *Journal of the Franklin Institute*, vol. 249, no. 1, pp. 57–83,

Jan. 1950.

- [19] G. L. Matthaei, L. Young and E. M. T Jones, *Microwave Filters, Impedance-Matching Networks and Coupling Structures*, Artech House Books, Dedham, Mass. 1980.
- [20] P. V. Nikitin, K. V. S. Rao and S. Lam, “UHF RFID tag characterization: overview and state-of-the-art”, *Proceedings of 34th Annual AMTA Symposium*, Bellevue, WA, Oct. 2012.
- [21] P. Iliev, P. Le Thuc, C. Luxey and R. Staraj, “Antenna design method for RFID UHF tags”, *IEEE International Conference on Electronics, Circuits and Systems (ICECS)*, pp. 562–565, Dec. 2007.
- [22] G. Marrocco, “The art of UHF-RFID antenna design: impedance matching and size-reduction techniques”, *IEEE Antennas and Propagation Magazine*, vol. 50, no. 1, pp. 66–79, Feb. 2008.
- [23] A. H. Rida, Y. Li, S. Serkan Basat, A. Ferrer-Vidal, S. Nikolaou, and M. M. Tentzeris, “Design, development and integration of novel antennas for miniaturized UHF RFID tags”, *IEEE Transactions on Antennas and Propagation*, vol. 57, no. 11, pp. 3450–3457, Nov. 2009.
- [24] D. D. Deavours, “Analysis and design of wideband passive UHF-RFID tags using a circuit model”, *IEEE International Conference on RFID*, pp. 283–290, May 2009.
- [25] F. Paredes, G. Zamora, J. Bonache, and F. Martin, “Dual-band impedance-matching networks based on split-ring resonators for applications in RF identification (RFID)”, *IEEE Transactions on Microwave Theory and Techniques*, vol. 58, no. 4, pp. 1159–1166, April 2010.
- [26] H. W. Son and C. S. Pyo, “Design of RFID tag antennas using an inductively coupled feed”, *Electronics Letters*, vol. 41, no. 18, pp. 994–996, Sep. 2005
- [27] Li Yang, S. Serkan Basat and M. M. Tentzeris, “Design and development of novel inductively coupled RFID antennas”, *IEEE International Symposium on Antennas and Prop. Society*, pp. 1035–1038, July 2006

- [28] N. Popovic and P. Manojlovic, “UHF RFID antenna: A printed dipole antenna with CPS matching circuit and inductively coupled feed”, *International Conference on Telecommunication in Modern Satellite, Cable, and Broadcasting Services (TELSIKS)*, pp. 445–448, Oct. 2009.
- [29] Y. Zheng and L. Xiuping, “Inductively coupled RFID tag antenna design and measurement”, *International Conference on Microwave and Millimeter Wave Technology (ICMMT)*, pp. 1546–1548, May 2010.
- [30] G. Marrocco, “RFID antennas for the UHF remote monitoring of human subjects”, *IEEE Transactions on Antennas and Propag.*, vol. 55, no. 6, , pp. 1862–1870, June 2007.
- [31] H. Kwon and B. Lee, “Compact slotted planar inverted-F RFID tag mountable on metallic objects”, *Electronics Letters*, vol. 41, no. 24, pp. 1308–1310, Nov. 2005.
- [32] S. Aroor and D. D. Deavours, “A dual-resonant microstrip-based UHF RFID “cargo” tag”, in *IEEE MTT-S International Microwave Symposium Digest*, pp. 579–582, June 2008.
- [33] L. Mo, H. Zhang, and H. Zhou, “Broadband UHF RFID tag antenna with a pair of U slots mountable on metallic objects”, *Electronics Letters*, vol. 44, no. 20, pp. 1173–1174, Sep. 2008.
- [34] J. Choo, J. Ryoo, J. Hong, H. Jeon, C. Choi and M. M. Tentzeris, “T-matching networks for the efficient matching of practical RFID tags”, *European Microwave Conference*, pp. 5–8, Sep.-Oct. 2009.
- [35] N. A. Mohamed, K. R. Demarest and D. D. Deavours, “Analysis and synthesis of UHF RFID antennas using the embedded T-match”, *IEEE International Conference on RFID*, pp. 230–236, April 2010.
- [36] S. Uda and Y. Mushiake, *Yagi-Uda Antenna*. Tohoku University: Research Institute of Electrical Communication, 1954.
- [37] C. A. Balanis, *Antenna Theory: Analysis and Design*, 3rd ed., John Wiley & Sons Inc., NY, 2005.

- [38] R. W. Lampe, "Design formulas for an asymmetric coplanar strip folded dipole", *IEEE Trans. Antennas Propagation*, vol. AP-33, no. 9, pp. 1028–1031, Sep. 1985.
- [39] W. Lampe, Correction to "Design formulas for an asymmetric coplanar strip folded dipole", *IEEE Trans. Antennas Propagation*, vol. AP-34, no. 4, pp. 611, April 1986.
- [40] H. J. Visser, "Improved design equation for asymmetric coplanar strip folded dipoles on a dielectric slab", *Antennas and Propagation International Symposium*, pp. 1–6, June 2007.
- [41] D. M. Dobkin and S. Weigand, "Environmental effects on RFID tag antennas", *IEEE MTT-S International Microwave Symposium*, pp. 135–138, June 2005.
- [42] D. M. Dobkin, *The RF in RFID: Passive UHF RFID in Practice*, Newnes, 2007.
- [43] L. J. Chu, "Physical limitations of omni-directional antennas", *J. Appl. Phys.*, vol. 19, pp. 1163–1175, Dec. 1948.
- [44] R. F. Harrington, "Effect of antenna size on gain, bandwidth, and efficiency", *J. Res. Nat. Bureau Standards*, vol. 64D, no. 1, pp. 1–12, Jan.-Feb. 1960.
- [45] H. A. Wheeler, "Small antennas", *IEEE Trans. Antennas Propag.*, vol. AP-23, no. 4, pp. 462–469, July 1975.
- [46] F. Paredes, G. Zamora, F. J. Herraiz-Martinez, F. Martín and J. Bonache, "Dual-band UHF-RFID tags based on meander line antennas loaded with spiral resonators", *IEEE Antennas and Wireless Propagation Letters*, vol. 10, pp. 768–771, July 2011.
- [47] "Item-level visibility in the pharmaceutical supply chain: a comparison of HF and UHF RFID technologies", white paper by Philips, TAGSYS, and Texas Instruments, available at <http://www.pharmaceuticalonline.com/doc/Item-Level-Visibility-In-The-Pharmaceutical-S-0002>.

- [48] D. Desmons, “UHF Gen 2 for item-level tagging”, presented at the *RFID World Meeting*, Dallas, Feb.-March 2006.
- [49] “UHF Gen 2 for Item-level Tagging”, Impinj RFID Technology series paper, available at http://www.impinj.com/files/MR_GP_ED_00003_ILT.pdf.
- [50] C. Ajluni, “Item-level RFID takes off”, *RF Design magazine*, Sept. 2006
- [51] P. Harrop, “Near field UHF vs. HF for item level tagging”, IDTechEx article, available at <http://202.71.128.164/download/>.
- [52] D. D. Uysal, J. P. Emond and D. W. Engels, “Evaluation of RFID performance for a pharmaceutical distribution chain: HF vs. UHF”, *IEEE International Conference on RFID*, pp. 27–34, April 2008.
- [53] P. V. Nikitin, K. V. S. Rao and S. Lazar, “An overview of near field UHF RFID”, *IEEE International Conference on RFID*, pp. 167–174, March 2007.
- [54] H. W. Liu, C. F. Yang, C. H. Weng, H. L. Kuo, K. H. Wu and Y. S. Lin, “An UHF reader antenna design for near-field RFID applications”, *IEEE Asia Pacific Microwave Conference (APMC)*, pp. 2394–2397, Dec. 2009.
- [55] W. Choi, J. S. Kim, J. H. Bae, G. Choi and J. S. Chae “Near-field antenna for a radio frequency identification shelf in the UHF band”, *IET Microwave Antennas and Propagation*, vol. 4, no. 10, pp. 1538–1542, Oct. 2010.
- [56] J. H. Cho, J. Kim, J. W. Kim, K. Lee, K. D. Aim and S. Kim, “An NFC transceiver with RF-powered RFID transponder mode”, *IEEE Asian Solid-State Circuits Conference, ASSCC'07*, pp. 172–175, Nov. 2007.
- [57] J. Choo, J. Ryoo, I. Park, J. Hong, K. Park and J. Lee, “A novel multi-loop tag for near field communication in UHF band”, *IEEE Asia-Pacific Microwave Conference Proceedings (APMC)*, pp. 1–4, Dec. 2007.
- [58] P. Iliev, P. Le-Thuc, R. Staraj and C. Luxey, “Near field/far field RFID tag antenna”, *IEEE Proceedings of the Fourth European Conference on Antennas and Propagation (EuCAP)*, pp. 1–4, April 2010.

- [59] M. Dhaouadi, M. Mabrouk and A. GhaZel, “Magnetic antenna for near-field UHF RFID tag”, *IEEE 18th International Conference on Microwave Radar and Wireless Communications (MIKON)*, pp. 1–2, June 2010.
- [60] M. Dhaouadi, M. Mabrouk, A. GhaZel and S. Tedjini, “Electromagnetic analysis of UHF near-field RFID tag antenna”, *IEEE XXXth URSI General Assembly and Scientific Symposium*, pp. 1–4, Aug. 2011.
- [61] P. K. Gentner, M. Wiessflecker, H. Arthaber, A. L. Scholtz and C. F. Mecklenbrauker, “Measured wideband near-field characteristics of an UWB RFID tag with on-chip antenna”, *IEEE International Conference on Ultra-Wideband (ICUWB)*, pp. 479–483, Sep. 2011.
- [62] J. Dong and X. Li, “UHF near-field tags design based on split ring resonator”, *IEEE Asia-Pacific Microwave Conference Proceedings (APMC)*, pp. 1794–1797, Dec. 2011.
- [63] X. Qing, C. K. Goh and Z. N. Chen, “Segmented loop antenna for UHF near-field RFID applications”, *Electronics Letters*, vol. 45, no. 17, 872–873, Aug. 2009.
- [64] H. W. Liu, K. H. Wu and C. F. Yang, “UHF reader loop antenna for near-field RFID applications”, *Electronics Letters*, vol. 46, no. 1, pp. 10–11, Jan. 2010.
- [65] X. Qing, Z. N. Chen and C. K. Goh, “UHF near-field RFID reader antenna with capacitive couplers”, *Electronics Letters*, vol. 46, no. 24, pp. 1591–1592, Nov. 2010.
- [66] X. Qing, C. K. Goh and Z. N. Chen, “A broadband UHF near-field RFID antenna”, *IEEE Transactions on Antennas and Propagation*, vol. 58, no. 12, pp. 3829–3838, Dec. 2010.
- [67] A. L. Borja, A. Belenguer, J. Cascon and J. R. Kelly, “A reconfigurable passive UHF reader loop antenna for near-field and far-field RFID applications”, *IEEE Antennas and Wireless Propagation Letters*, vol. 11, pp. 580–583, May 2012.
- [68] J. Shi, X. Qing, Z. N. Chen and C. K. Goh, “Electrically large dual-loop antenna for UHF near-field RFID reader”, *IEEE Transactions on Antennas*

and Propagation, vol. 61, no. 3, pp. 1019–1025, March 2013.

- [69] X. Li and Z. Yang, “Dual-printed-dipoles reader antenna for UHF near-field RFID applications”, *IEEE Antennas and Wireless Propagation Letters*, vol. 10, pp. 239–242, Feb. 2011.
- [70] J. W. Cao, Z. M. Xie and X. Z. Lai, “A compact near field UHF RFID reader antenna using SRR”, *IEEE International Conference on Machine Learning and Cybernetics (ICMLC)*, vol. 1, pp. 330–332, July 2011.
- [71] A. Ren, C. Wu, Y. Gao and Y. Yuan, “A robust UHF near-field RFID reader antenna”, *IEEE Transactions on Antennas and Propagation*, vol. 60, no. 4, pp. 1690–1697, April 2012.
- [72] G. V. Eleftheriades and K. G. Balmain, *Negative Refraction Metamaterials: Fundamental Principles and Applications*, Wiley, Hoboken, NJ, 2005.
- [73] N. Engheta and R. W. Ziolkowski, *Electromagnetic Metamaterials: Physics and Engineering Explorations*, Wiley, Hoboken, NJ, 2006.
- [74] C. Caloz and T. Itoh, *Electromagnetic Metamaterials: Transmission Line Theory and Microwave Applications: The Engineering Approach*, Wiley, Hoboken, NJ, 2006.
- [75] R. Marqués, F. Martín and M. Sorolla, *Metamaterials with Negative Parameters: Theory, Design and Microwave Applications*, Wiley, Hoboken, NJ, 2008.
- [76] A. K. Iyer and G. V. Eleftheriades, “Negative refractive index metamaterials supporting 2-D waves”, *IEEE International Symposium on Microwave Theory and Techniques*, pp. 1067–1070, Digest, Seattle, USA, June 2002,
- [77] A. A. Oliner, “A planar negative-refractive-index medium without resonant elements”, *CNCIUSNC URSI National Radio Science Meeting*, p. 41, San Antonio, USA, June 2002.
- [78] C. Caloz and T. Itoh, “Novel microwave devices and structures based on the transmission line approach of meta-materials”, *IEEE International Symposium on Microwave Theory and Techniques*, pp. 195–198, Digest,

Philadelphia, USA, June 2003.

- [79] F. Martín, F. Falcone, J. Bonache, R. Marqués and M. Sorolla, “Split ring resonator-based left handed coplanar waveguide”, *Appl. Phys. Lett.*, vol. 83, no. 22, pp. 4652–4654, Dec. 2003.
- [80] J. B. Pendry, A. J. Holden, D. J. Robbins and W. J. Stewart, “Magnetism from conductors and enhanced nonlinear phenomena”, *IEEE Trans. Microwave Theory Tech.*, vol. 47, no. 11, pp. 2075–2084, Nov. 1999.
- [81] R. Marqués, F. Medina and R. Rafii-El-Idrissi, “Role of bianisotropy in negative permeability and left-handed metamaterials”, *Phys. Rev. B*, vol. 65, pp. 144440 (1–6), 2002.
- [82] J. D. Baena, J. Bonache, F. Martín, R. Marqués Sillero, F. Falcone, T. Lopetegi, M. A. G. Laso, J. Garcia-Garcia, I. Gil, M. F. Portillo and M. Sorolla. “Equivalent-circuit models for split-ring resonators and complementary split-ring resonators coupled to planar transmission lines”, *IEEE Transactions on Microwave Theory and Techniques*, vol. 53, no. 4, pp. 1451–1461, April 2005.
- [83] F. Aznar, J. Bonache and F. Martin, “Improved circuit model for left-handed lines loaded with split ring resonators”, *Appl. Phys. Lett.*, vol. 92, no. 4, pp. 043512 (1–3), Feb. 2008.
- [84] A. Sanada, C. Caloz and T. Itoh, “Characteristics of the composite right/left-handed transmission lines”, *IEEE Microwave Wireless Comp. Lett.*, vol. 14, no. 2, pp. 68–70, Feb. 2004.
- [85] W. W. Hansen, “*Radiating Electromagnetic Waveguide*”, U.S., Patent 2.402.622, 1940.
- [86] T. Tamir, “*Leaky Wave Antennas*”, in *Antenna Theory*, R. E. Collin and F. J. Zucker, Eds. McGraw-Hill, NY, 1969.
- [87] A. Oliner, “*Leaky-Wave Antennas*”, in *Antenna Engineering Handbook*, R. C. Johnson, Ed. McGraw-Hill, NY, 1993.

- [88] D. R. Jackson, C. Caloz and T. Itoh, “Leaky-Wave Antennas”, *Proceedings of the IEEE* vol. 100, no. 7, pp. 2194–2206, July 2012.
- [89] A. Grbic, G. V. Eleftheriades, “Experimental verification of backward-wave radiation from a negative refractive index metamaterial”, *J. Appl. Phys.*, vol. 92, no. 10, pp. 5930–5935, Nov. 2002.
- [90] L. Liu, C. Caloz and T. Itoh, “Dominant mode leaky-wave antenna with backfire-to-endfire scanning capability”, *Electron. Lett.*, vol. 38, no. 23, pp. 1414–1416, Nov. 2002.
- [91] A. Grbic, and G. V. Eleftheriades, “Leaky CPW-based slot antenna arrays for millimeter-wave applications”, *IEEE Trans. Antennas Propag.*, vol. 50, no. 11, pp. 1494–1504, Nov. 2002.
- [92] I Arnedo, J. Illescas, M. Flores, M. A. G. Laso, F. Falcone, J. Bonache, J. García-García, F. Martín, J. A. Marcotegui, R. Marques and M. Sorolla, “Forward and backward leaky wave radiation in split-ring-resonator-based metamaterials”, *IET Microw. Antennas Propag.*, vol. 1, no. 1, pp. 65–68, Feb. 2007.
- [93] M. A. Antoniades and G. V. Eleftheriades, “A CPS leaky-wave antenna with reduced beam squinting using NRI-TL metamaterials”, *IEEE Trans. Antennas Propag.*, vol. 56, no. 3, pp. 708–721, March 2008.
- [94] S. Paulotto, P. Baccarelli, F. Frezza and D. R. Jackson, “Full-wave modal dispersion analysis and broadside optimization for a class of microstrip CRLH leaky-wave antennas”, *IEEE Trans. Microw. Theory Tech.*, vol. 56, no. 12, pp. 2826–2837, Dec. 2008.
- [95] R. Siragusa, E. Perret, P. Lemaitre-Auger, H. Van Nguyen, S. Tedjini and C. Caloz, “A tapered CRLH interdigital/stub leaky-wave antenna with minimized side-lobe levels”, *IEEE Microwave Wireless Comp. Lett.*, vol. 11, pp. 1214–1217, Oct. 2012.
- [96] O. Losito, M. Gallo, V. Dimiccoli, D. Barletta and M. Bozzetti, “A tapered design of a CRLH-TL leaky wave antenna”, *IEEE Proceedings of the 5th European Conference on Antennas and Propagation (EUCAP)*, pp. 357–360, April. 2011.

- [97] Y. Chi and F. Chen, “CRLH leaky-wave antenna based on ACPS technology with 180° horizontal plane scanning capability”, *Trans. Antennas Propag.*, vol. 61, no. 2, pp. 571–577, Feb. 2013.
- [98] C. Caloz and T. Itoh, “Array factor approach of leaky-wave antennas and application to 1-D/2-D composite right/left-handed (CRLH) structures”, *IEEE Microwave and Wireless Components Letters*, vol. 14, no. 6, pp. 274–276, June 2004.

CHAPTER 3

Single Resonant Passive Circuit Network for Conjugate Matching and Bandwidth Optimization

The purpose of this chapter is to obtain the passive circuit network required for tag bandwidth broadening, by introducing a single resonance with conjugate matching at the intermediate frequency of the UHF-RFID band⁴ [1]. Bandwidth optimization of the resulting network is validated by means of the Bode criterion, formulated in Section 2.2.4. According to this analysis, a global band UHF-RFID tag prototype is designed and fabricated.

⁴ The intermediate frequency of the UHF-RFID band has been chosen to be the central frequency of the USA band, $f_0 = 915$ MHz, throughout this chapter.

3.1 Circuit Network Analysis

Let us consider the schematic depicted in Fig. 3.1, where the load to be matched consists of a parallel combination of a capacitance C_c and a resistance R_c , effectively modelling an UHF-RFID chip. An eventual impedance matching network is inserted between the tag antenna and the load, to consider the most general case. Maximum power transfer between the antenna and the chip is achieved for conjugate matching, i.e., $Z_{chip} = Z_N^*$ (or $Y_{chip} = Y_N^*$), since this forces the power reflection coefficient [2],[3]

$$|S|^2 = \left| \frac{Z_{chip} - Z_N^*}{Z_{chip} + Z_N} \right|^2 = \left| \frac{Y_N^* - Y_{chip}}{Y_N + Y_{chip}} \right|^2 = \frac{(G_N - G_{chip})^2 + B^2}{(G_N + G_{chip})^2 + B^2} \quad (3.1)$$

to be zero. In (3.1), $Y_N = G_N + jB_N$, $Y_{chip} = G_{chip} + jB_{chip}$, and $B = B_N + B_{chip}$. Since the chip impedance depends on the input power applied to the chip, for the evaluation of the maximum read range, Z_{chip} must be considered at the threshold power.

Obviously, conjugate matching cannot be fulfilled in a broad band. Therefore, we choose the intermediate frequency of the UHF-RFID frequency span, f_0 , to force conjugate matching. This means that the conductances and susceptances must satisfy $G_N = G_{chip}$ and $B_N = -B_{chip}$, respectively, at f_0 . In order to minimize the power reflection coefficient in the vicinity of f_0 , B must be minimized and G_N must be constant and equal to G_{chip} . This result is inferred from the second-order Taylor expansion of the power reflection coefficient in the vicinity of f_0 :

$$\Delta |s(G_N, B)|^2 = \frac{(G_N - G_{chip})^2 + B^2}{4G_{chip}^2} \quad (3.2)$$

Then, the frequency derivative of the susceptance B

$$\frac{dB}{d\omega} = \frac{dB_N}{d\omega} + \frac{dB_{chip}}{d\omega} \quad (3.3)$$

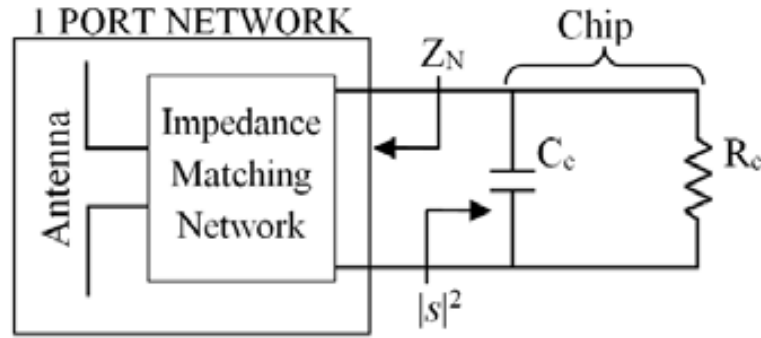


Fig. 3.1 Schematic of a typical UHF-RFID tag in the most general case. An impedance matching network is located in between the chip (modeled as a RC parallel load) and the tag antenna.

must be as small as possible. As it is mentioned in Section 2.2.3, UHF-RFID chips exhibit high-impedance phase-angle and small resistance within the UHF-RFID frequency range. Thus, it can be considered a low-loss one port network in which the energy loss per period is a small fraction of the stored energy. This can be expressed in terms of the quality factor of the chip equivalent-circuit model as $Q \gg 1$ [4],[5], which is well satisfied by the typical values of the RFID integrated circuits available in the market today [6]-[8]. It follows that a low-loss network (with impedance Z_N) cascaded to the chip, such that $Z_N^* = Z_{\text{chip}}$ (same Q) at the operating frequency f_0 , should be considered to minimize the power reflection coefficient around the tag resonance frequency. It was proven in [4] that the Foster's reactance theorem [9]-[11] is also valid for low-loss networks at frequencies far from the network resonance frequencies. From the Foster's theorem, both terms in the right hand side of (3.3) are positive; therefore, to minimize (3.3), it is necessary to reduce the slope of B_N , at f_0 and in the vicinity, as much as possible (notice that the second term is determined by the chip capacitance). In the case of a Foster network, it was demonstrated in [12] that the minimum frequency derivative of any negative susceptance corresponds to the value introduced by a simple inductor.

From the previous analysis, it follows the relevant conclusion that the maximum bandwidth achievable by a typical (single resonant) RFID tag, exhibiting conjugate matching at the central frequency of the UHF band, is obtained by cascading a parallel combination of a resistor (which provides a pure conductance G_N such that $G_N = G_{\text{chip}}$) and an inductor, with susceptance $B_N = -B_{\text{chip}}$ at f_0 , to the chip. This should be (ideally) the network describing the antenna or the antenna plus the matching network (see Fig. 3.1) for maximum bandwidth.

It is important to point out that a series combination of an inductor and a resistor cascaded to the chip, providing conjugate matching at f_0 , can be considered to achieve a bandwidth very close to the optimum. This is a direct consequence of the fact that a low-loss network is required for bandwidth optimization. In order to demonstrate it, let us consider a low-loss network formed by a series combination of a resistor with resistance R_s and an inductor with reactance χ_s ($Q \gg 1$, therefore $\chi_s \gg R_s$). The conductance G_N and susceptance B_N of such a network can be approximated by

$$G_N = \frac{R_s}{R_s^2 + \chi_s^2} \approx \frac{R_s}{\chi_s^2} \quad (3.4)$$

$$B_N = \frac{-\chi_s}{R_s^2 + \chi_s^2} \approx \frac{-1}{\chi_s} \quad (3.5)$$

Notice that B_N in (3.5) is approximated by the minimum achievable susceptance in a Foster network, obtained in the previous analysis. However, the conductance G_N in (3.4) is approximated by a frequency dependent function, rather than a constant value which is required for achieving maximum bandwidth, as mentioned before. A first-order Taylor expansion of G_N in the vicinity of f_0

$$G_N = G_{chip} \left(3 - 2 \frac{f}{f_0} \right) \quad (3.6)$$

shows that the maximum variation of G_N from the optimum value G_{chip} , that is evaluating (3.6) at the UHF-RFID frequency limits, leads to $G_N = 0.86G_{chip}$ at the maximum frequency (960 MHz) and $G_N = 1.13G_{chip}$ at the minimum frequency (840 MHz). From (3.2) it follows that a variation less than 0.005 in comparison with the optimum power reflection coefficient is expected at any frequency in the vicinity of f_0 .

3.2 Limitation of the –3 dB Bandwidth

By considering the required network for maximum bandwidth obtained in the previous section, the optimum –3 dB bandwidth (inferred by forcing (3.1) to be 1/2) is given by

$$\Delta f_{-3dB} \leq \frac{1}{\pi R_c C_c} \quad (3.7)$$

and $dB/d\omega = 2C_c$ at f_0 . Such upper limit depends only on the constituent elements of the lumped equivalent-circuit model of the chip. It is shown in **Table 3.1** the calculated value for the case of considering the UHF-RFID chips presented in **Table 2.4**. It can be appreciated that, in all cases, the upper limit for the -3 dB bandwidth is higher than the UHF-RFID frequency band (840-960 MHz), being in some cases more than twice higher. On the other hand, notice that a -3 dB level of the power reflection coefficient $|s|^2$ corresponds to the same value for the power transmission coefficient τ , since $\tau = (1 - |s|^2)$. It follows from (2.1) that such matching level involves a 30 % reduction of the peak read range obtained by considering conjugate matching between the chip and the antenna⁵. Thus, by considering an UHF tag with a peak read range of about 10 m⁶, the achieved read range at that frequency when $|s|^2 = -3$ dB is reduced to 7 m, which is an acceptable value for most UHF-RFID applications. Therefore, expression (3.7) gives valuable information for RFID designers in order to choose the best chip from those available.

For a real network, deviations from the ideal network (a parallel LR load) providing the optimum bandwidth are expected. Whereas for the ideal network $dB/d\omega = 2C_c$ at f_0 , in

Table 3.1 Upper limit for the -3 dB bandwidth for different UHF-RFID chips available in the market today

Chip	Δf_{-3dB}^{\max} (MHz)
Impinj Monza 4	160
Impinj Monza 5	208
Impinj Monza X-2K Dura	199
Alien Higgs 3	250
Alien Higgs 4	250
NXP UCODE G2XM/ G2XL	198

⁵ The tag read range, given by (2.1), is reduced about 30 %, with respect to the value obtained with perfect matching, by considering both the tag gain, G_r , and the minimum power threshold necessary to powers up the chip, P_{chip} , constant values within the -3 dB bandwidth.

⁶ Most of the UHF Gen 2 tags currently available in the market exhibit a peak read range around 10 m.

the case of considering a real network the frequency derivative of the susceptance B evaluated at f_0 can be expressed as⁷ $dB/d\omega = (k+1)C_c$, where $k \geq 1$ is a factor that indicates how much the susceptance seen by the chip deviates from the purely inductive behaviour ($k = 1$). By using the susceptance slope concept for real resonators [13],[14], expression (3.7) can be generalized as

$$\Delta f_{-3dB} = \frac{2}{\pi(k+1)R_c C_c} = \frac{2}{(k+1)} \Delta f_{-3dB}^{\max} \quad (3.8)$$

Expression (3.8) provides a useful formula for RFID designers which allows to predict the degradation of the -3 dB bandwidth, as compared to the maximum achievable bandwidth (given by (3.7)), i.e., the bandwidth that results by using the optimum network (a parallel LR network). Notice that k can be easily determined from the antenna input impedance at f_0 . Indeed, k is given by:

$$k = \frac{1}{C_c} \left. \frac{dB_N(\omega)}{d\omega} \right|_{\omega_0} \quad (3.9)$$

with $\omega_0 = 2\pi f_0$.

3.3 Design of a Broadband UHF-RFID Tag

The design of the complete system for tag bandwidth maximization is carried out in this section. Since the design of a global band tag is pursued, the central frequency of the operating band was chosen to be roughly the intermediate frequency of the UHF-RFID band ($f_0 = 915$ MHz).

⁷ It has been expressed the frequency derivative of the susceptance of a generic network, $dB_N/d\omega$, evaluated at the tag resonance frequency, f_0 , as a proportional value (being k the constant of proportionality) of the frequency derivative of the susceptance of the chip at f_0 , $dB_{\text{chip}}/d\omega = C_c$.

3.3.1 Equivalent-Circuit Model for Tag Bandwidth Optimization

Let us now consider a typical integrated circuit for the RFID tag (the *NXP UCODE G2XM* chip). The impedance reported by the manufacturer of this integrated circuit at the intermediate frequency is $Z_{\text{chip}}(f_0) = 16 - j148 \Omega$. As indicated in Section 2.2.3, the chip can be modeled by a parallel combination of a resistance R_c and a capacitance C_c . These values were calculated from the input impedance of the chip transformed to its equivalent RC parallel circuit, giving $R_c = 1385 \Omega$ and $C_c = 1.16 \text{ pF}$. The whole system for bandwidth optimization is depicted in Fig. 3.2. As it has been shown in Section 3.1, the low-loss one port network depicted in Fig. 3.1 should be replaced by a parallel combination of a resistor and an inductor, providing conjugate matching at f_0 . Since the required resonance frequency is $f_0 = (LC_c)^{-1/2}/2\pi$, the inductance value corresponding to the susceptance B_N was found to be $L = 26 \text{ nH}$.

The simulated power reflection coefficient of the circuit of Fig. 3.2 was obtained by using the *Agilent ADS* circuit simulator. Evaluation of (2.5) shows that the Bode area for the chip considered in this work is $2700 \text{ MHz}\cdot\text{dB}$, as indicated in Table 2.4. For comparison, a numerical simulation, based on the trapezoidal rule, in order to obtain the area for the reflection coefficient of the circuit depicted in Fig. 3.2, was carried out by using the *Matlab* commercial software. As it was expected from the analysis of Section 3.1, the value of that area is exactly the same than the upper limit determined by the Bode criterion. Thus, it has been demonstrated that the circuit of Fig. 3.2 gives the upper limit for the operating bandwidth by achieving conjugate matching at the intermediate frequency. Obviously, the bandwidth evaluated when the power reflection coefficient equals to -3 dB reaches the upper limit calculated from equation (3.7),

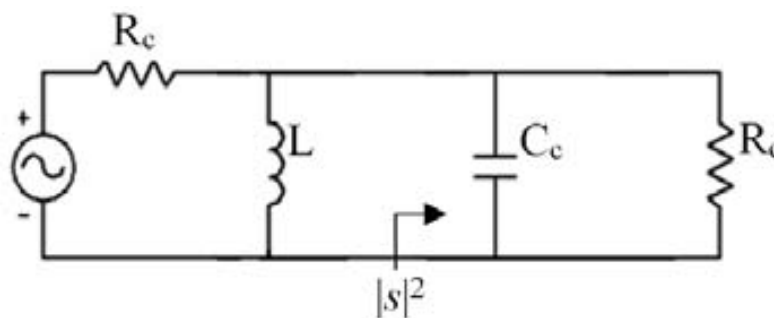


Fig. 3.2 Equivalent-circuit model of an UHF-RFID tag for bandwidth maximization and complex conjugate matching at the UHF-RFID intermediate frequency (915 MHz). For the RFID chip considered in this work, the value of the circuit parameters are $R_c = 1385 \Omega$, $C_c = 1.16 \text{ pF}$ and $L = 26 \text{ nH}$.

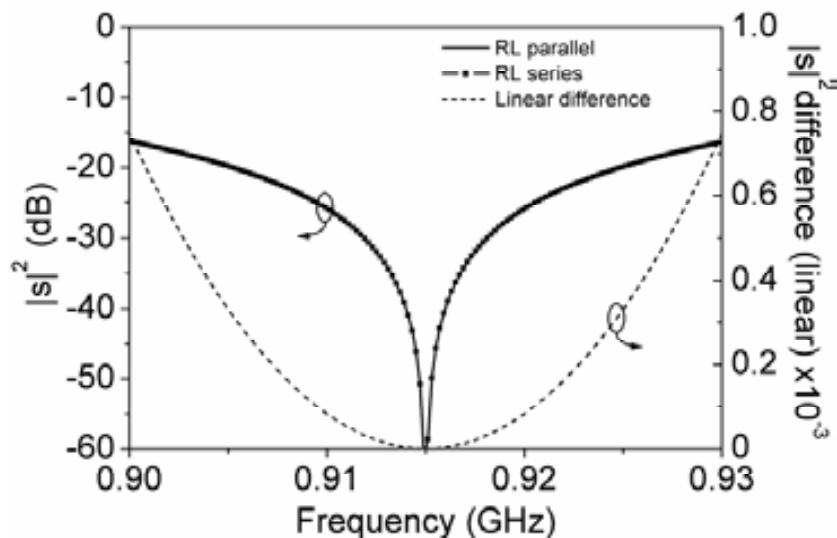


Fig. 3.3 Power reflection coefficient obtained from (3.2) in the case of considering a parallel and a series RL circuit cascaded to the *NXP UCODE G2XM* chip.

which corresponds to 198 MHz. On the other hand, as indicated in Section 3.1, a series combination of an inductor and a resistor cascaded to the chip, providing conjugate matching at f_0 , can be used to obtain roughly the optimum bandwidth. This can be observed in Fig. 3.3, where a plot of the power reflection coefficient in the vicinity of f_0 obtained from (3.2) is depicted, considering the cases of a parallel RL circuit (using $G_N = G_{\text{chip}}$) and a series RL circuit (using G_N given by equation (3.6)) cascaded to the chip. Notice that the difference expressed in linear between both coefficients is in the order of 10^{-3} .

3.3.2 Tag Antenna Design

Considering the previous requirements to achieve optimum bandwidth and conjugate matching at the operating frequency, a broadband RFID tag is designed in this section. In order to avoid the use of an external matching network, the tag antenna should have a lumped-element equivalent-circuit model based on the parallel RL circuit of Fig. 3.2, at the frequency range of interest. As it is well known, to obtain a purely inductive behavior by means of a planar semi-lumped element, physical dimensions must be much smaller than the wavelength, thus minimizing distributed effects. As it was mentioned in Section 2.2.5, there exists a tradeoff between antenna size miniaturization and maximum achievable gain and bandwidth. Thus, reducing the electrical size of the tag antenna (in order to accurately describe it by a parallel RL circuit) causes gain

degradation and, consequently, read range reduction. Taking it into account, the following design procedure was used to obtain the layout of the proposed tag antenna. A narrow open rectangular loop with 1 mm strip width, connected to the chip at the aperture (located at the center of one of the longer sides), was considered as a starting point. Such a loop, with an input impedance essentially inductive, cascaded to the chip provides an *RLC* shunt resonance. By varying the length (longer side) of the rectangular loop, the resonance frequency can be adjusted to the desired frequency, f_0 . Finally, the required antenna resistance is achieved by tailoring the length and width of the loop, in the opposite region to chip location (without modifying neither the width of the arms connected to the chip nor the dimensions of the slot created by the loop). By this means, a tag antenna directly matched to the chip, based on a folded dipole, has been designed on a commercial low loss microwave substrate, the *Rogers RO3010* substrate with dielectric constant $\epsilon_r = 10.2$ and thickness $h = 1.27$ mm. The proposed tag antenna, depicted in Fig. 3.4(a), is an asymmetric, coplanar strip, folded dipole. The dimensions of the tag antenna are roughly $0.27\lambda \times 0.02\lambda$, λ being the wavelength at 915 MHz. These small dimensions force the direction of the antenna current density to be different at both arms, as in the case of a conventional folded dipole working at the so called transmission line mode [15]-[18]. Although a conventional folded dipole is usually designed for working mainly at the antenna mode, where the current density direction is the same at both arms and consequently the radiation efficiency is typically higher, an asymmetrical design of the folded dipole can improve substantially the radiation efficiency achieved at the transmission line mode. Hence, the asymmetrical folded dipole radiates as a result of its unbalanced condition.

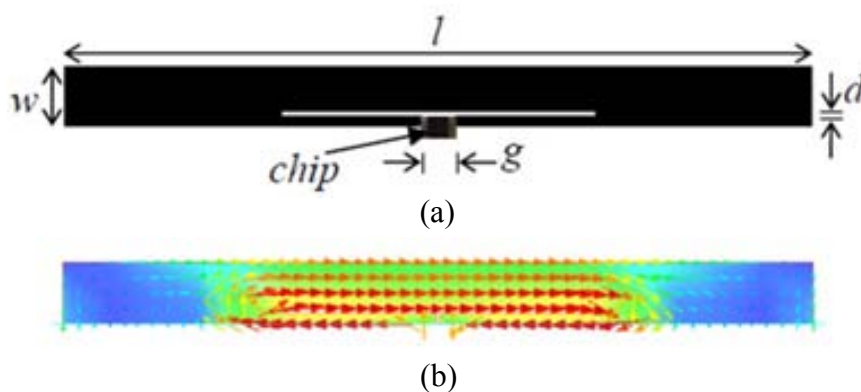


Fig. 3.4 (a) Layout of the proposed RFID tag antenna for bandwidth optimization and conjugate matching. The dimensions are $l = 90$ mm, $w = 7$ mm, $g = 4$ mm and $d = 0.5$ mm, and (b) current distribution of the proposed tag antenna at 915 MHz.

The power reflection coefficient of the presented RFID tag is depicted in Fig. 3.5(a). It can be seen that conjugate matching is achieved at the frequency of interest. Fig. 3.5(b) shows the input admittance of the tag antenna in comparison to the input admittance of the RL circuit of Fig. 3.2. Both results were obtained by using the *Agilent Momentum* commercial software. It can be seen that, at the UHF-RFID frequency range, the input admittance of the tag antenna can be approximated by the RL circuit required for bandwidth optimization and conjugate matching at f_0 . The area for the reflection coefficient of Fig. 3.5(a) has been calculated by using the trapezoidal approach used in Section 3.3.1. The value of this area for the lossy and lossless case was found to be more than 80% of the upper limit determined by the Bode criterion. The -3 dB bandwidth can be obtained through (3.8), where, inferred from (3.9), $k = 1.44$ for the lossless case and $k = 1.78$ for the lossy case, corresponding to 82% and 71%, respectively, of the upper limit of 198 MHz determined by (3.7). Then, the resulting theoretical bandwidths are 162 MHz in the lossless case and 142.5 MHz in the lossy case. These results were corroborated by obtaining the -3 dB bandwidths from electromagnetic simulation, giving 162 MHz (82% of the upper limit) and 144 MHz (73% of the upper limit) for the lossless and lossy case, respectively. The simulated gain reaches the value of 1 dB at the operating frequency and the radiation pattern is similar to that of a conventional $\lambda/2$ dipole.

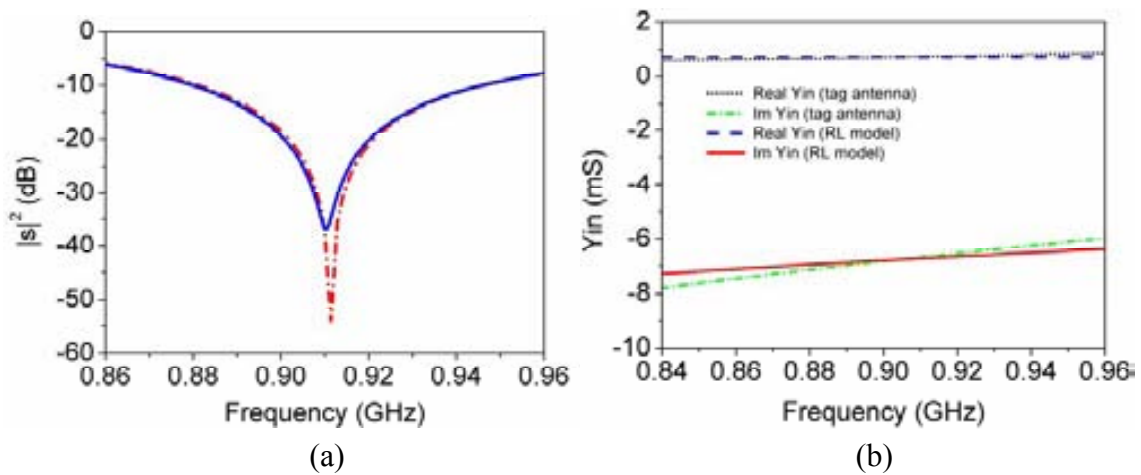


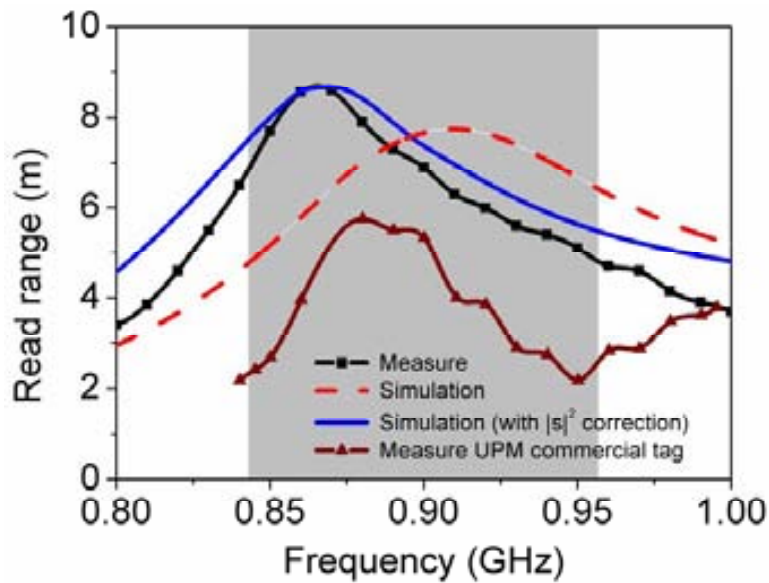
Fig. 3.5 (a) Power reflection coefficient for the lossless (red dashed line) and lossy case (blue solid line) of the proposed RFID tag and (b) input admittance of the proposed tag antenna compared with the input admittance of the RL circuit of Fig. 3.2.

3.4 Fabrication and Experimental Results

Firstly, it is important to highlight that the minimum power level necessary to activate the chip used in this work reported by the manufacturer is $P_{\text{chip}} = -15$ dBm. However, a measure of the sensitivity of this chip was carried out in [19] and [20], resulting in a frequency dependent value within the UHF-RFID frequency band. By taken this into account, and from electromagnetic and circuit co-simulation results, an evaluation of the theoretical read range was obtained and depicted in Fig. 3.6(b). The proposed RFID tag was fabricated and the read range was measured (see Fig. 3.6) through the procedure explained in Section 2.2.2. Very good performance through the entire UHF-RFID frequency band is achieved. The proposed tag exhibits a significant read range, higher than 5 m within the whole band (840-960 MHz) with roughly 9 m peak read range.



(a)



(b)

Fig. 3.6 (a) Photograph of the fabricated tag and (b) simulated and measured read range for the proposed RFID tag, considering $EIRP = 4$ W in the whole frequency band.

A 40 MHz frequency shift between the simulated and measured peak read range can be observed in Fig. 3.6(b). As explained in Section 2.2.4, the maximum read range of a typical RFID tag occurs at the frequency where conjugate matching between the chip and the antenna is achieved (see Fig. 2.15). Hence, the main cause of the shift in the measured read range is attributed to a frequency displacement of the power reflection coefficient $|s|^2$. This has been validated by obtaining the theoretical read range of the proposed structure by considering a 40 MHz frequency shift of the simulated $|s|^2$ towards lower frequencies (see Fig. 3.6b). Such shift can be due to a combination of different sources of error, such as variations in the imaginary part of the packaged chip impedance due to the flip-chip attachment process and to variations in ASIC assembly, which may cause changes in the chip impedance reported by the manufacturer [21]. Other reasons explaining this frequency shift are related to the accuracy of the electromagnetic simulators, and to tolerances in both geometrical and substrate parameters. Nevertheless, the measured read ranges of the proposed global band tag are very reasonable. A comparison of our fabricated tag with other commercially available tags only makes sense if the considered chips are identical. This is because the optimum bandwidth achievable by any tag depends on the chip impedance, as explained in Section 2.2.3, and the activation power is fundamental in determining the read range (see expression (2.1)). Hence, for comparison purposes, we include in Fig. 3.6(b) the measured read range of a wideband commercial tag (UPM Web) that uses identical chip to that of our proposed tag, as indicated in Table 2.5. Although the commercial tag has a higher area (50 mm x 30 mm), our tag exhibits much higher read range in the whole UHF-RFID band. From these results, it follows that the strategy for bandwidth optimization is efficient, and the specific designed tag is competitive.

3.5 Conclusions

In this chapter, bandwidth optimization in single resonant UHF-RFID tags has been considered. It has been demonstrated that, for a certain UHF-RFID chip that is modeled by a parallel RC circuit, the optimum network for bandwidth enhancement, providing conjugate matching, is simply a parallel combination of an inductor and a resistor cascaded to the chip. Bandwidth optimization has been validated by means of the Bode criterion, explained in Section 2.2.4. It has also been shown that a folded dipole antenna behaves as a parallel combination of an inductor and a resistor, and by designing this antenna to provide conjugate matching at f_0 , a bandwidth very close to the optimum value results. A formula that predicts the maximum achievable -3 dB bandwidth (i.e., the one that results by considering the ideal RL network with conjugate

matching) for a given UHF-RFID chip has been derived. It has also been inferred a generalized expression for the -3 dB bandwidth when any real network, corresponding to the antenna and matching network (if it is considered), is cascaded to the UHF-RFID chip.

According to this analysis, a broadband RFID tag prototype able to operate within the different worldwide regulated UHF-RFID bands has been designed and fabricated. The experimental results show a significant read range; over 5 m within the whole band (840-960 MHz) and almost 9 m peak read range. The area of the power reflection coefficient is more than 80% of the Bode area limit, and the corresponding -3 dB bandwidth is 73% of the upper limit for complex conjugate matching between the antenna and the chip at 915 MHz, which is in good agreement with the value (71% of the upper limit) predicted by using the proposed generalized expression for the -3 dB bandwidth. Thus, with the reported example, it is demonstrated that it is possible to evaluate if the designed tag is close to the maximum achievable bandwidth or if it still has some margin for improvement. Moreover, the proposed tag has been designed without using an external matching network, for cost and size reduction.

3.6 References

- [1] G. Zamora, F. Paredes, F. J. Herraiz-Martinez, and F. Martin and J. Bonache “On the bandwidth limitations of UHF-RFID tags”, *IET Microwaves Antennas and Propagation*. Accepted (May 2013).
- [2] K. Kurokawa, “Power waves and the scattering matrix”, *IEEE Trans. Microw. Theory Tech.*, vol. 13, no. 2, pp. 194–202, March 1965.
- [3] P. V. Nikitin, K. V. Seshagiri Rao, S. F. Lam, V. Pillai, R. Martinez, and H. Heinrich, “Power Reflection Coefficient Analysis for Complex Impedances in RFID Tag Design”, *IEEE Trans. Antennas and Propagation*, vol. 53, no. 9, pp. 2721–2725, Sep. 2005.
- [4] G. Nedlin, “Energy in lossless and low-loss networks, and Foster’s reactance theorem”, *IEEE Trans. Circuits Syst.*, vol. 36, no. 4, pp. 561–567, April 1989.
- [5] W. H. Boghosian, Comments on “Energy in lossless and low-loss networks, and Foster’s reactance theorem”, *IEEE Trans. Circuits Syst.*, vol. 36, no. 12,

pp. 1558, Dec. 1989.

- [6] Impinj RFID chips [Online]. Available at <http://www.impinj.com>.
- [7] Alien Technology RFID Ics [Online]. Available at <http://www.alientechnology.com>.
- [8] NXP UCODE smart label Ics [Online]. Available at www.nxp.com.
- [9] R. A. Foster, "A reactance theorem", *Bell Syst. Tech. J.*, vol. 3, pp. 259–267, 1924.
- [10] E. A. Guillemin, *Communication Networks*, vol. 2, Wiley, NY, 1935.
- [11] N. Balabanian and T. Bickart, *Linear Network Theory*, Chesterland, OH: Matrix, 1981.
- [12] G. Sisó, M. Gil, J. Bonache and F. Martin, "On the dispersion characteristics of metamaterial transmission lines", *J. Appl. Phys.*, vol. 102, no. 7, pp. 074911 (1–7), Oct. 2007.
- [13] G. L. Matthaei, L. Young and E. M. T Jones, *Microwave filters, impedance-matching networks and coupling structures*, Artech House Books, Dedham, Mass. 1980.
- [14] J. S. Hong and M. J. Lancaster, *Microstrip Filters for RF/Microwave Applications*. John Wiley, NY, 2001.
- [15] W. L. Weeks, *Antenna Engineering*, McGraw-Hill, NY, 1968.
- [16] H. Jasik, *Antenna Engineering Handbook*, McGraw-Hill, NY, 1961.
- [17] G. A. Thiele, E. P. Ekelman, and L. W. Henderson, "On the accuracy of the transmission line model of the folded dipole", *IEEE Trans. Antennas Propagation*, vol. 28, no. 5, pp. 700–703, Sep. 1980.

- [18] A. R. Clark and A. P. C. Fourie, “An improvement to the transmission line model of folded dipole”, *IEE Proc Microwave Antennas Propag*, Vol. 138, no. 6, 577–579, Dec. 1991.
- [19] P. V. Nikitin, K. V. Seshagiri Rao, “Effect of Gen2 protocol parameters on RFID tag performance”, *IEEE International Conference on RFID*, pp. 117–122, April 2009.
- [20] P. V. Nikitin, K. V. Seshagiri Rao, R. Martinez, S. F. Lam, “Sensitivity and Impedance Measurements of UHF-RFID Chips”, *IEEE Trans. Microw. Theory Tech.*, vol. 57, no. 5, pp. 1297–1302, May 2009.
- [21] K. V. Seshagiri Rao, P. V. Nikitin, and S. F. Lam, “Antenna design for UHF-RFID tags: a review and a practical application”, *IEEE Trans. Antennas and Propagation*, vol. 53, no. 12, pp. 3870–3876, Dec. 2005.

CHAPTER 4

Design and Synthesis Methodology for UHF-RFID Tags Based on the T- match Network

In this chapter, a new and very simple systematic method for the design and synthesis of global band UHF-RFID tags based on the T-match network is proposed [1]. Such method is based on the required equivalent-circuit network for bandwidth broadening in single resonant UHF tags with conjugate matching, obtained in Chapter 3. Moreover, the frequency limits related to the validity of the presented approach are studied, and the dependence of the achieved tag bandwidth with the antenna impedance is also discussed. To illustrate the potential of the approach, an RFID tag is designed and synthesized through this method and the read range of the fabricated prototype is measured.

4.1 Previous Equivalent-Circuit Models of T-match Based Tags

As indicated in Chapter 1, the T-match structure is the most common matching network used for the efficient matching of UHF-RFID tags. Since this network is electrically small at the UHF-RFID regulated bands (840-960 MHz), a lumped-element equivalent-

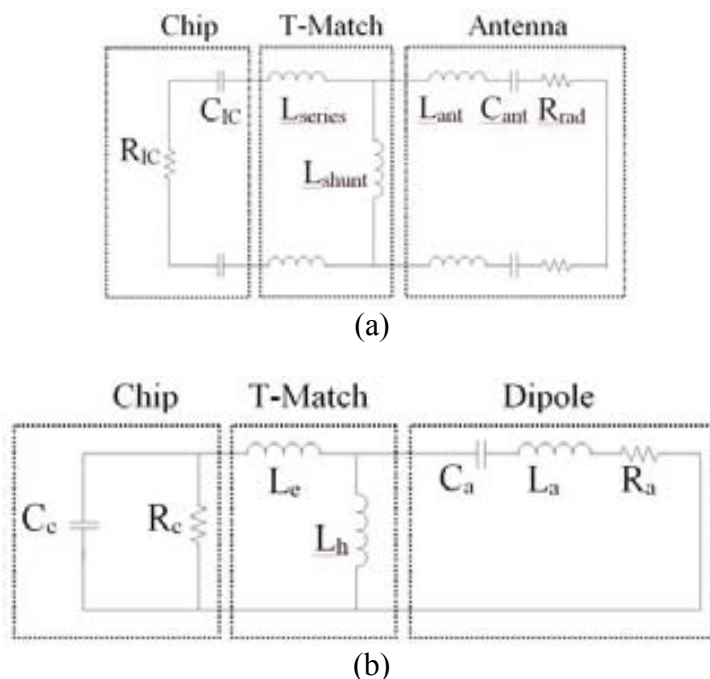


Fig. 4.1 (a) Balanced equivalent-circuit model of a T-match based UHF-RFID tag from [2], and (b) unbalanced equivalent-circuit model reported in [3].

circuit model for the T-match structure cascaded to a commercial RFID chip can be considered, which is of special interest for tag design. Some efforts to obtain an equivalent-circuit model for the T-match network cascaded to the chip can be found in the literature. In [2], the circuit diagram shown in Fig. 4.1(a) is proposed, whereas in [3] this balanced circuit is reduced to an unbalanced version, depicted in Fig. 4.1(b). Although this circuit is complete and reasonably accurate, the authors in [3] transformed the matching circuit from a series-shunt connection of L_e and L_h into a shunt-series connection with a scaled load impedance. This allows reformulating the tag antenna and matching circuit problem into a classical two stage bandpass filter. The main drawback of such approach is the difficulty to synthesize the tag antenna and matching circuit, once the circuit model is tuned. Moreover, the authors do not give details about how to synthesize the presented tags from the circuit model.

4.2 Proposed Circuit Approach and Requirements

Due to the symmetry of T-match based tags and the differential mode excitation, forced by the chip, the electric wall concept has been used in order to obtain a new equivalent-

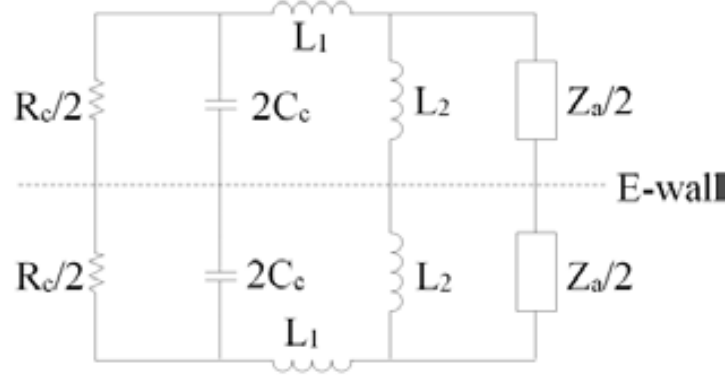


Fig. 4.2 Equivalent-circuit model of a T-match based UHF tag, using the electric wall concept.

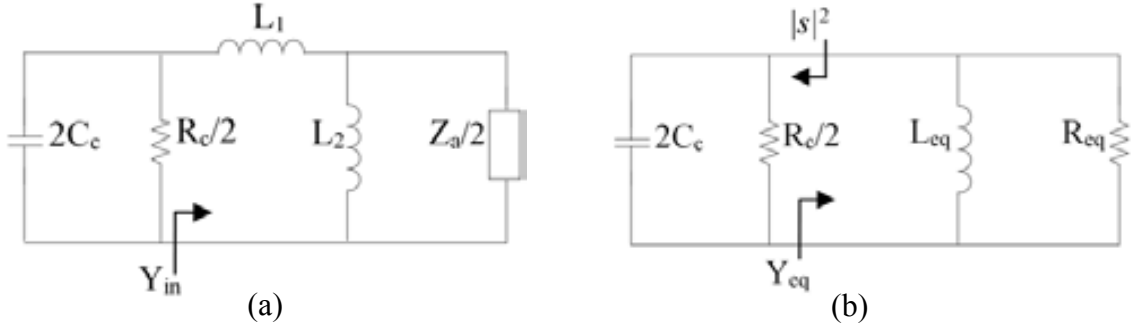


Fig. 4.3 (a) One half of the circuit of Fig. 4.2 and (b) transformed equivalent-circuit.

circuit model (see Fig. 4.2). The required values of the circuit elements can be obtained by considering only one-half of the network, as shown in Fig. 4.3(a). In this equivalent-circuit, the antenna impedance, $Z_a = R_a + j\chi_a$, is modeling any general impedance. It can be observed that the circuit cascaded between the chip and the antenna is an inductive transformer [4]. Thus, the circuit of Fig. 4.3(a) can be modeled by the equivalent-circuit depicted in Fig. 4.3(b). To demonstrate this, the admittances $Y_{in} = G_{in} + jB_{in}$ and $Y_{eq} = G_{eq} + jB_{eq}$, given by

$$G_{in} = \frac{2L_2^2 R_a}{|Z_a|^2 (L_1 + L_2)^2 + 4\omega^2 L_1^2 L_2^2 + 4\omega\chi_a L_1 L_2 (L_1 + L_2)} \quad (4.1)$$

$$B_{in} = \frac{-\left[|Z_a|^2 (L_1 + L_2) + 4\omega^2 L_2^2 L_1 + 2\omega\chi_a (L_2^2 + 2L_1 L_2)\right]}{\omega \left[|Z_a|^2 (L_1 + L_2)^2 + 4\omega^2 L_1^2 L_2^2 + 4\omega\chi_a L_1 L_2 (L_1 + L_2)\right]} \quad (4.2)$$

$$Y_{eq} = G_{eq} + jB_{eq} = \frac{1}{R_{eq}} - j\frac{1}{\omega L_{eq}} \quad (4.3)$$

are forced to be equal. Comparing the real part one obtains:

$$R_{eq} = \frac{|Z_a|^2 (L_1 + L_2)^2 + 4\omega^2 L_1^2 L_2^2 + 4\omega\chi_a L_1 L_2 (L_1 + L_2)}{2L_2^2 R_a} \quad (4.4)$$

If $|Z_a|^2 (L_1 + L_2)^2 \gg |4\omega^2 L_1^2 L_2^2 + 4\omega\chi_a L_1 L_2 (L_1 + L_2)|$ is satisfied, then expression (4.4) can be approximated by

$$R_{eq} = \left(1 + \frac{L_1}{L_2}\right)^2 \left(\frac{R_a^2 + \chi_a^2}{2R_a}\right) = \frac{n^2}{2G_a} \quad (4.5)$$

where $n = 1 + (L_1/L_2)$ and $G_a = R_a / (R_a^2 + \chi_a^2)$ is the antenna conductance. The imaginary parts of the admittances lead to:

$$L_{eq} = \frac{|Z_a|^2 (L_1 + L_2)^2 + 4\omega^2 L_1^2 L_2^2 + 4\omega\chi_a L_1 L_2 (L_1 + L_2)}{|Z_a|^2 (L_1 + L_2) + 4\omega^2 L_2^2 L_1 + 2\omega\chi_a (L_2^2 + 2L_1 L_2)} \quad (4.6)$$

which can be approximated by:

$$L_{eq} = L_1 + L_2 \quad (4.7)$$

provided $|Z_a|^2 (L_1 + L_2)^2 \gg |4\omega^2 L_1^2 L_2^2 + 4\omega\chi_a L_1 L_2 (L_1 + L_2)|$ and $|Z_a|^2 (L_1 + L_2) \gg |4\omega^2 L_2^2 L_1 + 2\omega\chi_a (L_2^2 + 2L_1 L_2)|$ (notice that the first condition is the same than the one required for expression (4.5)). It can be demonstrated through simple algebra that these two inequalities are satisfied if

$$\frac{|Z_a|}{2} \gg |Z_{L_2}| \quad (4.8)$$

$$|\chi_a| \leq |Z_{L_2}| \frac{L_1 + L_2}{\max\left\{L_1, \frac{L_2}{2}\right\}} \quad (4.9)$$

where $|Z_{L_2}| = \omega L_2$. Hence, the circuit of Fig. 4.3(a) can be approximated by the circuit of Fig. 4.3(b), where R_{eq} and L_{eq} are obtained from (4.5) and (4.7), respectively, as long as conditions (4.8) and (4.9) are satisfied.

4.3 Design and Synthesis of T-match Based Tags

A systematic methodology for the design and synthesis of a global band T-match based tag is presented in this section. Let us consider the circuit of Fig. 4.3(b), assuming that conditions (4.8) and (4.9) are well satisfied, as a model for T-match based tags. The central frequency of the operating band is chosen to be the intermediate frequency of the UHF-RFID band, $f_0 = 898 \text{ MHz}$ ⁸. Then, R_{eq} in (4.5) must be equal to $R_c/2$ and L_{eq} in (4.7) must be equal to $1/(2\omega_0^2 C_c)$, where $\omega_0 = 2\pi f_0$, to achieve complex conjugate matching at f_0 . It is clear that, for a given chip and Z_a , the inductances L_1 and L_2 can be easily calculated from (4.5) and (4.7). However, in spite of the possibility of satisfying conditions (4.8) and (4.9) by means of an antenna with a complex impedance, resonant antennas designed at f_0 are very good candidates for using the proposed circuit approach. This is because, regardless of the considered chip, condition (4.9) will be easily satisfied in the vicinity of the antenna resonance frequency since χ_a approaches zero. Therefore, the proposed equivalent-circuit model will predict the frequency response of the designed tag in a wider bandwidth when a resonant antenna is considered.

Let us now consider the particular case of using a resonant tag antenna designed to exhibit a purely resistive impedance R_a at f_0 . It is important to point out that even if

⁸ In this chapter, the intermediate frequency of the UHF-RFID band has been chosen to be the geometric average between the frequency limits of this band ($f_0 = 898 \text{ MHz}$). Notice that the criterion is different in chapter 3.

conditions (4.8) and (4.9) are very well satisfied, a frequency shift of the tag resonance is expected since R_{eq} and L_{eq} are exactly determined by (4.4) and (4.6) rather than (4.5) and (4.7), respectively. However, this shift can be avoided by taking it into account in the T-match design stage. Let us see how it is possible to correct this frequency displacement by means of an analysis of the power reflection coefficient of Fig. 4.3(b), given by [5],[6]

$$|s|^2 = \left| \frac{Y_{eq}^* - 2Y_{chip}}{Y_{eq} + 2Y_{chip}} \right|^2 = \frac{(G_{eq} - 2G_c)^2 + B^2}{(G_{eq} + 2G_c)^2 + B^2} \quad (4.10)$$

where Y_{chip} is the chip admittance, $G_{chip} = 1/R_c$, $G_{eq} = 1/R_{eq}$ and $B = B_{eq} + 2B_{chip}$ is the total susceptance of the circuit given by the sum of the susceptance of L_{eq} and two times the susceptance of the chip. Let us assume a constant resistive value for the antenna impedance such that $Z_a = R_a \leq R_c$ in the circuit of Fig. 4.3(a), in order to be transformed to the circuit of Fig. 4.3(b), where R_{eq} and L_{eq} are given by (4.4) and (4.6), respectively. By using (4.6), it can be demonstrated (see Appendix A) that the susceptance B vanishes at a frequency $\omega \geq \omega_0$, since $L_{eq} \leq L_1 + L_2 = 1/(2\omega_0^2 C_c)$. This corresponds to a frequency shift of the tag resonance, $\Delta\omega = 2\pi\Delta f$, towards higher frequencies, which depends only upon the antenna resistance, for a given chip (see Appendix A). Such shift is depicted in Fig. 4.4 in the case of considering four different commercial chips [7]-[9].

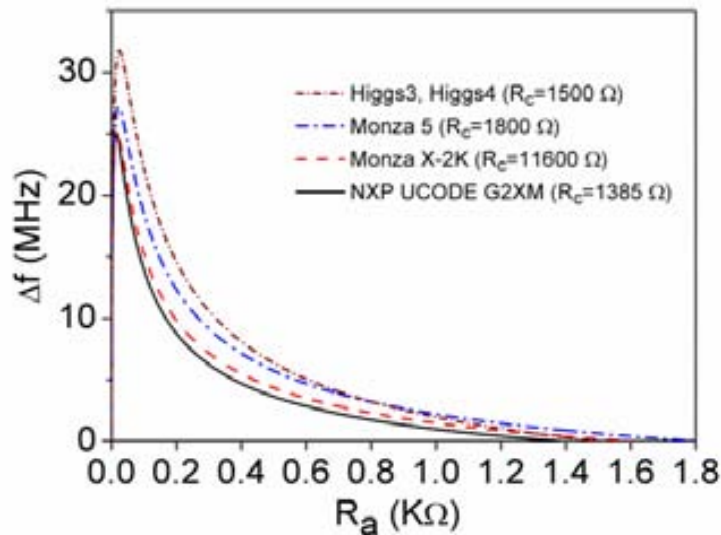


Fig. 4.4 Frequency increment of the tag resonance (with respect to f_0) as a function of the antenna resistance, R_a , in the case of considering four different commercial chips.

It can be seen that Δf decreases as R_a approaches the chip resistance, R_c , and becomes higher as R_a moves away (decreasing) from R_c . Moreover, a reduction of the matching level (with respect to conjugate matching) will take place at this frequency, as long as R_a differs from R_c . From (4.4) it follows that the exact expression for G_{eq} evaluated at the tag resonance

$$G_{eq} = \frac{2R_a\omega_0^4C_c^2}{R_aR_c\omega_0^4C_c^2 + (\omega_0 + \Delta\omega)^2 \left(1 - \sqrt{\frac{R_a}{R_c}}\right)^2} \quad (4.11)$$

is always less than or equal to $2G_{chip}$, and becomes lower as R_a moves away (decreasing) from R_c . Then, by evaluating (4.10) at the tag resonance ($B = 0$), and introducing (4.11) into this expression, this matching level reduction can be inferred.

Let us now consider any general complex antenna impedance $Z_a = R_a + j\chi_a$, designed to exhibit a real impedance value at $f_0 + \Delta f$ (being Δf the shift related to this real impedance value). Obviously, the same power reflection coefficient as in the previous case (where a constant antenna impedance value was considered) is achieved at $f_0 + \Delta f$, since $B = 0$ and G_{eq} is given by (4.11) at this frequency. Furthermore, it can be demonstrated from (4.10) that the minimum power reflection coefficient occurs roughly at that frequency when $B = 0$, even in the case of considering G_{eq} as a frequency dependent function, provided G_{eq} is close to $2G_{chip}$ at that frequency (see Appendix B). Notice that if conditions (4.8) and (4.9) are satisfied, R_{eq} is approximately given by (4.5) and, therefore, $G_{eq} \approx 2G_{chip}$ at the antenna resonance frequency, namely, $f_0 + \Delta f$. This can also be seen from equation (4.11), since G_{eq} approaches $2G_{chip}$ as R_a goes near R_c . Thus, by forcing equation (4.5) to be $R_c/2$ at the antenna resonance frequency, $f_0 + \Delta f$, and $L_{eq} = 1/(2\omega_0^2C_c)$ in (4.7), the tag resonance will be located at $f_0 + \Delta f$, and the matching level at this frequency can be approximately inferred by introducing (4.11) into (4.10) and forcing $B = 0$ and $R_a = Z_a(f_0 + \Delta f)$.

4.3.1 Design of a T-match Based Tag using a Resonant Antenna

From the above analysis, it can be concluded that the proposed method should be applied by means of a resonant antenna designed at f_0 and the T-match network designed by forcing $R_{eq} = R_c/2$ at f_0 in (4.5) and $L_{eq} = 1/(2(\omega_0 - \Delta\omega)^2C_c)$ in (4.7), in order to obtain the tag resonance at the desired frequency, f_0 (notice that a linear

approximation of Δf with respect to f_0 has been considered, since $\Delta f \ll f_0$). The shift Δf is obtained from that curve corresponding to a given chip (see Fig. 4.4), evaluated at $R_a = Z_a(f_0)$. Then, from (4.5), the factor n can be rewritten in terms of the chip resistance, R_c , and the antenna resistance evaluated at f_0 , $R_a(f_0)$, given $n = 1 + (L_1/L_2) = (R_c/R_a(f_0))^{1/2}$. Thus, the inductances L_1 and L_2 can be calculated from (4.5) and (4.7) and are obtained as

$$L_1 = \frac{1}{2(\omega_0 - \Delta\omega)^2 C_c} \left(1 - \frac{1}{n}\right) \quad (4.12)$$

$$L_2 = \frac{1}{2n(\omega_0 - \Delta\omega)^2 C_c} \quad (4.13)$$

Then, the required conditions (4.8) and (4.9) lead to

$$|Z_a| \gg \frac{1}{n\omega_0 C_c} \quad (4.14)$$

$$|\chi_a| \leq \begin{cases} \frac{1}{\omega_0 C_c} & \text{if } 1 \leq n \leq \frac{3}{2} \\ \frac{1}{2\omega_0 C_c (n-1)} & \text{if } n > \frac{3}{2} \end{cases} \quad (4.15)$$

where, it has been considered $\omega \approx \omega_0$ and $(\omega_0 - \Delta\omega) \approx \omega_0$, since variations of ω relative to ω_0 are less than 7% within the whole UHF-RFID band and $\Delta\omega \ll \omega_0$. Notice that condition (4.15) does not play any role to achieve complex conjugate matching at f_0 , since $\chi_a = 0$ at this frequency (this condition will be used in Section 4.3.3 to discuss the frequency range of validity of the proposed circuit approach). However, expression (4.14) lead to a simple condition, in which the required antenna resistance $R_a(f_0)$ depends only upon the RFID chip and the intermediate frequency as $R_a(f_0) \gg 1/(\omega_0^2 C_c^2 R_c)$. Therefore, the greater the value of $R_a(f_0)$, the better satisfied the required condition. However, since R_{eq} is forced to be $R_c/2$ at f_0 , as indicated before, it follows from (4.5) that $R_a(f_0)$ must be less than or equal to R_c . Hence, it can be

concluded that the presented approach is valid at the intermediate frequency, if the antenna resistance accomplishes

$$\frac{1}{\omega_0^2 C_c^2 R_c} \ll R_a(f_0) \leq R_c \quad (4.16)$$

Notice that condition (4.16) forces $(R_c C_c)^2 \gg 1/\omega_0^2$, which is well satisfied by the typical values of the RFID integrated circuits available in the market today, such as Impinj Monza 5, Impinj Monza X-2K Dura, Alien Higgs 3, Alien Higgs 4 and NXP UCODE G2XM [7]-[9].

4.3.2 Tag Bandwidth Related to the Antenna Impedance

Let us now demonstrate that a degradation of the maximum achievable tag bandwidth, by means of the proposed equivalent-circuit approach and considering conjugate matching at f_0 , will be mainly determined by the derivative of the antenna resistance at f_0 . It was demonstrated in [10] that the optimum equivalent-circuit network necessary for bandwidth broadening in single resonant UHF-RFID tags with conjugate matching is a parallel combination of an inductor and a resistor cascaded to the chip, according to the Bode's limit [11],[12]. However, the proposed circuit approach consists of a parallel combination of an inductor and a frequency dependent resistor, cascaded to the chip. Hence, bandwidth degradation with respect to the optimum will be obtained as long as the conductance G_{eq} differs from $2G_{chip}$. In a first order approximation, this reduction of the tag bandwidth is determined by the frequency derivative of the antenna resistance at f_0 , and it does not depend on the frequency derivative of the antenna reactance χ_a , since this term is cancelled (see Appendix C). This result is deduced from the first-order Taylor expansion of the conductance G_{eq} , obtained from (4.5), in the vicinity of f_0 :

$$G_{eq} = 2G_{chip} \left(1 - \frac{R_a'(f_0)}{R_a(f_0)} (f - f_0) \right) \quad (4.17)$$

where $R_a'(f_0)$ is the frequency derivative of the antenna resistance evaluated at f_0 . Notice that, for a given value of $R_a(f_0)$, the further $R_a'(f_0)$ is from zero, the further G_{eq} is from $2G_{chip}$, and consequently a higher degradation of the tag bandwidth will be obtained. By introducing (4.17) into (4.10) and expanding the susceptance $B = B_{eq} + 2B_{chip}$ (using

$L_{eq} = 1/(2\omega_0^2 C_c)$, the approximated bandwidth at a fixed value for the power reflection coefficient can be inferred, within the frequency range of validity of the proposed circuit approach.

4.3.3 Frequency Range of Validity of the Proposed Approach

Let us now focus on the validity of the presented approach beyond the tag resonance frequency. As it has been pointed out, a T-match based tag designed following the steps indicated in Section 4.3.1 will exhibit a frequency response centered at the desired frequency f_0 . Therefore, such response will be similar to that of the proposed equivalent-circuit of Fig. 4.3(b), using (4.5) and (4.7) and designing the T-match network at f_0 . It follows that, in order to determine the frequency range of validity of the proposed approach, a comparison between these two frequency responses makes sense. Then, assuming that the tag antenna satisfies the required condition at the resonance frequency (see expression (4.16)), an examination of condition (4.14) reveals that it will be satisfied within the whole UHF-RFID band provided $|Z_a| \geq R_a(f_0)$. It can be easily demonstrated that this condition holds true in the case of considering a canonic *RLC* series load as antenna impedance. Thus, in this particular case, condition (4.14) is accomplished in all frequencies and, consequently, the frequency limits around the tag resonance from which the proposed approach no longer predicts the frequency response of the designed tag are determined by (4.15). Therefore, in order to satisfy such condition within the entire UHF-RFID band, the frequency derivative of χ_a must be small. Conversely, if we consider the antenna impedance modeled by an *RLC* shunt load around the resonance frequency, it can be demonstrated that $|Z_a| \leq R_a(f_0)$ and, therefore, both expressions (4.14) and (4.15) must be taken into account in order to obtain the frequency limits from which the proposed approach becomes invalid. The same conclusion can be applied when any general frequency dependent complex antenna impedance is considered. Thus, in such cases, both the frequency derivatives of χ_a and R_a should be small to enhance the frequency range of validity.

4.3.4 Synthesis of a T-match Based Tag using a Resonant Antenna

A simple method for the synthesis of T-match based tags using a resonant antenna is proposed in this section. In order to synthesize the T-match network, we start by considering a closed loop consisting of a narrow conductor strip (e.g. 0.2 mm width)

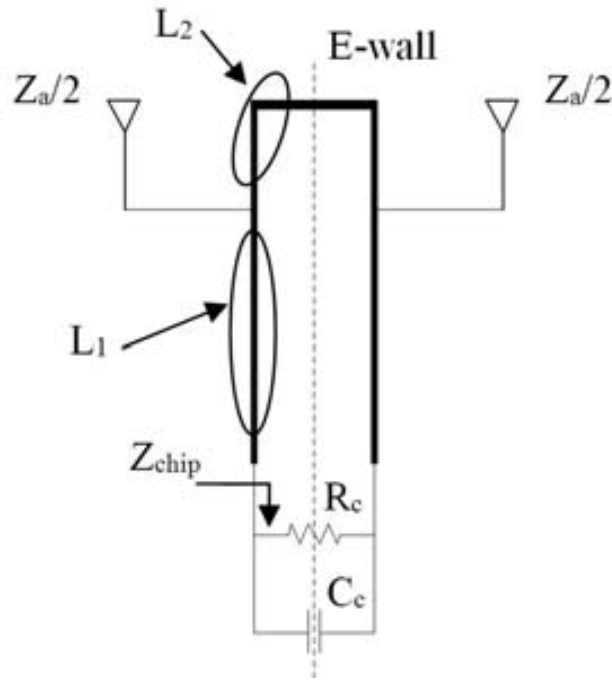


Fig. 4.5 Model of an UHF-RFID T-match based tag.

connected to a differential port with impedance Z_{chip} , as depicted in Fig. 4.5. This loop exhibits an inductive behavior at the UHF-RFID frequency band. To achieve the required dimensions for the loop inductance, a sweep of the length of the loop is carried out by means of electromagnetic simulations (by using the *Agilent Momentum* commercial software), until the resonance frequency appears at $f_0 - \Delta f$. Then, the inductance corresponding to one half of the loop must be divided into L_1 and L_2 by connecting the antenna at the adequate position (see Fig. 4.5). To this end, a sweep of the position of the antenna connection is carried out to achieve the calculated values for these inductances. The final position is obtained when the tag resonance reaches the desired frequency f_0 .

4.4 Design of a Broadband UHF-RFID Tag using the Proposed Method

Let us now consider a typical integrated circuit for the RFID tag (the NXP UCODE G2XM chip). As indicated in Chapter 1, the chip can be modeled by a parallel combination of a resistance $R_c = 1385 \Omega$ and a capacitance $C_c = 1.16 \text{ pF}$. From (4.16) it follows that $17 \Omega \ll R_a(f_0) \leq 1385 \Omega$. Thus, the tag antenna has to be designed to exhibit an antenna resistance at the operating frequency according to (4.16). As a proof

of concept for the presented method, an antenna for tag implementation has been designed on a commercial low loss microwave substrate, the *Rogers RO3010* substrate with dielectric constant $\epsilon_r = 10.2$ and thickness $h = 0.254$ mm. As it was pointed out in Section 4.3, the use of a resonant antenna is appropriate to ensure the validity of the presented approach around the operating frequency f_0 . The proposed antenna is a meandered coplanar strip, folded dipole working at the so called antenna mode [13]-[16]. and exhibits a purely resistive impedance at the intermediate frequency, $R_a(f_0) = 220 \Omega$ (see Fig. 4.6). Then, in order to design the T-match network at the correct frequency, $f_0 - \Delta f$, the frequency shift Δf was inferred by using expression

(A.4), from Appendix A, and it was found to be 8 MHz. This result perfectly agrees with the shift obtained in Fig. 4.7, where a simulation (by means of the *Agilent ADS* circuit simulator) of the power reflection coefficient of the circuit of Fig. 4.3(b), using (4.5) and (4.7) and designing the T-match network at f_0 , with a sweep of the antenna impedance $Z_a = R_a$ from 20Ω to 1385Ω , is depicted. As expected in this analysis, perfect conjugate matching at the desired frequency f_0 is achieved when $R_a = R_c$ and, consequently, $L_1 = 0$ and $L_2 = 1/(2\omega_0^2 C_c)$. This is because in this case, approximation (4.7) becomes an exact expression for L_{eq} and $G_{eq} = 2G_{chip}$. As it was previously predicted, a frequency shift of the tag resonance from f_0 towards higher frequencies and a reduction of the matching level at this frequency are observed as R_a decreases from R_c . It can be seen in Fig. 4.7 that such frequency shift and matching level reduction at the resonance frequency become more significant as the value of R_a moves away from R_c . Thus, the T-match network was designed at 890 MHz, which corresponds to 8 MHz below f_0 . From (4.12) and (4.13), the elements of the T-match network were found to be $L_1 = 8.3$ nH and $L_2 = 5.5$ nH. Then, the synthesis method explained in Section 4.3.4

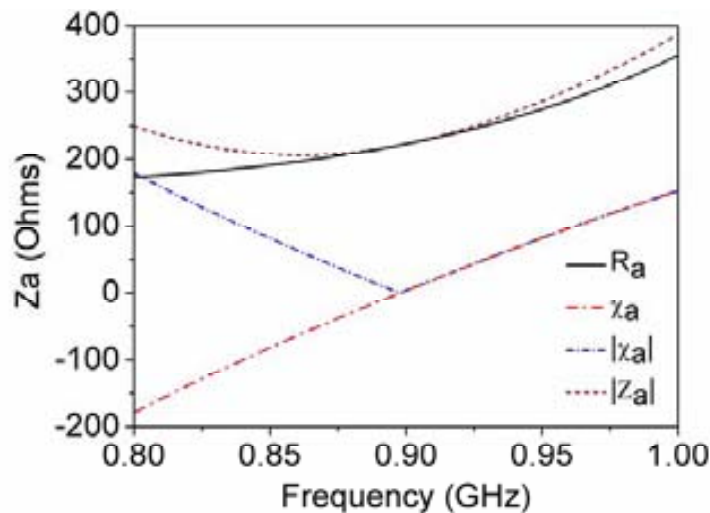


Fig. 4.6 Input impedance of the designed tag antenna.

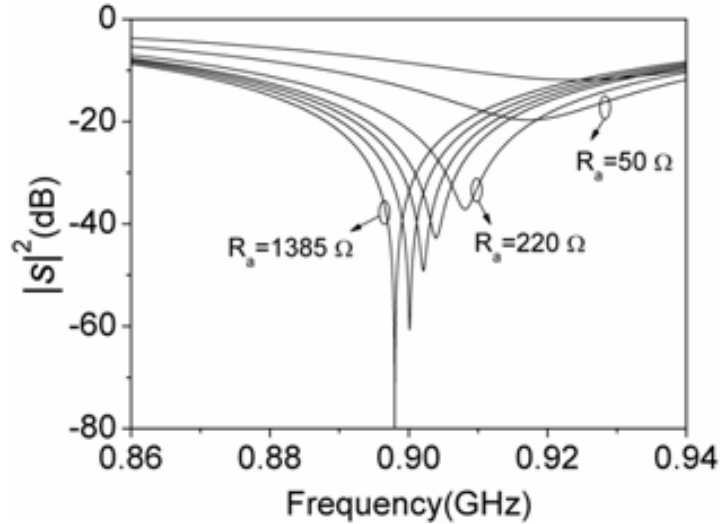


Fig. 4.7 Simulated power reflection coefficient of the circuit of Fig. 4.3(a), by sweeping the antenna impedance Z_a from 20Ω to 1385Ω .

was applied. The layout of the designed tag is depicted in Fig. 4.8(a). The dimensions are $l = 120 \text{ mm}$, $w = 30 \text{ mm}$, $g = 4.9 \text{ mm}$, $c = 8.7 \text{ mm}$, $d_1 = 12 \text{ mm}$, $d_2 = 9 \text{ mm}$ and $d_3 = 9 \text{ mm}$. All the strips of the antenna have the samewidth (3 mm) and the width of the T-match network is 0.2 mm. The total length of the T-match closed loop was found to be 30 mm, and the tag antenna was connected to the loop at a distance of 10.2 mm from the chip.

The power reflection coefficient of the designed RFID tag is depicted in Fig. 4.8(b). It can be seen that conjugate matching is achieved at the intermediate frequency f_0 of the UHF-RFID frequency band. Very good agreement is observed between the power reflection coefficient obtained from the equivalent-circuit approach and the electromagnetic simulation within the entire UHF-RFID band, except in the low frequency region. Although the tag antenna exhibits purely resistive impedance at the resonance frequency f_0 , the antenna resistance is not constant with frequency, as it is shown in Fig. 4.6. Hence, both conditions (4.14) and (4.15) must be examined to discuss the validity of the approach applied in this work within the UHF-RFID band, as it was mentioned in Section 4.3.3. For the considered chip and antenna impedance we obtain $|Z_a| \gg 61 \Omega$ and $|\chi_a| \leq 51 \Omega$. Thus, the condition for the antenna reactance is satisfied between 867 MHz and 930 MHz. However, although the condition for the absolute value of the antenna impedance is well satisfied at frequencies higher than f_0 and in the vicinity, there is a frequency region within the low UHF-RFID band where such condition is less satisfied. Therefore, good agreement is expected between the power reflection coefficients of the equivalent-circuit approach and the electromagnetic

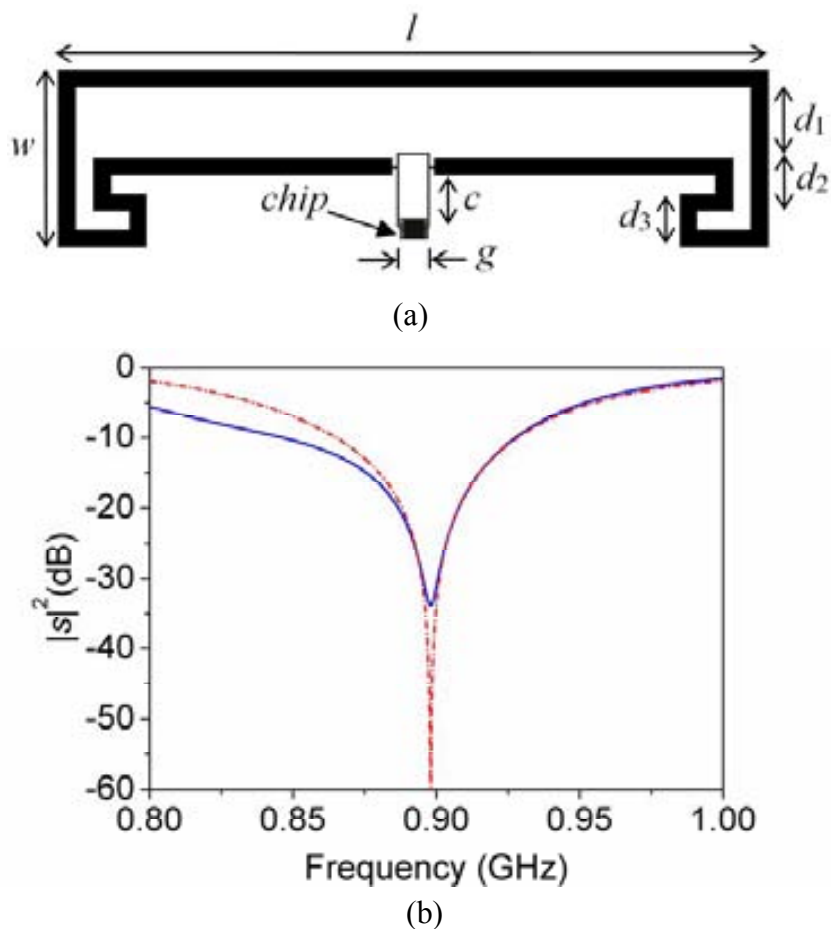


Fig. 4.8 (a) Layout of the designed T-match based tag. (b) Electrical simulation of the return loss of the proposed equivalent-circuit (red dashed line) and electromagnetic simulation of the return loss of the designed tag (blue solid line).

response of the designed tag within the whole UHF-RFID band except in the low frequency region.

As indicated in Section 4.3.2, by introducing (4.17) into (4.10), the approximated bandwidth at a fixed value for the power reflection coefficient can be predicted, within the frequency range of validity of the proposed circuit approach. Thus, the -15 dB bandwidth was found to be 35 MHz, which is similar to the obtained by means of the electromagnetic simulation of the designed tag (39 MHz). The simulated gain reaches the value of 1.4 dB at the operating frequency and the radiation pattern is similar to that of a conventional $\lambda/2$ dipole in the whole UHF-RFID band, as it is shown in Fig. 4.9.

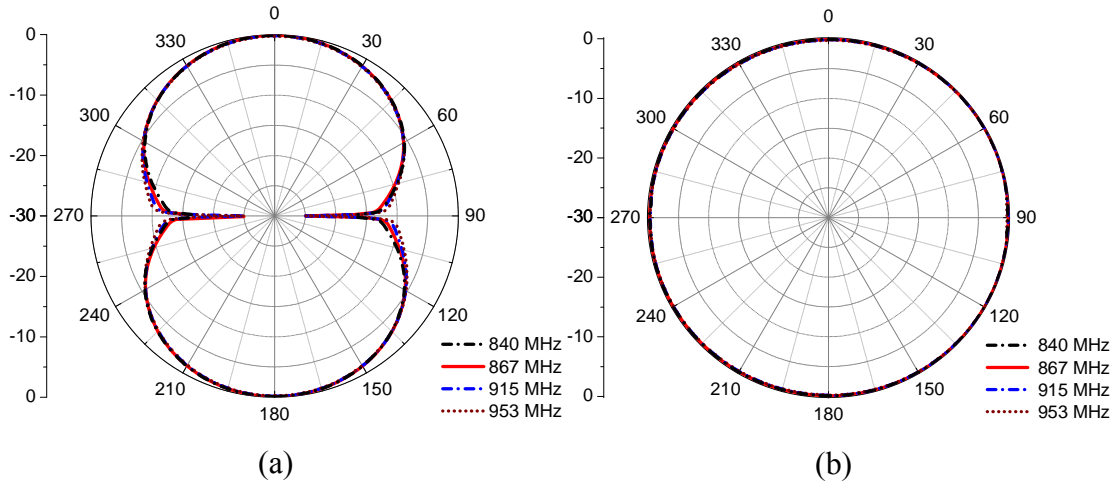


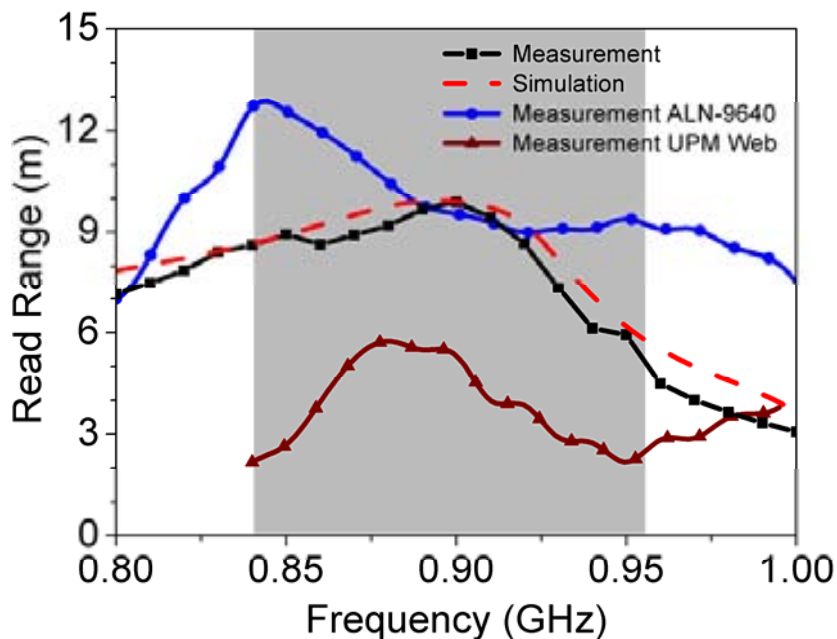
Fig. 4.9 (a) Electric plane radiation pattern of the designed T-match based tag and (b) magnetic plane. The proposed tag has a radiation pattern similar to that of a conventional $\lambda/2$ dipole in the whole UHF-RFID band.

4.5 Fabrication and Experimental Results

The proposed RFID tag was fabricated and the read range was measured (see Fig. 4.10) following the method's steps described in Section 2.2.2. As it was mentioned in Section 3.4, the chip used in this work has a different threshold power than the reported by the manufacturer [17],[18]. From electromagnetic and circuit co-simulation results, an evaluation of the theoretical read range was obtained and depicted in Fig. 4.10(b). Very good agreement between the theoretical and measured read ranges can be observed. The fabricated tag exhibits a significant read range within the whole UHF-RFID band (840-960 MHz), with a peak value of 10 m at 898 MHz. The read range of a commercially available tag (*UPM Web*) that uses the *NXP UCODE G2XM* chip and the T-match network is also shown in Fig. 4.10(b) for comparison purposes. It can be seen that our fabricated tag exhibits a substantially superior read range in the whole UHF-RFID band. Despite the fact that comparing RFID tags only makes sense if they use the same chip (the chip impedance and P_{chip} are key parameters in determining the read range), we have also included in Fig. 4.10(b) the read range of the commercial tag *Alien ALN-9640*. Such tag uses a chip (the *Alien Higgs 3*) with $P_{\text{chip}} = -18$ dBm, whereas $P_{\text{chip}} = -15$ dBm for the *NXP UCODE G2XM* chip (according to the manufacturer specifications). In spite of this significant difference in the threshold power, the read range at 898 MHz is comparable in both the *ALN-9640* tag and our proposed tag. Therefore, the proposed approach for the design of global band UHF-RFID tags is simple and competitive in terms of the main figure of merit: the read range.



(a)



(b)

Fig. 4.10 (a) Photograph of the fabricated RFID tag and (b) simulated and measured read range. The measured read ranges of the *UPM Web* tag (that uses the tag chip of our prototype), and the *Alien ALN-9640* tag of Table 2.5, are also shown for comparison purposes.

4.6 Synthesis Technique of the Proposed Method

In this section, a description of the steps required to apply the method proposed in this chapter is given. The design and synthesis process is illustrated on a flow chart shown in Fig. 4.11. Such process starts by chosen an UHF-RFID chip available in the market (e.g. see **Table 2.4**). Then, the values of the lumped elements of the equivalent-circuit model of the chip, R_c and C_c , will be determined. In the next step, a resonant antenna with a real input impedance at the resonance frequency, ω_0 , such that $1/(\omega_0^2 C_c^2 R_c) \ll R_a \leq R_c$ is designed (or selected). Preferably, the tag antenna should

exhibit a frequency derivative of the antenna impedance at ω_0 as low as possible, in order to maximize the frequency range of validity of the proposed approach and the achieved tag bandwidth (the latter mainly controlled by the derivative of the antenna resistance with frequency, evaluated at ω_0). From R_a and the considered chip, the parameters $n = (R_c/R_a)^{1/2}$ and Δf can be inferred. The shift Δf is obtained from the associated function of the antenna resistance R_a (given by equation

(A.4)) for a given chip (e.g. see Fig. 4.4). To finish the design stage, the inductances L_1 and L_2 are calculated by using equations (4.12) and (4.13). The synthesis of the designed T-match based tag starts by considering a closed loop consisting of a narrow conductor strip (e.g. 0.2 mm) connected to the input reactance of the considered chip. A sweep of the length of the loop is performed by means of electromagnetic simulations until the resonance frequency appears at $f_0 - \Delta f$, as illustrated in Fig. 4.12(a). Finally, a sweep of the antenna connection is carried out as shown in Fig. 4.12(b) until the tag resonance reaches the desired frequency, f_0 .

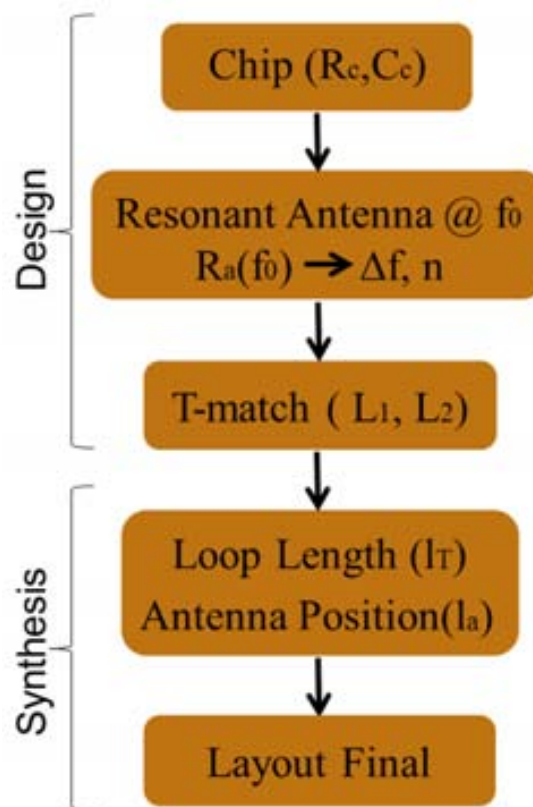


Fig. 4.11 T-match based UHF tag design and synthesis process.

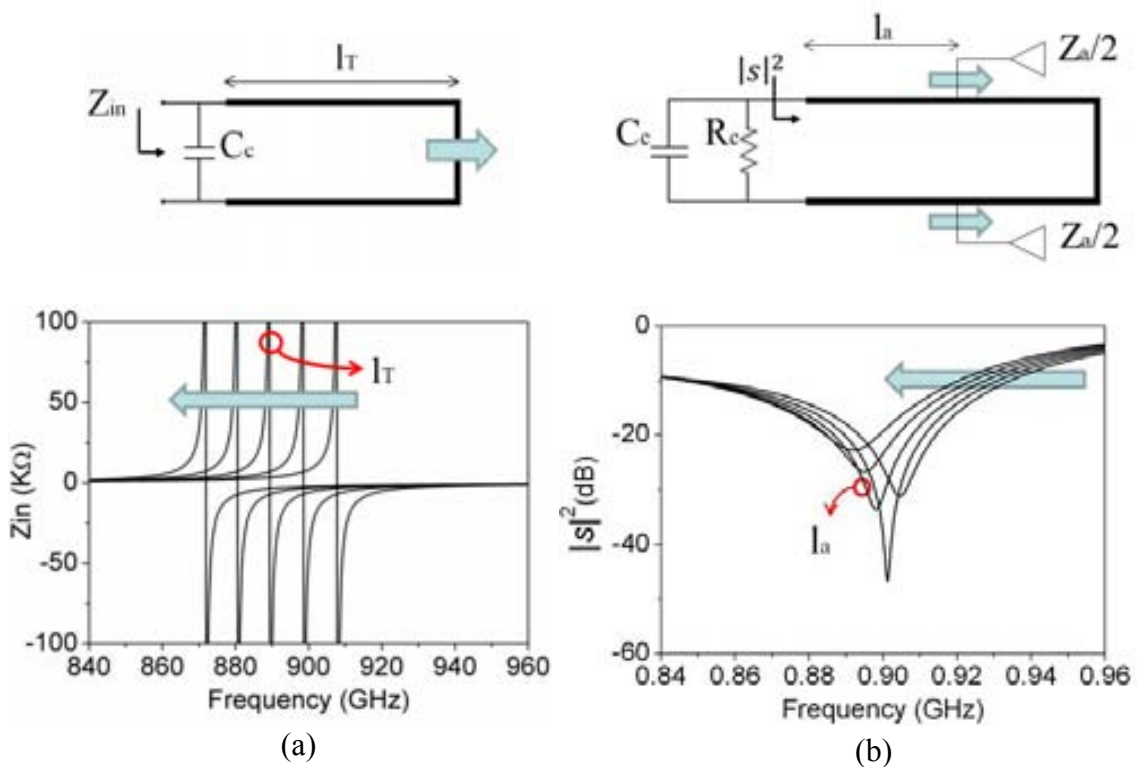


Fig. 4.12 Synthesis of the T-match based tag. (a) Sweep of the length of the loop to obtain l_T , and (b) sweep of the position of the antenna connection to obtain the tag resonance at f_0 .

4.7 Conclusions

In this chapter, a systematic and simple method for the design of UHF-RFID tags, based on the T-match network, has been introduced. This method is based on the equivalent-circuit network required for bandwidth broadening in single resonant UHF tags obtained in Chapter 3 that includes the tag antenna, the chip and the matching network. The frequency limits related to the validity of the presented approach have been analyzed, and the dependence of the achieved tag bandwidth with the antenna impedance is also discussed. As a proof of concept, a global band tag has been designed using this method, and the read range of the fabricated prototype has been measured and compared to those of commercially available tags. The results reveal that the designed tag is very competitive, and point out that the proposed circuit-based approach is very useful for the synthesis of T-match based tags.

4.8 References

- [1] G. Zamora, S. Zuffanelli, F. Paredes, F. Martín and J. Bonache, “Design and synthesis methodology for UHF-RFID tags based on the T-match network”, *IEEE Trans. Microw. Theory Tech.* Submitted (June 2013).
- [2] D. M. Dobkin, *The RF in RFID: Passive UHF RFID in Practice*, Newnes, 2007.
- [3] D. D. Deavours, “Analysis and design of wideband passive UHF-RFID tags using a circuit model”, *IEEE International Conference on RFID*, pp. 283–290, May 2009.
- [4] P. H. Young, *Electronic Communication Techniques*, 3rd ed., Macmillan Publishing Company, NY, 1994.
- [5] K. Kurokawa, “Power waves and the scattering matrix”, *IEEE Trans. Microw. Theory Tech.*, vol. MTT-13, no. 3, pp. 194–202, March 1965.
- [6] P. V. Nikitin, K. V. Seshagiri Rao, S. F. Lam, V. Pillai, R. Martinez, and H. Heinrich, “Power Reflection Coefficient Analysis for Complex Impedances in RFID Tag Design”, *IEEE Trans. Antennas and Propagation*, vol. 53, no. 9, pp. 2721–2725, Sep. 2005.
- [7] Impinj RFID chips [Online]. Available at <http://www.impinj.com>.
- [8] Alien Technology RFID Ics [Online]. Available at <http://www.alientechnology.com>.
- [9] NXP UCODE smart label ICs [Online]. Available at www.nxp.com.
- [10] G. Zamora, F. Paredes, F. J. Herraiz-Martinez, and F. Martin and J. Bonache “On the bandwidth limitations of UHF-RFID tags”, *IET Microwaves Antennas and Propagation*. Accepted (May 2013).
- [11] H. W. Bode, “Network analysis and feedback amplifier design”, pp. 360–371,

D. Van Nostrand co., N.Y., 1945.

- [12] R. M. Fano, “Theoretical Limitations on the Broadband Matching of Arbitrary Impedances”, *Journal of the Franklin Institute*, vol. 249, no. 1, pp. 57–83, Jan. 1950.
- [13] W. L. Weeks, *Antenna Engineering*. McGraw-Hill, NY, 1968.
- [14] H. Jasik, Ed., *Antenna Engineering Handbook*, McGraw-Hill, NY, 1961.
- [15] G. A. Thiele, E. P. Ekelman, and L. W. Henderson, “On the accuracy of the transmission line model of the folded dipole”, *IEEE Trans. Antennas Propagation*, vol. 28, no. 5, pp. 700–703, Sep. 1980.
- [16] A. R. Clark and A. P. C. Fourie, “An improvement to the transmission line model of folded dipole”, *IEE Proc Microwave Antennas Propag*, Vol. 138, no. 6, 577–579, Dec. 1991.
- [17] P. V. Nikitin, K. V. Seshagiri Rao, “Effect of Gen2 protocol parameters on RFID tag performance”, *IEEE International Conference on RFID*, pp. 117–122, April 2009.
- [18] P. V. Nikitin, K. V. Seshagiri Rao, R. Martinez, S. F. Lam, “Sensitivity and impedance measurements of UHF-RFID chips”, *IEEE Trans. Microw. Theory Tech.*, vol. 57, no. 5, pp. 1297–1302, May 2009.

CHAPTER 5

Microwave and UHF-RFID Devices Based on Metamaterial Concepts for Reader Applications

This chapter is focused on the design of RFID devices based on metamaterial concepts for reader applications. Firstly, a composite right/left-handed (CRLH) slot line leaky-wave antenna (LWA) is designed and fabricated [1]. The antenna, implemented by loading a slot line with SRRs, is designed to exhibit a balanced dispersion relation, with a continuous transition between the left-handed and the right-handed bands at 2.5 GHz. Moreover, a practical application of the LWA for microwave RFID readers in the field of automatic vehicle identification (AVI) is also proposed. Finally, a strategy to design near field (NF) UHF communication devices capable to confine the electromagnetic power in a controlled space is explained.

5.1 Fundamental Mode LWA using Slot Line and SRR-Based Metamaterials for Microwave RFID Reader Applications

The design of a slot line based LWA is carried out in this section. We start by designing a balanced CRLH CPW unit cell, with a sufficiently wide central strip to minimize field coupling between both slots. In the next step, one half of the structure is removed to obtain the unit cell of the LWA, which is expected to exhibit similar dispersion relation, as explained later. Finally, the length of the LWA is chosen such that almost all the incident power is radiated before reaching the antenna end termination.

It was experimentally verified in [2] that by positioning two equally excited parallel slots ($f = 3$ GHz with dielectric constant $\epsilon_r = 16$) at a distance of 2.5 cm (that is roughly a quarter wavelength), the field coupling between slots is weaker than -28.36 dB. Thus, the coupling between the two slots in a CPW can be neglected when they are placed far enough. This means that a CPW transmission line with the two slots separated far enough can be thought of as two independent slot transmission lines sharing the same substrate, with a 180° phase shift between the magnetic currents in both slots. Therefore, a symmetric CPW with a wide central strip should have similar propagation characteristics than the slot line resulting by removing one half of the CPW structure.

5.1.1 Design of a Balanced CPW CRLH Transmission Line

The propagation characteristics of a CRLH CPW transmission line based on SRRs and wires can be obtained through the analysis of the dispersion relation. This can be inferred from the lumped element equivalent-circuit model of the elemental cell (see Fig. 2.21). The resulting dispersion diagram exhibits backward wave propagation at low frequencies and forward wave propagation at high frequencies. Typically, a frequency gap is present between the left-handed and the right-handed bands of the transmission line, unless it is designed to be balanced. In this case, the gap collapses and there is a continuous transition between the left-handed and the right-handed band at the so-called transition frequency, where the phase velocity is ideally infinity and the group velocity takes a finite value. Following the indications described in [3], a balanced CRLH CPW unit cell with a wide central strip was designed. The dispersion diagram, inferred from electromagnetic simulation by using the *Agilent Momentum* commercial software, is

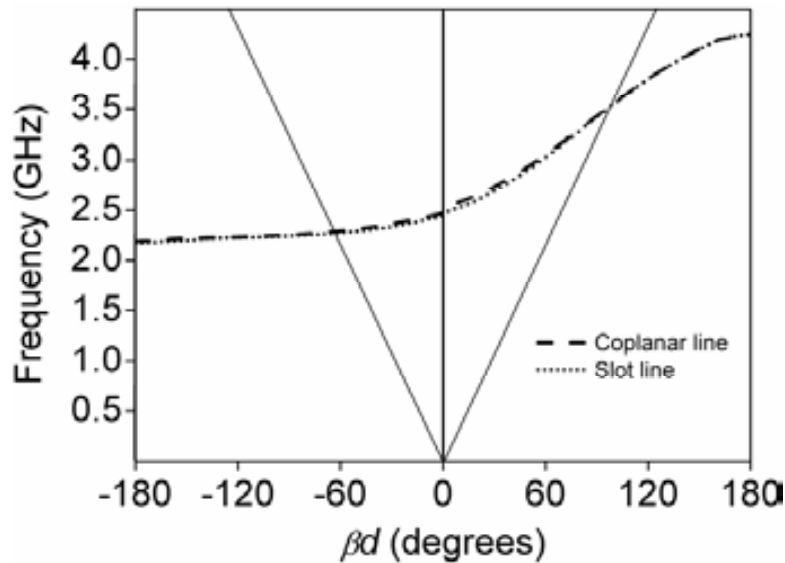


Fig. 5.1 Dispersion diagram (phase constant) of the CPW (dashed line) and slot line (dotted line) inferred from electromagnetic simulation.

depicted in Fig. 5.1. It can be seen that perfect balance is achieved, the transition frequency being $f_0 = 2.5$ GHz.

5.1.2 Proposed Structure

The proposed implementation of the CRLH slot line leaky-wave structure is shown in Fig. 5.2. The antenna is essentially a host slot line periodically loaded with SRRs, placed in the back side of the substrate, and thin metal wires connecting both conductors at those positions coincident with the centers of the SRRs. The dominant mode of a slot line is a TE mode, quite similar to the TE_{10} mode of rectangular waveguides [4]. Thus, the magnetic field in the proposed configuration has a component polarized along the ring axis, providing appropriate excitation of the SRRs.

The unit cell was obtained by removing one of the halves of the CPW unit cell designed in the previous section. The length of the basic cell is 23.5 mm, approximately 5 times smaller than the free-space wavelength ($\lambda_0 = 120$ mm) at 2.5 GHz. Fig. 5.1 shows the dispersion relation of the unit cell obtained from electromagnetic simulation. As expected, good agreement between the dispersion diagrams obtained from the electromagnetic simulation of the slot line and the CPW is observed. It can be appreciated that the SRR-loaded slot line also exhibits perfect balance at roughly

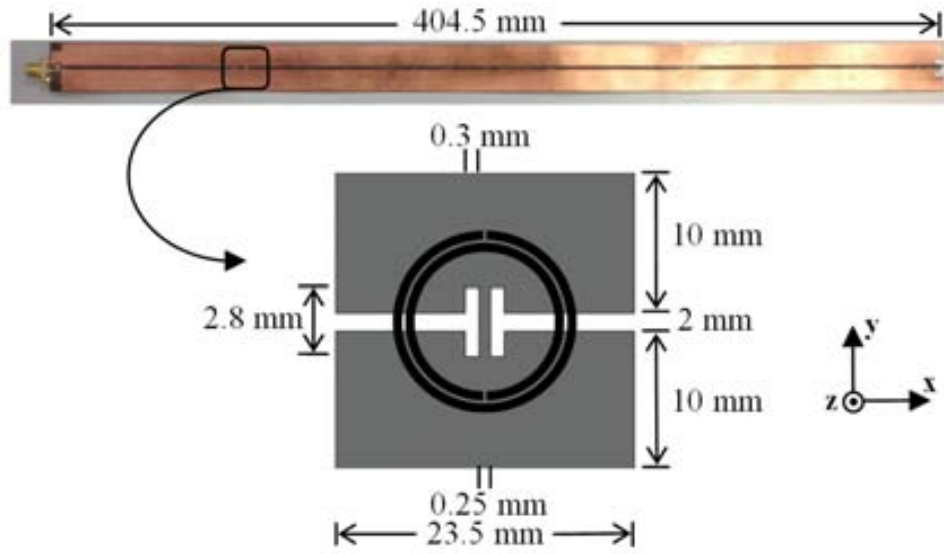


Fig. 5.2 Fabricated LWA and dimensions. The external radius, rings width and rings separation of the SRRs are 5.5 mm, 0.5 mm and 0.25 mm, respectively.

2.5 GHz, with a continuous transition between the left-handed and the right-handed bands. Since the periodicity of the proposed structure is much less than a wavelength, the resulting antenna is a quasi-uniform LWA. The radiation characteristics of uniform (or quasi-uniform) leaky-wave antennas are determined by the complex propagation constant of the considered leaky mode:

$$\gamma = \alpha + j\beta \quad (5.1)$$

where α is the attenuation constant of the wave propagating along the waveguide and accounts for the radiated and dissipated power density per unit length. If the structure is uniform (or quasi-uniform) longitudinally, α and β are constant along its length. Then, the angle, θ_m , between the maximum of the radiation beam and the broadside direction (see Fig. 5.3) is almost the same as the angle of leakage and is given by [5]-[7]

$$\sin(\theta_m) \approx \frac{\beta}{k_0} \quad (5.2)$$

where k_0 is the free-space wavenumber. It can be deduced from (5.2) that if $|\beta| < k_0$, then radiation may occur, and the angle θ_m can be either positive or negative. According

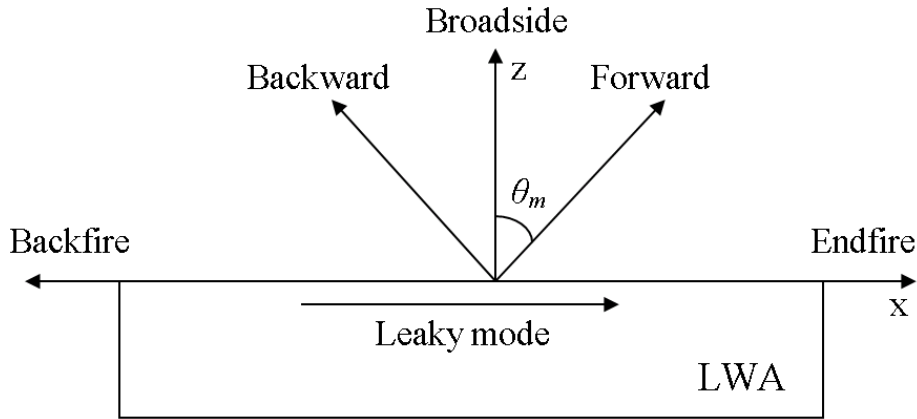


Fig. 5.3 A side view of a LWA and different directions of leaky-wave radiation.

to this, backward leaky-wave radiation is expected if $|\beta| < k_0$ and $\beta < 0$, whereas forward leaky-wave radiation will occur if $|\beta| < k_0$ and $\beta > 0$.

The proposed structure allows for backward and forward leaky-wave radiation, as it can be observed in Fig. 5.1, since portions of both the left-handed and the right-handed bands within the light cone exist. The light cone is the area enclosed between the straight thin lines in Fig. 5.1, and determines the boundaries between slow and fast-wave propagation relative to free space. Moreover, broadside radiation is also possible at 2.5 GHz since a continuous transition between the left-handed and the right-handed band is achieved at this frequency (see Fig. 5.1). As it was shown in [8], the analysis of a single unit cell is inaccurate for the determination of the attenuation constant α of leaky periodic structures. This is due to mutual coupling and edge effects. However, as the number of the considered unit cells increases, edge effects become less significant and the obtained attenuation constant is more accurate [9]. Therefore, in order to determine the required number of unit cells, N , the attenuation constant was computed by simulating an N -element two-port structure, using the *Agilent Momentum* commercial software. Fig. 5.4 shows the normalized attenuation constant α/k_0 at the design frequency of 2.5 GHz. It can be observed that more than 15 elements are required to achieve convergence to a value of $\alpha/k_0 = 0.076$. This value was used to obtain the length of the LWA from the expression for the power flow along a lossy periodic structure with periodicity d [10]

$$P_n = P_0 e^{-2\alpha nd} \quad (5.3)$$

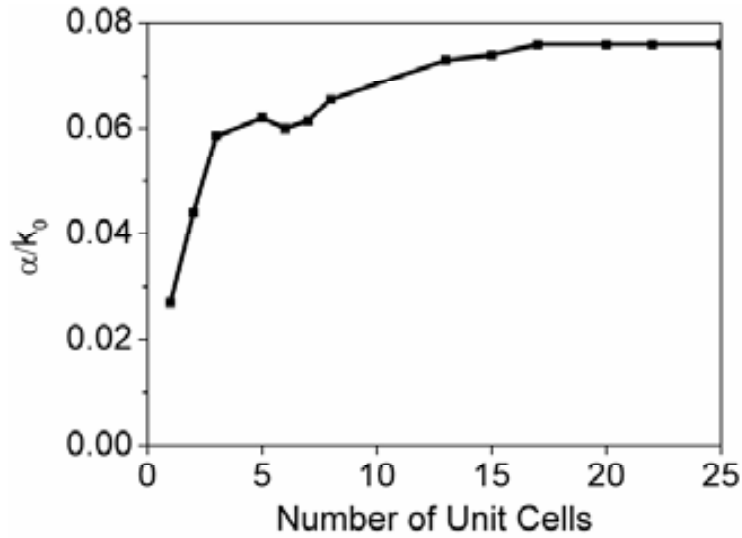


Fig. 5.4 Attenuation constant versus number of unit cells at 2.5 GHz.

where P_0 is the power delivered to the LWA and P_n is the power at the n th terminal of the periodic structure. For 95 % of the power dissipated before reaching the antenna termination and using the converged value of $\alpha/k_0 = 0.076$, we find that the needed number of unit cells is $N = 17$.

5.1.3 Simulation and Experimental Results

An *Arlon Cuclad 250XL* substrate with a dielectric constant $\epsilon_r = 2.43$, a loss tangent $\tan\delta = 0.002$ and thickness $h = 0.49$ mm was used to fabricate the designed antenna. According to simulation, the Bloch impedance of the loaded line around the transition frequency is about 150Ω . This impedance was matched to the 50Ω connector using a semi-lumped microstrip-to-slot line transition acting as an inductive transformer-based matching network [11]. A photograph of the radiating structure terminated with a 150Ω load, with the impedance matching network and with the input connector, is shown in Fig. 5.2. The measured and simulated gains are depicted in Fig. 5.5. The maximum measured gains are 7.1 dB and 11.3 dB for the left-handed and right-handed bands, respectively. There is a relatively good agreement between measured and simulated data. The angle of the maximum beam θ_m as a function of frequency is also plotted in Fig. 5.5, showing good agreement between measurement and simulation. The measured backward to forward scanning range is from -50° to $+60^\circ$ while maintaining an acceptable gain level (above -2 dB).

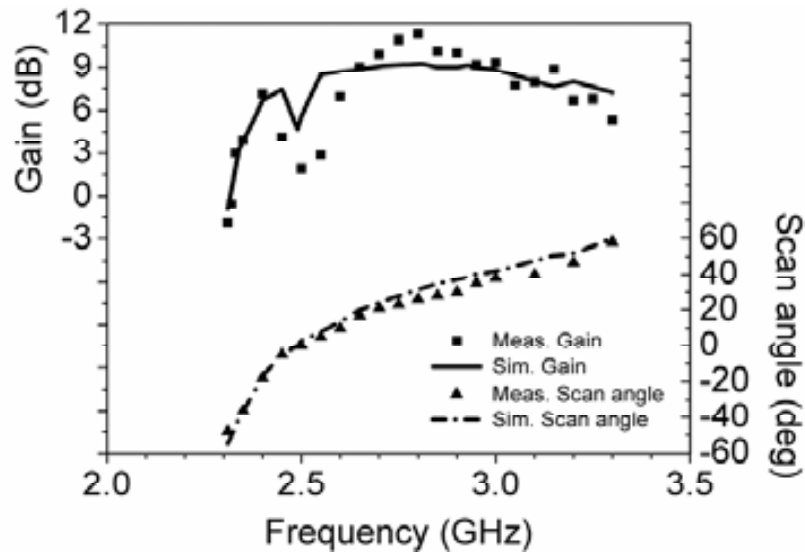


Fig. 5.5 Simulated and measured antenna gain and scanning angle of the proposed LWA.

The measured and simulated normalized radiation patterns are shown in Fig. 5.6. As it can be appreciated, backward, broadside and forward leaky-wave radiation is obtained as frequency increases from the left-handed to the right-handed frequency band. The simulated orthogonal pattern at 2.5 GHz is depicted in Fig. 5.7. It can be observed that, while the radiated beam is directive in the xz -plane (see Fig. 5.6), it is fat in the perpendicular direction (yz -plane), thus resulting in a fan beam. The highest cross-polarization level is -16.7 dB.

As compared to other planar CRLH one-dimensional LWAs that report experimental data on antenna performance [12],[13]-[17] the proposed implementation exhibits a good balance between size, gain and scanning capability (see Table 5.1). The scanning

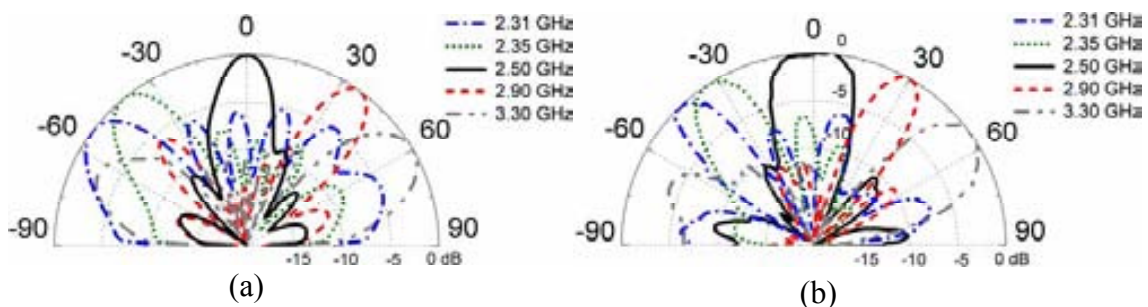


Fig. 5.6 (a) Simulated and (b) measured normalized radiation patterns of the proposed LWA at the longitudinal plane. Actually, the radiation patterns are specular, i.e., only the upper half semi-space of the xz -plane is shown in the figures.

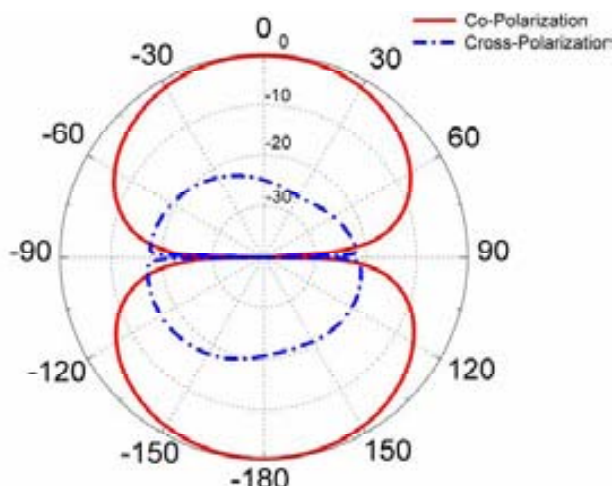


Fig. 5.7 Simulated orthogonal plane radiation pattern of the proposed LWA at 2.5 GHz.

Table 5.1 Comparison of various planar CRLH LWAs

Reference	Unit cell length	# cells (% rad. power)	Scan angle	Scan freq. (GHz)	Maximum Gain
[6]	$\lambda_o/13$	24 (66%)	$-20^\circ, +20^\circ$	3.4-4.3	7dB
[9]	$\lambda_o/6$	20 (68%)	$+11^\circ, +67^\circ$	4.1-5.9	--
[10]	$\lambda_o/11$	41(95%)	$-42^\circ, +47^\circ$	4.0-5.5	15dB ^(a)
[11]	$\lambda_o/11$	12(--)	--	--	5.4dB
[12]	$\lambda_o/10$	16(--)	$-60^\circ, +25^\circ$	1.1-3.2	--
[13] ^(b)	$\lambda_o/10$	10(70%)	$-60^\circ, +60^\circ$	2.2-2.8	3.2dB
This work	$\lambda_o/5$	17 (95%)	$-50^\circ, +60^\circ$	2.3-3.3	11.3dB

^(a)Simulated value; ^(b)This LWA uses chip capacitors.

spans in the table are limited to threshold gains of -2 dB, and f_0 is the transition frequency, except for the antenna of ref. [13], not balanced, where f_0 is the lower frequency of the right handed band. It is noteworthy that the proposed antenna produces specular radiation beams, contrary to those LWAs implemented in microstrip technology.

5.1.4 Automatic Vehicle Identification (AVI) Applications

A practical RFID application for the proposed LWA could be automatic vehicle identification (AVI) based on microwave RFID systems. AVI technology permits fully automatic and unique identification of vehicles at specific interrogation points and

offers potential benefits in many fields including fleet control, revenue collection, traffic operations, transportation planning and safety enforcement. AVI systems essentially comprise three functional elements: the vehicle-mounted transponder, the roadside reader and a communication system with associated antennas or sensors. There are three main technologies used for AVI applications. The technologies are inductive loop systems, optical and infrared systems, and radio frequency and microwave systems. The history of the loop detector extends to 50 years ago when it was first developed in the 1960s. Inductive loop detectors have become the most widely utilized sensors in traffic management systems for more than 30 years because of its simple design. The main problem of the loops is reliability, since loop detectors tend to fail due to the very hard environment of the pavement, the temperature variation, and the resulting shifts in the pavement, which can make the loop detector nonfunctional. Moreover, these systems have an additional problem concerning maintenance, since cutting into the pavement to repair the defective loops may shorten the lifetime of the pavement or resulting in pavement damage. On the other hand, Optical and infrared techniques were used in a number of early AVI systems, as well. These technologies suffer the problem of requiring clear visibility, resulting in a significant degradation of the system performance in presence of snow, rain, ice, fog or dirt. Finally, RF and microwave approaches using RFID technologies are extensively used at present, since these technologies provide better performance in terms of accuracy, cost and ease of use, in comparison with inductive loop and optical and infrared techniques, in most applications. These systems may work in a wide variety of frequencies including LF, HF, UHF and Microwave RFID bands. Obviously, the choice of a specific RFID frequency band depends on the requirements of the considered application and the inherent characteristics of each technology. Microwave RFID (2.4-2.5 GHz) AVI systems using active tags are often used to enhance security and provide fast access in many places such as gated communities, universities and colleges, hospitals and manufacturing or industrial locations, due to their ability to provide longer read ranges, faster read rates, and more complex protocols that are required to provide safety.

Specifically, the proposed LWA is suitable for applications where a unique gate or barrier is used for bi-directional vehicle access control, as in the case of the real scenarios illustrated in Fig. 5.8. In these examples it can be observed different access control applications including hospital access, access control of trucks, security gates and security areas controlled by hydraulic rising bollards. In such applications, two readers are used for vehicle access control in both directions, as indicated in Fig. 5.8(a) and Fig. 5.8(b). Alternatively, these two readers can be replaced by just one reader using the proposed LWA working at 2.45 GHz (within the LH operating region), since the



Fig. 5.8 Examples of AVI systems for (a) hospital access control, (b) access control of trucks, (c) access control in gated communities, and (d) area controlled by hydraulic rising bollards.

specular radiation produced by the LWA allows for bi-directional vehicle identification. This would reduce the cost of the infrastructure necessary to implement the required microwave RFID AVI systems. Furthermore, the LWA exhibits higher gain in comparison with the commonly used antennas (typically patch antennas) and it helps to increase the read range for the same transmitted RF power, or equivalently the transmitted power can be decreased to achieve the same read range. In compliance with maximum allowed 4W EIRP for microwave RFID systems, it implies lower power consumption by the transmitter and thus longer battery life.

5.2 Design Strategy of Near Field Communication Devices for UHF-RFID Reader Applications

The objective of this section is to explain a design strategy of a near field (NF) communication device to be used in a UHF-RFID reader. This device should be able to

work with electric field in order to be usable with standard UHF-RFID tags (long read range), but it should also be able to confine the electric field in a certain predefined region that ensures that only tags within this region (the coverage zone) can be read. Thus, the existing problem in the retail item management, described in Section 2.2.5.1, should be solved.

The presented method is based on an evanescent solution so that there is an exponential decay of the field versus distance and therefore do not give rise to significant components of radiated field, but allowing an arbitrary near field coverage zone. As a result, the proposed strategy avoids giving rise to multiple and undesired readings at different points. Evanescent solutions or surface-waves (also called trapped waves because it carries its energy within a small distance from the interface) are known in natural environments, but these media do not have the ability to sufficiently control as to impose field confinement levels at will. Furthermore, this mode of operation based on evanescent waves has been used in the design of the so-called surface-wave antennas. Much like leaky-wave antennas, surface-wave antennas belong to the family of traveling-wave antennas. The main difference between surface waves and leaky waves is that the former are slow waves (purely bound), whereas the latter are fast waves with respect to free space. Antennas based on surface waves radiate through the introduction of discontinuities or by the excitation of arrays of radiating elements, as surface waves by themselves do not have the ability to radiate.

The principle of operation of the proposed approach is based on metamaterials. Generally, these types of artificial media can control the phase constant of the signal that travels through them. Such control can be used either for designing radiating structures based on LWAs (showed in Section 5.1) or for confining the electromagnetic field around the metamaterial structure in the following way. Let us consider a lossless one-dimensional metamaterial structure M , depicted in Fig. 5.9. The parameter β corresponds to the phase constant (or wavenumber) of the signal traveling through the metamaterial structure M , k_0 corresponds to the wavenumber of the signal propagating in air (signal induced by the metamaterial structure into the air) and k_x and k_y correspond to the projection of the longitudinal and transverse components of k_0 . Then, the wavenumber β can be tailored appropriately by designing the metamaterial structure M by modifying the metamaterial guiding structure adjusting the effective dielectric permittivity (ϵ) and the magnetic permeability (μ) of the metamaterial structure.

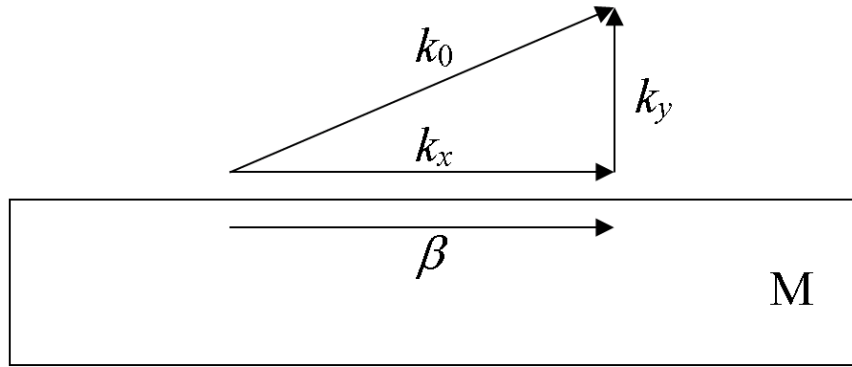


Fig. 5.9 Lossless metamaterial structure M and wavenumbers of the signal traveling through the metamaterial (β) and propagating in air (k 's).

The magnitude of the vector k_0 will depend solely on the environment surrounding the metamaterial structure M, in this case the air, and can therefore be calculated as ω/c , where ω is the angular frequency of the signal and c the speed of light in air. On the other hand, to ensure compliance with the relations of continuity at the interface between the metamaterial structure M and the surrounding environment is necessary that the vector β matches with k_x . Thus, from the separability condition for the wave equation, it can be obtained the governing relation between the magnitude of the vector β and the k vectors [18]

$$k_0^2 = k_x^2 + k_y^2 = \beta^2 + k_y^2 \quad (5.4)$$

wherein by isolating k_y

$$k_y = \pm \sqrt{k_0^2 - \beta^2} \quad (5.5)$$

Hence, by properly adjusting the value of β , there are obtained real and imaginary values of the parameter k_y . This result will depend on the sign of the discriminant of (5.5), that is, the sign of $k_0^2 - \beta^2$. Recalling the general solution of the two-dimensional plane wave propagation in free space it is obtained that the spatial term of the solution contains a propagation factor of the form [10]:

$$e^{-j\vec{k}_0\vec{r}} = e^{-jk_x x} e^{-jk_y y} \quad (5.6)$$

The real values of k_y lead to the so-called progressive wave antennas (radiative solutions) under which the value of β can control the emission direction of the antenna, as it has been done in the leaky-wave antenna designed in this chapter.

By contrast, the proposed method makes use of the flexibility for controlling the propagation characteristics in order to impose values of β leading to imaginary values of k_y and thus avoiding the radiation but allowing the control of the distribution of electric and magnetic fields around the metamaterial structure M. By designing the metamaterial structure M in order to get imaginary values of the parameter k_y ($\beta^2 > k_0^2$) it is obtained

$$e^{-j\vec{k}_0\vec{r}} = e^{-jk_x x} e^{-j\alpha y} \quad (5.7)$$

where α is a positive real number. That supposes an exponentially decrease of the electric and magnetic fields as it is moved away from the surface of the metamaterial structure M (in the y direction). Since the value of β can be adjusted in the design stage of the metamaterial structure M, it is possible to impose the level of confinement of the electromagnetic field around the structure, ensuring that near the communication device (or reader) the field would be large enough to provide a good read but in no case can lead to undesired readings in reading adjacent communication devices. Since the obtained device does not radiate, the dimensions of the structure can be done arbitrarily large (increasing the number of unit cells) to increase the coverage area.

Just like the design of LWAs, the slot line waveguide is also a good candidate to implement NF communication devices for UHF-RFID readers. The reason is that, by using this technology, the entire metamaterial structure M would constructively contribute to the formation of electric and magnetic fields and avoids the cancellation of currents (which causes field cancelation) that exists in different conventional planar technologies, as it was pointed out in Section 2.3.2. Such device can be designed by following the same steps than the used in Section 5.1 for the design of a LWA, except that the NF device must be designed to support slow waves at the operating frequency, rather than fast waves.

The presented design strategy is patent pending and we are currently working on the implementation and measurement of the early prototypes. A good candidate to initially take advantage of this technology could be the textile industry, since there is an immediate necessity of using the UHF-RFID tags, already in use for clothing inventory, in payment points.

5.3 Conclusions

In this chapter, a new planar LWA that exploits the CRLH characteristics of a SRRs-loaded slot line is presented. The proposed antenna consists of a 17-cell CRLH slot line, designed to exhibit a continuous transition from the left-handed to the right-handed band at 2.5 GHz. The presented antenna is able to produce backward, broadside and forward leaky-wave radiation from its fundamental TE mode. The proposed prototype has been successfully tested, exhibiting a backward to forward scanning range from -50° to $+60^\circ$ with significant gain. The measured gain reaches the maximum values of 7.1 dB and 11.3 dB for the left-handed and right-handed bands, respectively. Moreover, it has been shown how the designed structure can be used as microwave RFID reader antenna in the field of AVI.

Finally, a methodology for designing NF communication devices able to confine the electric and magnetic field in a controlled coverage region have been presented. This approach allows solving the problem of the UHF-RFID technology in retail item management applications, consisting in the impossibility of using the same conventional UHF-RFID tags for payment and inventory applications by using the NF readers that exist today.

5.4 References

- [1] G. Zamora, S. Zuffanelli, F. Paredes, F. J. Herraiz-Martinez, F. Martín and J. Bonache, "Fundamental mode leaky-wave antenna (LWA) using slot line and split-ring-resonator (SRR) based metamaterial", *IEEE Antennas and Wireless Propagation Letters*. Submitted (May 2013).
- [2] S. B. Cohn, "Slot line on a dielectric substrate", *IEEE Trans. Microw. Theory*

- Tech.*, vol. 17, no. 10, pp. 768–778, Oct. 1969.
- [3] J. Selga, M. Gil, F. Aznar, J. Bonache and F. Martín, “Composite right/left-handed coplanar waveguides loaded with split ring resonators and their application to high-pass filters”, *IET Microw. Antennas Propag.*, vol. 4, no. 7, pp. 822-827, July 2010.
- [4] G. H. Robinson and J.L. Allen “Application of the slot line to miniature ferrite devices”, *IEEE Trans. Microw. Theory Tech.*, vol. 17, no. 12, pp. 1097–1101, Dec. 1969.
- [5] A. Oliner, “Leaky-wave antennas”, in *Antenna Engineering Handbook*, R. C. Johnson, Ed. McGraw-Hill, NY, 1993.
- [6] T. Tamir, “Leaky wave antennas”, in *Antenna Theory*, R. E. Collin and F. J. Zucker, Eds. McGraw-Hill, NY, 1969.
- [7] D. R. Jackson, C. Caloz and T. Itoh, “Leaky-wave antennas”, *Proceedings of the IEEE* vol. 100, no. 7, pp. 2194–2206, July 2012.
- [8] T. Kokkinos, C. D. Sarris, and G. V. Eleftheriades, “Periodic FDTD analysis of leaky-wave structures and applications to the analysis of negative-refractive-index leaky-wave antennas”, *IEEE Trans. Microw. Theory Tech.*, vol. 54, no. 4, pp. 1619–1630, Jun. 2006.
- [9] A. Grbic, and G. V. Eleftheriades, “Leaky CPW-based slot antenna arrays for millimeter-wave applications”, *IEEE Trans. Antennas Propag.*, vol. 50, no. 11, pp. 1494–1504, Nov. 2002.
- [10] D. M. Pozar, *Microwave Engineering*, 2nd ed. Wiley, NY, 1998.
- [11] P. H. Young, *Electronic Communication Techniques*, 3rd ed., Macmillan Publishing Company, NY, 1994.
- [12] L. Liu, C. Caloz and T. Itoh, “Dominant mode leaky-wave antenna with backfire-to-endfire scanning capability”, *Electron. Lett.*, vol. 38, no. 23, pp. 1414–1416, Nov. 2002.

- [13] M. A. Antoniadis and G. V. Eleftheriades, “A CPS leaky-wave antenna with reduced beam squinting using NRI-TL metamaterials”, *IEEE Trans. Antennas Propag.*, vol. 56, no. 3, pp. 708–721, March 2008.
- [14] S. Paulotto, P. Baccarelli, F. Frezza and D. R. Jackson, “Full-wave modal dispersion analysis and broadside optimization for a class of microstrip CRLH leaky-wave antennas”, *IEEE Trans. Microw. Theory Tech.*, vol. 56, no. 12, pp. 2826–2837, Dec. 2008.
- [15] R. Siragusa, E. Perret, P. Lemaitre-Auger, H. Van Nguyen, S. Tedjini and C. Caloz, “A tapered CRLH interdigital/stub leaky-wave antenna with minimized side-lobe levels”, *IEEE Microwave Wireless Comp. Lett.*, vol. 11, pp. 1214–1217, Oct. 2012.
- [16] O. Losito, M. Gallo, V. Dimiccoli, D. Barletta and M. Bozzetti, “A tapered design of a CRLH-TL leaky wave antenna”, *IEEE Proceedings of the 5th European Conference on Antennas and Propagation (EUCAP)*, pp. 357–360, April. 2011.
- [17] Y. Chi and F. Chen, “CRLH leaky-wave antenna based on ACPS technology with 180° horizontal plane scanning capability”, *Trans. Antennas Propag.*, vol. 61, no. 2, pp. 571–577, Feb. 2013.
- [18] F. J. Zucker, “Surface-wave antennas”, in *Antenna Engineering Handbook*, 3rd ed., R. C. Johnson, Ed. McGraw-Hill, NY, 1993.

CHAPTER 6

Conclusions and Future Work

This thesis is framed within the RFID technology and has been focused on the design of tags and near field communication devices to operate within the UHF-RFID frequency band, and reader antennas for the microwave RFID frequency band. For this purpose, fundamental bandwidth limitations on the design of UHF-RFID tags have been investigated. This study has been conducted by obtaining the optimum equivalent-circuit network necessary for bandwidth broadening in single resonant UHF-RFID tags with conjugate matching. Based on this equivalent-circuit network, a new systematic methodology for the design of T-match UHF-RFID tags based on conjugate matching has been proposed, since the T-match structure is the most common matching network used for the efficient matching of UHF-RFID tags and there is a lack of systematization in the design methodology. Also, a new strategy for the design of a near field communication device to be connected to a standard UHF-RFID reader (replacing the reader antenna) has been proposed by using metamaterial concepts. Moreover, a metamaterial-inspired LWA has been proposed, to be applied in certain microwave RFID AVI applications, in order to reduce costs.

The contents of this work have been divided into five chapters (excluding the conclusions and future work). In **Chapter 1**, the motivation and general objectives have

been pointed out. The most important aspects discussed in the rest of the chapters are summarized in the following paragraphs:

In **Chapter 2**, a broad overview of RFID technology is given. RFID is placed in the context of automatic identification procedures and compared with the well-known optical barcode technology. The different RFID operating frequency ranges and their main features and applications are introduced, and RFID standardization is summarized. A brief history of RFID and a market prediction for the near future is also presented. The state of the art of RFID systems operating within the UHF regulated frequency bands is analyzed, and the most relevant characteristics of UHF-RFID systems are explained in detail, including the operating principle and the regulated frequency bands, the most important parameter indicative of the performance of an RFID system (the read range), the lumped equivalent-circuit model of UHF-RFID chips and the physical bandwidth limitations of UHF-RFID systems. The concept of metamaterials is defined and metamaterial transmission lines based on a coplanar waveguide (CPW) and SRRs are described. Finally, leaky-wave antennas (LWAs) are briefly described, focusing the attention on planar implementations using metamaterial transmission lines, since a LWA based on metamaterial concepts is proposed in Chapter 5 for RFID reader applications.

In **Chapter 3**, bandwidth optimization in single resonant UHF-RFID tags has been considered. It has been demonstrated that the optimum network for bandwidth enhancement, providing conjugate matching, is simply a parallel combination of an inductor and a resistor cascaded to the UHF-RFID chip. Bandwidth optimization has been validated by means of the Bode criterion. It has also been shown that a folded dipole antenna behaves as a parallel combination of an inductor and a resistor, and by designing this antenna to provide conjugate matching at 915 MHz, a bandwidth very close to the optimum value results. A formula that predicts the maximum achievable -3 dB bandwidth (i.e., the one that results by considering the ideal RL network with conjugate matching) for a given UHF-RFID chip has been derived. It has also been inferred a generalized expression for the -3 dB bandwidth when any real network, corresponding to the antenna and matching network (if it is considered), is cascaded to the UHF-RFID chip. According to this analysis, a global band RFID tag prototype has been designed and fabricated. The experimental results show a significant read range; over 5 m within the whole band (840-960 MHz) and almost 9 m peak read range. The area of the power reflection coefficient has been obtained resulting in more than 80% of the Bode area limit, and the corresponding -3 dB bandwidth is 73% of the upper limit for complex conjugate matching between the antenna and the chip at 915 MHz, which is

in good agreement with the value (71% of the upper limit) predicted by using the proposed generalized expression for the -3 dB bandwidth. Thus, with the reported example, it is demonstrated that it is possible to evaluate if the designed tag is close to the maximum achievable bandwidth or if it still has some margin for improvement.

In **Chapter 4**, a systematic and simple method for the design of UHF-RFID tags, based on the T-match network and conjugate matching, has been presented. This method is based on the equivalent-circuit network required for bandwidth broadening in single resonant UHF tags obtained in Chapter 3 that includes the tag antenna, the chip and the matching network. The frequency limits related to the validity of the presented approach have been analyzed, and the dependence of the achieved tag bandwidth with the antenna impedance is also discussed. As a proof of concept, a global band tag has been designed using this method, and the read range of the fabricated prototype has been measured and compared to those of commercially available tags. The results reveal that the proposed circuit-based approach is very useful for the implementation of T-match based tags.

Chapter 5 is devoted to the design of RFID devices based on metamaterial concepts for reader applications. A planar leaky-wave antenna (LWA) that exploits the composite right/left-handed (CRLH) characteristics of a SRRs-loaded slot line is presented. It consists of a 17-cell CRLH slot line, designed to exhibit a continuous transition from the left-handed to the right-handed band at 2.5 GHz. The presented antenna is able to produce backward, broadside and forward leaky-wave radiation from its fundamental TE mode. The proposed prototype has been successfully tested, exhibiting a backward to forward scanning range from -50° to $+60^\circ$ with significant gain. The measured gain reaches the maximum values of 7.1 dB and 11.3 dB for the left-handed and right-handed bands, respectively. It has been shown how the designed structure can be used as microwave RFID reader antenna in the field of automatic vehicle identification (AVI). Moreover, a new methodology for designing near field (NF) communication devices able to confine the electric and magnetic field in a controlled coverage region has been presented. This approach allows solving the problem of the UHF-RFID technology in retail item management applications, consisting in the impossibility of using the same conventional UHF-RFID tags for payment and inventory applications by using the NF readers that exist today.

As a **general conclusion**, the objectives proposed in the first chapter have been satisfactorily achieved. With the work and the investigations carried out in this thesis, we have generated new design strategies that can be useful for RFID designers in order

to implement competitive RFID tags and communication devices for UHF reader applications, as well as reader antennas for cost reduction in microwave RFID systems.

Future Work

Different **future research lines** can emerge from this thesis. For instance, a straightforward application derived from the LWA proposed in Section 5.1 could be RFID tag miniaturization. This can be achieved by designing small CRLH resonant antennas based on a single unit cell (or a couple of unit cells) of the designed LWA. A CRLH resonant antenna is obtained by terminating a metamaterial transmission line opened to free space by a short or an open circuit. Unlike the working principle of a LWA (based on a progressive waves propagating along a guiding structure and gradually leaking out a small amount of energy in the form of coherent radiation), in resonant antennas, the presence of a standing wave produces radiation based on the resonance mechanism. The controllable electromagnetic properties of CRLH structures allows for the possibility of further tag miniaturization in comparison with conventional right-handed (RH) resonant antennas (e.g. a patch antenna), due to the small electrical size of the constituent cells and the possibility of exhibiting negative and zero-order resonances, in addition to positive resonances.

Regarding the design strategy of near field communication devices for UHF-RFID reader applications presented in Section 5.2, the fabrication and measurement of different prototypes should be carried out, in order to check the results predicted by the theory.

Additional research lines on the field of RFID are also being studied in the research group GEMMA/CIMITEC to which the author belongs.

- One of these research lines is focused on the fabrication of low cost RFID tags and reader antennas in polyethylene terephthalate (PET) flexible substrates (inlays) by means of a standard and large production technique known as screen printing or serigraphy. So far, an UHF-RFID reader antenna prototype based on a patch antenna, by using PET substrate and conductive ink with silver particles as a metallization, has been designed and fabricated. The results demonstrate the potential capability of a further cost reduction of UHF-RFID systems by using these low-cost reader antennas.

- Another research line is devoted to the integration of UHF-RFID technology into mobile phones, in order to take advantage of the benefits provided by the UHF technology and the already in use near field communication (NFC) technology at the same time. So far, a UHF-RFID reader antenna has been fabricated and tested mounted on a conventional mobile phone and good performance has been observed.
- Finally, the design of UHF-RFID tags to be mounted on metallic objects is also being studied. This research activity is very promising since the preliminary results demonstrate a significant improvement of the read ranges achieved from the fabricated small-size prototypes, in comparison with conventional tags for metallic objects that have similar dimensions. Moreover, an innovative design strategy for UHF-RFID tags mounted on optical discs (such as DVDs) has been developed and it is currently being considered for publication in the *IEEE Transactions on antennas and propagation* international journal. In this work, a worldwide UHF-RFID tag prototype, for direct mounting on a DVD disc, is designed and fabricated and the measured read range demonstrates that the presented method drastically improves the performance within the whole UHF-RFID band, compared with the DVD tags found in the literature. This design strategy is patent pending and we are currently working on the transfer of the technology to industry.

APPENDIX A

Calculation of the Frequency Shift of the Tag Resonance

Let us consider the circuit depicted in Fig. 4.3(a), where the tag antenna has a purely resistive impedance such that $Z_a = R_a \leq R_c$. This circuit can be exactly modeled by the one depicted in Fig. 4.3(b), where R_{eq} and L_{eq} are given by (4.4) and (4.6), respectively. Now, if we use equations (4.5) and (4.7) in the circuit of Fig. 4.3(b) rather than (4.4) and (4.6), one can obtain the inductances L_1 and L_2

$$L_1 = \frac{1}{2\omega_0^2 C_c} \left(1 - \frac{1}{n} \right) \quad (\text{A.1})$$

$$L_2 = \frac{1}{2n\omega_0^2 C_c} \quad (\text{A.2})$$

It follows that the exact expression for the inductance L_{eq} in the circuit of Fig. 4.3(b) can be expressed as

$$L_{eq} = (L_1 + L_2) \left[\frac{4\omega^2 (L_1 + L_2)^2 \left(1 - \frac{1}{n}\right)^2 + R_a R_c}{4\omega^2 (L_1 + L_2)^2 \left(1 - \frac{1}{n}\right) + R_a R_c} \right] \quad (\text{A.3})$$

where $n \geq 1$. Hence, it is clear from (A.3) that $L_{eq} \leq L_1 + L_2$ and, therefore, the susceptance $B = B_{eq} + 2B_{chip}$ vanishes at a frequency $\omega \geq \omega_0$. This frequency can be inferred by forcing $B = 0$ and using (A.3), giving a frequency increment, $\Delta\omega$, of the tag resonant with respect to ω_0 which can be written as

$$\Delta\omega = \sqrt{\frac{\omega_0^2 C_c (1 - \sqrt{R_a/R_c}) - \omega_0^4 C_c^3 R_a R_c + \sqrt{\left[\omega_0^2 C_c (1 - \sqrt{R_a/R_c}) - \omega_0^4 C_c^3 R_a R_c\right]^2 + 4\omega_0^6 C_c^4 R_a R_c (1 - \sqrt{R_a/R_c})^2}}{2C_c (1 - \sqrt{R_a/R_c})^2}} - \omega_0 \quad (\text{A.4})$$

APPENDIX B

Minimum Power Reflection Coefficient

Let us now consider the circuit depicted in Fig. 4.3(a), where the tag antenna has any general complex impedance $Z_a = R_a + j\chi_a$ and χ_a being an arbitrary frequency dependent function. This circuit can be exactly modeled by the one depicted in Fig. 4.3(b), where R_{eq} and L_{eq} are given by (4.4) and (4.6), respectively. Then, $G_{eq} = 1/R_{eq}$ also results in an arbitrary frequency dependent function. Let us demonstrate that in the case when $G_{eq} \approx 2G_{chip}$, the minimum power reflection coefficient occurs roughly at that frequency when the total susceptance $B = B_{eq} + 2B_{chip}$ vanishes. The power reflection coefficient, $|s|^2$, from the circuit of Fig. 4.3(b) is given by expression (4.10). By forcing the frequency derivative of (4.10) to be zero, it is found that

$$2BB'G_{eq} = G'_{eq} (B^2 + 4G_{chip}^2 - G_{eq}^2) \quad (B.1)$$

where B' and G'_{eq} are the frequency derivatives of the susceptance B and the conductance G_{eq} , respectively. Notice that all the parameters in (B.1) are frequency dependent functions, except G_{chip} . It can be deduced that equation (B.1) is satisfied at that frequency when $B = 0$, provided that $G_{eq} = 2G_{chip}$.

APPENDIX C

First Order Taylor Expansion of the Conductance G_{eq} at the vicinity of f_0

Let us consider the circuit depicted in Fig. 4.3(b), where the conductance G_{eq} and the inductance L_{eq} are obtained from (4.5) and (4.7), respectively. Hence, G_{eq} is a frequency dependent function given by

$$G_{eq} = \frac{2}{n^2} \left(\frac{R_a(f)}{R_a^2(f) + \chi_a^2(f)} \right) \quad (C.1)$$

that can be approximated by its first order Taylor expansion in the vicinity of f_0 , that is when $R_a(f) = R_a(f_0)$ and $\chi(f_0) = 0$ and, therefore, $G_{eq} = 2G_{chip}$ since $n^2 = R_c/R_a$. It follows that G_{eq} can be approximated, in the vicinity of f_0 , by:

$$G_{eq} = 2G_{chip} \left(1 - \frac{R'_a(f_0)}{R_a(f_0)} (f - f_0) \right) \quad (C.2)$$

where $R'_a(f_0)$ is the frequency derivative of the antenna resistance evaluated at f_0 .

Author list of publications

International Journals

1. F. Paredes, G. Z. Gonzalez, J. Bonache, and F. Martin, “Dual-band impedance-matching networks based on split-ring resonators for applications in RF identification (RFID)”, *IEEE Trans. Microw. Theory Tech.*, vol. 58, no. 5, pp. 1159–1166, April 2010.
2. F. Paredes, G. Zamora, F. J. Herraiz-Martinez, F. Martín and J. Bonache, “Dual-band UHF-RFID Tags Based on Meander Line Antennas Loaded with Spiral Resonators”, *IEEE Antennas and Wireless Propagation Letters*, vol. 10, pp. 768–771, July 2011.
3. F. J. Herraiz-Martínez, G. Zamora, F. Paredes, F. Martín and J. Bonache, “Multiband Printed Monopole Antennas loaded with OCSRRs for PANs and WLANs”, *IEEE Antennas and Wireless Propagation Letters (Special issue)*, vol. 10, pp. 1528–1531, Dec. 2011.
4. F. J. Herraiz-Martinez, F. Paredes, G. Zamora, F. Martin and J. Bonache, “Printed Magnetoinductive-Wave (MIW) Delay Lines for Chipless RFID Applications”, *IEEE Transactions on antennas and propagation*, vol. 60, no. 11, pp. 5075–5082, Nov. 2012.
5. F. J. Herraiz-Martinez, F. Paredes, G. Zamora, F. Martin and J. Bonache, “Dual-band printed dipole antenna loaded with open complementary split ring resonators (OCSRRs) for wireless applications”, *Microwave and Optical Technology Letters*, vol.54, No. 4, pp. 1014–1017, April 2012.
6. F. Martín, Jordi Bonache, Miguel Durán-Sindreu, Jordi Naqui, Ferran Paredes, Gerard Zamora, “Artificial Transmission Lines”, Chapter for Wiley Eyclopedia of Electrical and Electronics Engineering, July 2012.

7. F. Paredes, G. Zamora, S. Zuffanelli, F. J. Herraiz-Martinez, J. Bonache and F. Martín, “Recent advances in multiband printed antennas based on metamaterial loading”, *Advances in Optoelectronics (Special Issue)*, May 2012.
8. G. Zamora, F. Paredes, F. J. Herraiz-Martinez, F. Martín and J. Bonache, “On the Bandwidth Limitations of UHF-RFID Tags”, *IET Microwave Antennas and Propagation*. Accepted.
9. F. Paredes, G. Zamora, S. Zuffanelli, F. J. Herraiz-Martinez, F. Martín and J. Bonache, “Free-Space and On-metal Dual-Band Tag for UHF-RFID Applications in Europe and USA”, *Progress in Electromagnetic Research*. Accepted.
10. S. Zuffanelli, G. Zamora, F. Paredes, J. Bonache and F. Martín, “An approach for the design of passive UHF-RFID tag mounted on optical discs”, *IEEE Transactions on Antennas and Propagation*. Submitted.
11. G. Zamora, S. Zuffanelli, F. Paredes, F. J. Herraiz-Martinez, F. Martín and J. Bonache, “Fundamental mode leaky-wave antenna (LWA) using slot line and split-ring-resonator (SRR) based metamaterial”, *IEEE Antennas and Wireless Propagation Letters*. Submitted.
12. G. Zamora, S. Zuffanelli, F. Paredes, F. Martín and J. Bonache, “Design and synthesis methodology for UHF-RFID tags based on the T-match network”, *IEEE Trans. Microw. Theory Tech*. Submitted.

National and International Conferences

1. F. Paredes, G. Zamora, J. Bonache, F. Martín, “Dual-Band Impedance Matching Networks Based on a Perturbation Method”, *IEEE AP-S International Symposium on Antennas and Propagation and USNC/URSI National Radio Science Meeting*, Charleston (SC), USA, June 2009.
2. F. Paredes, G. Z. Gonzalez, J. Bonache, and F. Martín, “Perturbation method based on resonant type metamaterial transmission lines for dual-band matching networks”, *Mediterranean Microw. Symp.*, pp.1–4, Tanger, Morocco, November 2009.
3. F. Paredes, G. Zamora, F. Martín, J. Bonache, “Miniaturization of RFID Tag by Means of an Electrically Small Resonator”, *IEEE International Conference on Wireless Information Technology and Systems*, Honolulu, (HI), USA, August-September 2010.
4. F. Paredes, G. Zamora, Francisco Javier Herraiz-Martinez, F. Martín and J. Bonache, “Application of dispersion engineering to the optimization of RFID tags”, *Young scientist Meeting on Metamaterials (YSMM)*, Valencia, España, February 2011.

5. F. Paredes, G. Zamora, F. J. Herraiz-Martinez, F. Martín and J. Bonache, “Dual-band metallic tags for RFID applications”, *IEEE International Symposium on Antennas and Propagation and National Radio Science Meeting (IEEE APS-URSI)*, Spokane, Washington, USA, July 2011.
6. F. Paredes, G. Zamora, F. J. Herraiz-Martinez, F. Martín and J. Bonache, “Tags de RFID basados en dipolos meandro para operar en Europa y USA”, *Unión Científica Internacional de Radio (URSI)*, Leganés, España, Septiembre 2011.
7. F. J. Herraiz-Martinez, F. Paredes, G. Zamora, F. Martín and J. Bonache, “Dipolo Impreso de Doble Banda cargado con OCSRRs para aplicaciones inalámbricas”, *Unión Científica Internacional de Radio (URSI)*, Leganés, España. Septiembre 2011.
8. F. J. Herraiz-Martinez, J. Bonache, F. Paredes, G. Zamora and F. Martín, “Dual-band Printed Dipole Antenna Loaded with Open Complementary Split Ring Resonators (OCSRR)”, *Metamaterials: International Congress on Advanced Electromagnetic Materials in Microwaves and Optics*, Barcelona, Spain, October 2011.
9. M. Durán-Sindreu, P.Vélez, F. Paredes, G. Zamora, J. Bonache and F. Martín, “How can metamaterials help in aeronautics and transport?”, *META2012: 3rd International Conference on Metamaterials, Photonic Crystals and Plasmonics*, Paris, France, April 2012. **Invited.**
10. F. Paredes, G. Zamora, F. J. Herraiz-Martinez, F. Martín and J. Bonache, “Dual-band UHF-RFID Tags Based on Folded Dipole Antennas Loaded with Spiral Resonators”, *International Workshop on Antenna Technology (iWAT)*, Tucson (Az), USA, March 2012. **Invited.**
11. F. J. Herraiz-Martinez, E. Ugarte-Muñoz, D. Segovia- Vargas, F. Paredes, G. Zamora, F. Martín and J. Bonache, “Chipless RFID System Based on Magnetoinductive-Wave (MIW) Delay Lines”, *IEEE International Symposium on Antennas and Propagation and National Radio Science Meeting (IEEE APS-URSI)*, Chicago, USA, July 2012.
12. F. Paredes, G. Zamora, F. J. Herraiz-Martinez, F. Martín and J. Bonache, “Dipolo Doblado Cargado con Espiras Resonantes para Implementar Etiquetas RFID de Banda Dual”, *Unión Científica Internacional de Radio (URSI)*, Elche, España, Septiembre 2012.
13. F. J. Herraiz-Martinez, F. Paredes, G. Zamora, F. Martín and J. Bonache, D. Segovia-Vargas “Chipless RFID and Wireless Sensors Based on Planar Magnetoinductive-Wave (MIW) Delay Lines”, *Unión Científica Internacional de Radio (URSI)*, Elche, España, Septiembre 2012.

Patents

- Title:** *An optical disc with a wireless communication device, a wireless communication device and a method for its design and fabrication.*

Inventors: Jorge Bonache Albacete, Ferran Paredes Marco, Simone Zuffanelli, Ferran Martín Antolín and Gerard Zamora Gonzalez.

Applicants: Universitat Autònoma de Barcelona.

Applicantion number: EP13382232.0 (EPO: european patent office).
1310982.2 (UK-PO: United Kingdom patent office).
P201330926 (OEPM :Oficina española de patentes y marcas).

Date of applicantion: June 20, 2013.
- Title:** *Method for manufacturing a communication device to operate in near field and communication device thereof.*

Inventors: Jorge Bonache Albacete, Ferran Paredes Marco, Simone Zuffanelli, Ferran Martín Antolín and Gerard Zamora Gonzalez.

Applicants: Universitat Autònoma de Barcelona.

Applicantion number: EP13382287.4 (EPO: European patent office).
1312367.4 (UK-PO: United Kingdom patent office).
P201331049 (OEPM :Oficina española de patentes y marcas).

Date of applicantion: July 10, 2013.

